

**MULTIVORTEX MICROMIXING: NOVEL TECHNIQUES USING
DEAN FLOWS FOR PASSIVE MICROFLUIDIC MIXING**

A Dissertation

by

ARJUN PENUBOLU SUDARSAN

Submitted to the Office of Graduate Studies of
Texas A&M University
in partial fulfillment of the requirements for the degree of

DOCTOR OF PHILOSOPHY

December 2006

Major Subject: Chemical Engineering

**MULTIVORTEX MICROMIXING: NOVEL TECHNIQUES USING
DEAN FLOWS FOR PASSIVE MICROFLUIDIC MIXING**

A Dissertation

by

ARJUN PENUBOLU SUDARSAN

Submitted to the Office of Graduate Studies of
Texas A&M University
in partial fulfillment of the requirements for the degree of

DOCTOR OF PHILOSOPHY

Approved by:

Chair of Committee,	Victor M. Ugaz
Committee Members,	Michael A. Bevan
	Arul Jayaraman
	Ali Beskok
Head of Department,	N. K. Anand

December 2006

Major Subject: Chemical Engineering

ABSTRACT

Multivortex Micromixing: Novel Techniques Using Dean Flows for Passive
Microfluidic Mixing. (December 2006)

Arjun Penubolu Sudarsan, B.E., Bangalore University;

M.S., Texas A&M University

Chair of Advisory Committee: Dr. Victor M. Ugaz

Mixing of fluids at the microscale poses a variety of challenges, many of which arise from the fact that molecular diffusion is the dominant transport mechanism in the laminar flow regime. The unfavorable combination of low Reynolds numbers and high Péclet numbers implies that cumbersome long microchannels are required to achieve efficient levels of micromixing. Although considerable progress has been made toward overcoming these limitations (e.g., exploiting chaotic effects), many techniques employ intricate 3-D flow networks whose complexity can make them difficult to build and operate. In this research, we show that enhanced micromixing can be achieved using topologically simple and easily fabricated planar 2-D microchannels by simply introducing curvature and changes in width in a prescribed manner. This is accomplished by harnessing a synergistic combination of (i) Dean vortices that arise in the vertical plane of curved channels as a consequence of an interplay between inertial, centrifugal, and viscous effects, and (ii) expansion vortices that arise in the horizontal plane due to an abrupt increase in a conduit's cross-sectional area. We characterize

these effects using top-view imaging of aqueous streams labeled with tracer dyes and confocal microscopy of aqueous fluorescent dye streams, and by observing binding interactions between an intercalating dye and double-stranded DNA. These mixing approaches are versatile, scalable, and can be straightforwardly integrated as generic components in a variety of lab-on-a-chip systems.

DEDICATION

To my beloved fiancé Tapati,
my parents Rathna and Sudarsan,
my brother Vikram, and his family,
my wonderful friends, and
to the success and future of microfluidics

ACKNOWLEDGEMENTS

I express my sincere and heartfelt gratitude to my advisor Dr. Victor M. Ugaz for his invaluable supervision and support during this important phase of my career. The knowledge he has imparted on me during my M.S. and Ph.D. is indispensable and will go a long way into making my career successful.

Many thanks to Dr. Michael A. Bevan, Dr. Arul Jayaraman, and Dr. Ali Beskok for agreeing to serve on my committee.

It is impossible to adequately express my gratitude to Richard E. Beckham and Dr. Michael A. Bevan, not only for their invaluable training and assistance with confocal imaging experiments, but also for generously allowing me to access their confocal microscope at all hours of the day and night.

Use of the TAMU/CIMS Materials Characterization Facility and Dr. Orla M. Wilson are acknowledged for assistance with confocal imaging towards the latter part of this work.

I sincerely thank Michael Pendleton from the Microscopy and Imaging Center (MIC) at Texas A&M University for training and assistance with SEM imaging experiments. I would also like to thank E. Ann Ellis from the Microscopy and Imaging Center for assistance with sample preparation for SEM imaging.

I extend my thanks to my group members, Roger, René, Faisal, Nitin, Xiaojia and Jian for being a part of this research.

I am truly grateful to Dr. Sam Mannan for all his indispensable advice and encouragement over the past five years.

I would also like to thank the late Dr. Daniel Hanson for his extremely kind help and encouragement during the years I interacted with him.

A special thanks to Dr. Thomas Wood for several useful and insightful discussions over the past year.

I would like to take this opportunity to thank my friends Nikhil, Manish, Sunil, Deepa, Kiran, Sanjeev, Pooja, Jayant, Abhay, Amit, Ketan, and all my other friends in India who have helped me achieve my goals.

I thank my parents, my brother and his family, and Tapati for all their love and everything they have ever done for me.

Finally, I would like to thank the Artie McFerrin Department of Chemical Engineering for giving me the wonderful opportunity of pursuing my studies in this reputable university.

NOMENCLATURE

DNA	Deoxyribonucleic acid
PCR	Polymerase chain reaction
<i>Re</i>	Reynolds number
<i>Pe</i>	Péclet number
<i>Sc</i>	Schmidt number
SHM	Staggered herringbone mixer
SAR	Split-and-recombine
P-SAR	Planar split-and-recombine
ASM	Asymmetric serpentine mixer
PCB	Printed circuit board
DI	Deionized
SEBS	Polystyrene–(polyethylene/polybutylene)–polystyrene
SIS	Polystyrene–(polyisoprene)–polystyrene
SBS	Polystyrene–(butadiene)–polystyrene
SEM	Scanning electron microscopy
PDMS	Poly(dimethylsiloxane)
dsDNA	Double-stranded DNA

TABLE OF CONTENTS

	Page
ABSTRACT	iii
DEDICATION	v
ACKNOWLEDGEMENTS	vi
NOMENCLATURE	viii
TABLE OF CONTENTS.....	ix
LIST OF FIGURES	xii
LIST OF TABLES.....	xvii
 CHAPTER	
I INTRODUCTION.....	1
Micromixing.....	2
Micromixing strategies	6
Active micromixers.....	6
Passive micromixers.....	7
Lamination	8
Injection	11
Droplet	13
Rotation.....	14
Dean flows.....	25
Dean effects in planar 2-D configurations.....	35
Summary and motivation	38
Objectives.....	41
II EXPERIMENTAL PROCEDURES.....	44
Design and photomasks.....	44
Master mold fabrication using printed-circuit technology.....	45
Thermoplastic elastomer gels for device fabrication.....	49
Synthesis.....	51
Microchannel fabrication.....	51

CHAPTER	Page
	Fabrication of complex microstructures..... 54
	Solvent compatibility 60
	Biocompatibility 62
	SEM sample preparation and imaging..... 63
	Flow visualization and mixing characterization..... 66
	Top-view imaging..... 66
	Cross-sectional imaging 69
	Binding experiments 71
	Summary 71
III	SPIRAL MICROMIXERS..... 73
	Concept 76
	Design 76
	Flow visualization..... 80
	Summary 84
IV	PLANAR SPLIT-AND-RECOMBINE MIXING..... 87
	Concept 90
	Flow visualization in a two-split microchannel..... 92
	Planar split-and-recombine mixer (P-SAR) 95
	Design..... 95
	Flow visualization 96
	Optimal P-SAR design..... 100
	Mixing time 103
	Summary 107
V	ASYMMETRIC SERPENTINE MIXING 108
	Concept 109
	Flow visualization in a curved channel with an expansion 110
	Asymmetric serpentine mixer (ASM) 112
	Design..... 112
	Flow visualization 113
	Binding application..... 117
	Optimal ASM design 118
	ASM effective flow rate range 123
	Summary 126

CHAPTER	Page
VI	HYBRID MICROMIXING APPROACHES 128
	ASM combined with slanted barriers 129
	Concept..... 129
	Design..... 131
	Flow visualization 134
	ASM combined with spiral mixing sections 135
	Concept..... 135
	Design..... 136
	Flow visualization 137
	Summary 140
VII	CONCLUSIONS 142
	Micromixing designs investigated 143
	Spiral micromixers 143
	Planar split-and-recombine mixer 143
	Asymmetric serpentine mixer 144
	Hybrid mixing strategies 144
	Comparison with literature 145
	Fabrication 145
	Quantifying mixing 148
	Recommendations and future work 152
	LITERATURE CITED 156
	VITA 166

LIST OF FIGURES

FIGURE	Page
I-1 Laminar flow in a microchannel.....	3
I-2 Linear dependence of mixing length with Pe and Re	5
I-3 SEM image of a magnetic stirrer	7
I-4 Techniques for generating alternating lamellae of streams.....	8
I-5 Example of channel structure used to perform parallel lamination mixing	9
I-6 Example of channel structure used to perform serial lamination mixing	11
I-7 Example of an injection-type micromixer.....	12
I-8 Example of a droplet-based micromixer	14
I-9 Slanted wells for chaotic mixing	15
I-10 Staggered herringbone mixer	16
I-11 Barrier embedded micromixer.....	17
I-12 Three-dimensional serpentine channel mixer with C-shaped units	18
I-13 Micromixer utilizing the breakup process.....	19
I-14 Schematic of micromixer with Telsa structures	21
I-15 Schematic of square-spiral tower micromixer.....	22
I-16 Barrier embedded Kenics micromixer	23
I-17 Transverse Dean flow in a curved pipe.....	26
I-18 SEM image of micromixers based on conventional static mixers.....	27
I-19 Three-dimensional stirrer comprised of a series of square bends	28

FIGURE	Page
I-20	Idealized Dean flow phenomena in curved microchannels..... 29
I-21	Toroidal coordinate system 30
I-22	Cross-sectional investigation of Dean flow in a microchannel 32
I-23	Top-view imaging of Dean flow in a microchannel 33
I-24	Dean flow mixing at high flow rates..... 34
I-25	Dean effects in a circular microchannel..... 36
II-1	Overview of the printed-circuit board master fabrication process 46
II-2	Profile of etched structures on a PC board..... 48
II-3	Gel network formed by microphase separated SEBS triblock copolymers 50
II-4	Soft lithography using thermoplastic elastomer gels 52
II-5	Microfluidic channel structure constructed from SEBS gels 53
II-6	Cross-sectional SEM image of a bonded microchannel 54
II-7	Direct casting procedure to construct helical 3-D structures 55
II-8	Fabrication of an entangled bundle of microchannels 56
II-9	Fabrication of multilevel microstructures 57
II-10	Procedure used to generate multi-height channel structures 58
II-11	Examples of variable-height features..... 59
II-12	Fabrication of multi-height structures with herringbone patterns 60
II-13	Biocompatibility of SEBS elastomers..... 63
II-14	SEM images of channels before and after bonding 65
II-15	Top-view imaging setup..... 67

FIGURE	Page
II-16 Image processing using the top-view technique.....	68
II-17 Cross-sectional imaging using a LSM 5 PASCAL confocal microscope.....	69
II-18 Cross-sectional imaging using a Leica TCS SP5 confocal microscope	70
II-19 Typical cross-sectional image obtained from confocal laser scanning.....	71
III-1 Idealized Dean flow phenomena in a serpentine microchannel	75
III-2 Schematic of the spiral network incorporating three mixing sections.....	77
III-3 Dean number along the spiral contour at different Re	79
III-4 Mixing intensity comparison between a spiral and straight channel.....	81
III-5 Images of spiral mixing.....	82
III-6 Mixing intensity along the flow path of the first spiral section.....	83
III-7 Mixing intensity at the end of each spiral section	84
IV-1 Examples of selected SAR mixers from literature	89
IV-2 Concept of Dean induced planar split-and-recombine lamination	91
IV-3 P-SAR micromixer incorporating two split streams.....	92
IV-4 Evolution of lamellar structure in a two-split microchannel.....	93
IV-5 Dean induced lamination is a microchannel with two split streams.....	94
IV-6 Design of planar split-and-recombine micromixer.....	96
IV-7 Flow visualization in the first P-SAR element.....	97
IV-8 Cross-sectional images at $\kappa = 9.1$ images along the P-SAR micromixer	98
IV-9 Confocal cross-sectional images taken at the fourth recombination	99
IV-10 Mixing performance of P-SAR micromixer.....	100

FIGURE	Page
IV-11 Images for optimal P-SAR design	102
IV-12 Influence of flow and microchannel geometry on transverse rotation	103
IV-13 Comparison of conventional SAR and P-SAR mixer designs	105
IV-14 Mixing time for conventional SAR and P-SAR mixer designs.....	106
V-1 Multivortex phenomena in a microchannel.....	110
V-2 Multivortex micromixing.....	111
V-3 ASM design.....	112
V-4 Confocal cross-sectional images taken at the fourth expansion exit	113
V-5 Cross-sectional images at $\kappa = 8.6$ images along the ASM.....	114
V-6 Mixing levels measured at the fourth expansion exit	115
V-7 Mixing performance of ASM	116
V-8 Practical applicability of ASM	117
V-9 Flow images at different expansion locations with increasing κ	119
V-10 Optimal expansion ratio for the ASM design.....	121
V-11 Downstream distance to achieve 80% mixing at different Pe	122
V-12 Operating range of ASM and SHM for an aqueous system.....	125
VI-1 Schematic of microchannel with barriers along the channel floor	130
VI-2 Top-view images in a straight channel with barriers along the floor	131
VI-3 Design of ASM with slanted barriers.....	133
VI-4 Flow images in an ASM channel with barriers patterned along the floor	135
VI-5 Design of an ASM-spiral hybrid micromixer.....	137

FIGURE	Page
VI-6 Confocal cross-sectional images in the ASM-spiral hybrid micromixer	138
VI-7 Mixing performance of ASM-spiral hybrid micromixer	139
VI-8 Performance of ASM-spiral hybrid mixer as a function of Pe	140
VII-1 Comparison of mixing performance based on Re and footprint area	148
VII-2 Lengths required for 90% mixing as a function of Re	149
VII-3 Lengths required for 90% mixing as a function of Pe	150
VII-4 Lengths required for 90% mixing as a function of Sc	152

LIST OF TABLES

TABLE	Page
I-1 Summary of recent micromixer designs	24
I-2 Examples of work involving secondary flows in planar microchannels	37
I-3 Summary of techniques used to image and characterize mixing.....	39
I-4 Mixing characterization techniques in planar secondary flow systems.....	40
II-1 Swelling ratios for SEBS gels ranging from 9 – 33 wt% copolymer	61
III-1 Dimensions of the five different spiral channel designs investigated.....	78
V-1 Flow rates computed for the SHM for an aqueous working fluid.....	124
VII-1 Comparison of fabrication techniques of different micromixers.....	146

CHAPTER I

INTRODUCTION*

Microfluidics – the science and technology of processing and manipulating fluids in conduits having dimensions on the order of 10 – 100 μm , is becoming an increasingly important and mainstream technology in many chemical and biological process and analysis applications.¹⁻¹² The potential to replace large-scale conventional laboratory instrumentation with miniaturized and self-contained systems offers a variety of advantages that include reduced hardware costs, low reagent consumption, faster analysis speeds, and the capability of operating in a massively parallel scale in order to achieve high-throughput. Moreover, this technology provides for the capabilities of performing procedures that are extremely difficult or impossible to execute in the macro-scale.

This dissertation follows the style and format of *Analytical Chemistry*.

* Part of the data reported in this chapter is reprinted with permission from: Multivortex micromixing by Sudarsan, A.P.; Ugaz, V. M., *Proc. Natl. Acad. Sci. U. S. A.* **2006** *103*, 7228-7233. © 2006 by The National Academy of Sciences of the USA.

Although this technology is in its rudimentary stages, miniaturized microsystems have become indispensable in a number of established and emerging research areas including DNA and protein analysis,^{13, 14} polymerase chain reaction (PCR),^{15, 16} sorting,^{17, 18} nanoliter fluid manipulation,¹⁹ high-throughput screening,^{20, 21} biochemical networks,²² synthetic chemistry and catalysis,²³ computational problem solving,²⁴ and micromixing.²⁵ In terms of economics, the biochip market alone represented a \$400 million business in the year 2000 and was projected to grow at least a five-fold by 2005.²⁶ The number of microfluidic patents issued in the USA has steadily increased from under 50 in 1998 to over 350 in the year 2004.²⁷ In order to satisfy the demands of these increasingly sophisticated analysis tasks and for this technology to be successfully employed in μ TAS (Micro Total Analysis Systems) research, the ability to rapidly mix two or more reagent streams in a small device footprint is required.^{13, 25, 28-31}

Micromixing

Microfluidic mixing is a key process in a host of miniaturized analysis systems. A few of its recent applications include protein crystals,²⁸ kinetic studies of protein folding,^{31, 32} biosensors,³³ nucleation of hybridization enhancement,³⁴ DNA microarrays,^{35, 36} mixing of biological solutions,³⁷ and kinetic studies of liquid-phase reactions.³⁸ Although it is of fundamental importance, micromixing of reagent streams in small conduits continues to pose challenges owing to constraints associated with operating in a highly unfavorable laminar flow regime that is dominated by molecular diffusion (Figure I-1).

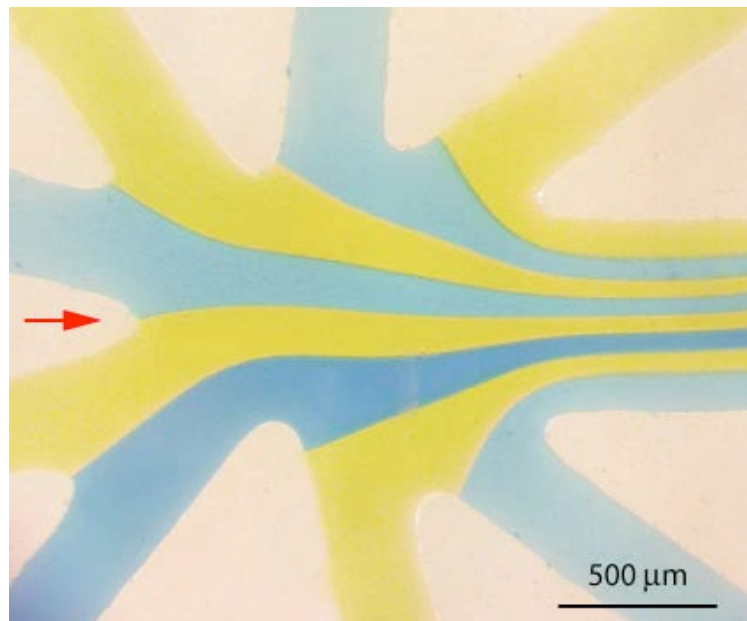


Figure I-1. Laminar flow in a microchannel. Aqueous streams labeled with blue and yellow food dyes are imaged at the entrance of a microchannel (600 μm wide, 29 μm tall) at a flow rate corresponding to $Re \sim 5$. Upon entering the channel the streams flow parallel to each other in the absence of any turbulence.

Typically, flow in planar smooth-walled micro-scale conduits are characterized by Reynolds numbers (Re) that are well below the threshold for turbulence (usually, $Re > 2000$ is required for turbulence in the macroscale). The Reynolds number represents the ratio between inertial and viscous effects and is given by the equation:

$$Re = Vd/\nu \quad (\text{I-1})$$

where V is the average flow velocity, d is the channel hydraulic diameter and ν is the kinematic viscosity of the fluid. Since $Re < 100$ in these smooth-walled planar microchannels, molecular diffusion is the predominant driving force for any mixing to

occur. Furthermore, values of the Péclet number (Pe), which is the ratio between mass transport due to convection and that of transverse diffusion, are relatively high in microchannels ($Pe > 100$):

$$Pe = Vd/D_{mol} \quad (I-2)$$

where D_{mol} is the molecular diffusivity. This relatively large discrepancy between convective and diffusive timescales implies that the downstream distances (Δy_m) over which fluids must travel to become completely intermixed can be on the order of several centimeters:

$$\Delta y_m \sim V \times (d^2/D) = Pe \times d \quad (I-3)$$

These mixing lengths scale linearly with Pe (and Re) and are generally prohibitively large resulting in the need to employ cumbersome long channels (Figure I-2). As a result, many of the benefits of miniaturization and the concept of lab-on-a-chip are often negated. To overcome these limitations, considerable effort has been directed toward the development of strategies to achieve rapid laminar flow mixing in microfluidic systems.

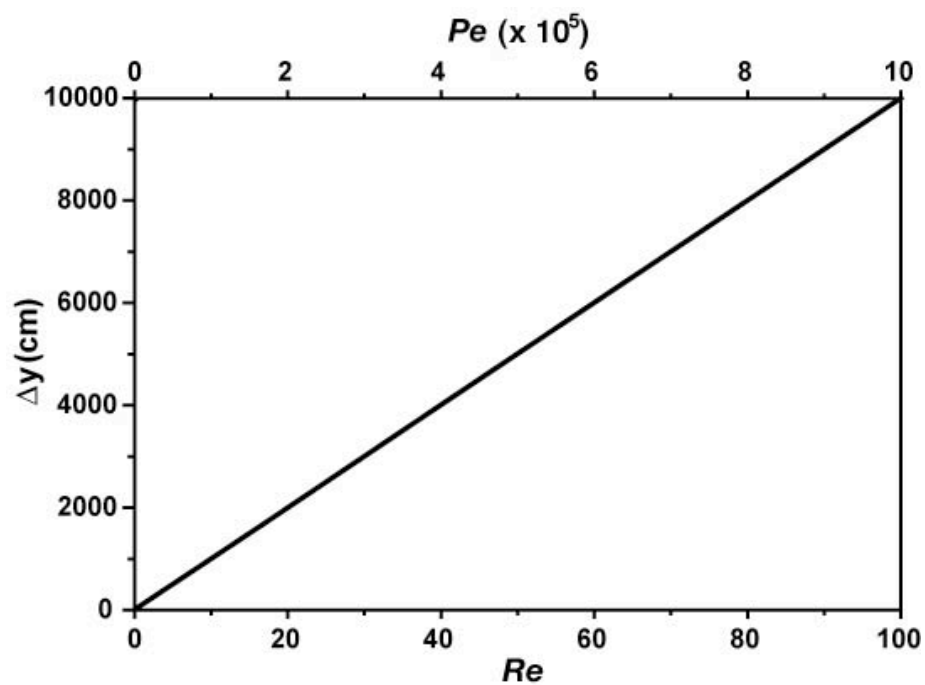


Figure I-2. Linear dependence of mixing length with Pe and Re . Typical microfluidic dimensions ($d = 100 \mu\text{m}$, $V = 0.01 - 100 \text{ cm/s}$, $D_{mol} = 10^{-6} \text{ cm}^2/\text{s}$) for a system of two aqueous streams were used to create this plot.

Micromixing strategies

In the past decade, a sizeable amount of research has been directed towards developing new micromixing strategies. Recent review papers give a holistic view of these micromixing techniques and applications.³⁹⁻⁴³ In general, mixing strategies can be classified as either *active* or *passive*, depending on the operational mechanism.

Active micromixers

Active micromixers employ external forces, beyond the energy associated with the flow, in order to perform mixing. Some examples of techniques developed to accomplish this include electro-osmosis,⁴⁴ magnetic stirring (Figure I-3),⁴⁵ bubble-induced acoustic actuation⁴⁶ and ultrasonic effects.⁴⁷ A distinct advantage over passive-type micromixers is that these systems can be activated on-demand. While generally effective in generating turbulence for rapid fluid mixing in short length-scales, these designs are often not easy to integrate with other microfluidic components and typically add substantial complexity to the fabrication process. Moreover, since high electric fields, mechanical shearing, or generation of nontrivial amounts of heat are involved, they are not well suited for use in applications involving sensitive species (e.g., biological samples).

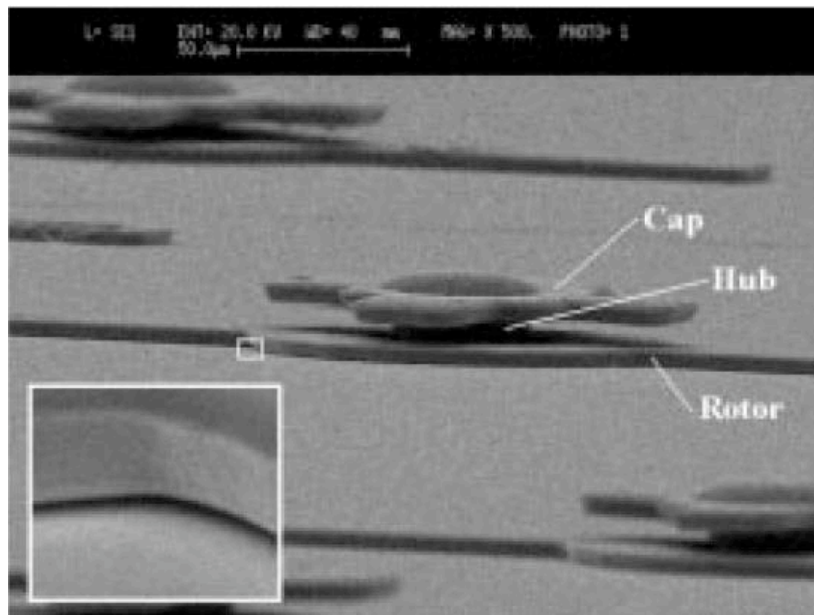


Figure I-3. SEM image of a magnetic stirrer. A rotating magnetic field causes the magnetic stirrer bar to rotate rapidly in the fluid environment. The overall height of the stirrer is 25 μm with a 0.5 μm gap between the rotor and substrate (inset). Individual microstirrers are separated by 500 μm from each other. Reprinted with permission from Lu, L.-H.; Liu, K. S. R., A magnetic microstirrer and array for microfluidic mixing, *J. Microelectromechan. Syst.* **2002**, *11*, 462-469. © 2000 IEEE.

Passive micromixers

Passive mixers, on the other hand, avoid these problems by exploiting characteristics of specific flow fields to mix species without application of external electrical or mechanical forces. These *gentle* designs are also often more straightforward to build and interface with other microfluidic components. Passive micromixers can be broadly sub-classified into designs based on *lamination*, *rotation*, *injection* and *droplet* techniques.

Lamination

Lamination-based mixers rely on the concept of repeated inter-layering of multiple parallel streams (a so-called *split-and-recombine* effect) in order to increase the interfacial area between species and accelerate the overall diffusive transport process. Both parallel and serial variations (Figure I-4) of this basic concept have been investigated.

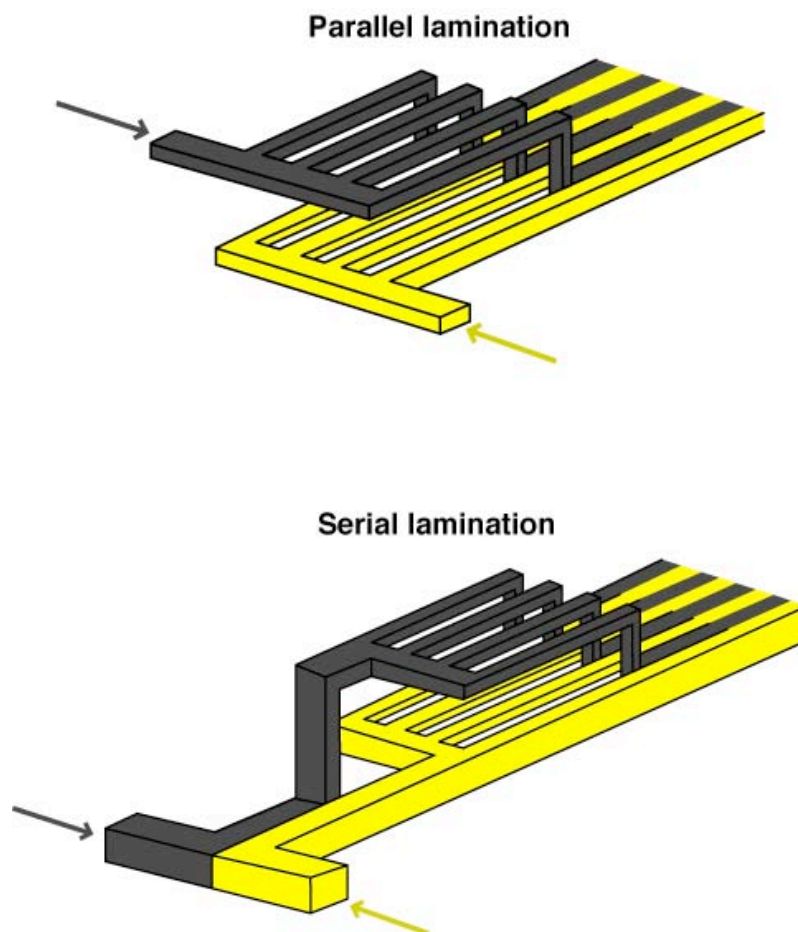


Figure I-4. Techniques for generating alternating lamellae of streams. Complex fabrication procedures are often required to create these 3-D structures required for both parallel and serial lamination.

Bessoth *et al.* demonstrated parallel lamination by splitting two species into sixteen streams on opposite sides of a silicon wafer, then bringing them together as alternating lamellae in a central zone where diffusive mixing occurred (Figure I-5).⁴⁸ The features on the silicon wafer were created by double-sided etching and then bonded by glass on either side to form a glass/silicon/glass sandwich. Kirner *et al.* have demonstrated another sandwich type mixer where all three chips were structured using microlithography.⁴⁹

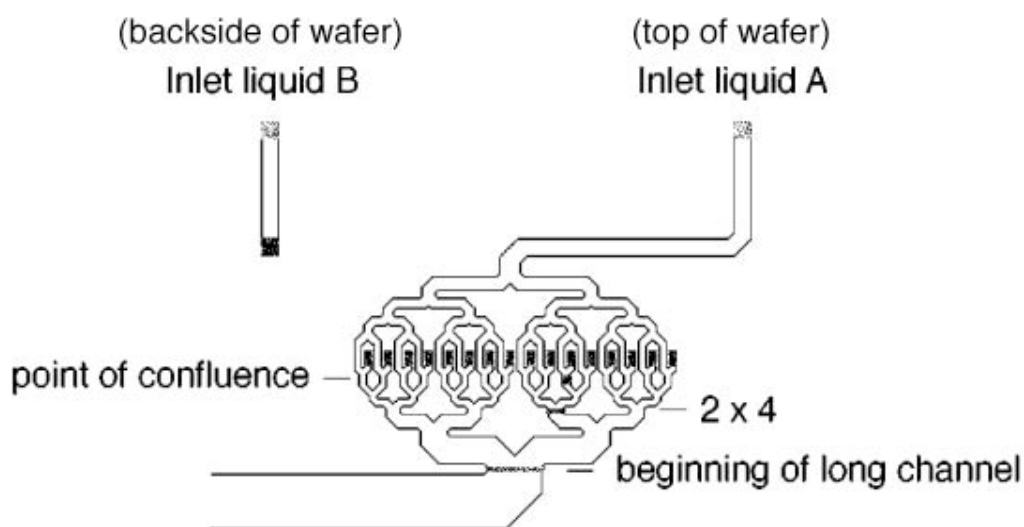


Figure I-5. Example of channel structure used to perform parallel lamination mixing. The two streams enter on either side of a wafer and are split to numerous streams before being brought together via through-holes. Mixing of the numerous lamellae by diffusion takes place in a single long channel. Channel depth ranged from 49 – 58 μm depending on the channel width (narrow down to 20 μm). The overall mixer microchip measured 5 mm \times 1 cm. Bessoth, F. G.; deMello, A. J.; Manz, A., Microstructure for efficient continuous flow mixing, *Anal. Commun.* **1999**, 36, 213-215 – Reproduced by permission of The Royal Society of Chemistry.

The idea of serial lamination mixing, where the streams to be mixed are separated from a common inlet channel, was suggested in early work by Schwesinger *et al.*⁵⁰ and Branbjerg *et al.*⁵¹ Usually, the streams are first directed in a horizontal conduit after which one or both of the streams are twisted vertically to initiate separation, followed by a sequence of turns to finally rejoin the fluids and create alternating lamellae.⁵² In reality however, if the fluid is subject to sudden changes in direction, distortion of the laminar profile is likely to occur making it extremely challenging to achieve multiple lamellae possessing identical cross-sectional profiles. In order to minimize these secondary flow effects, Schönfeld *et al.* have designed a split-and-recombine mixer incorporating minimal channel curvature capable of generating nearly ideal lamellar profiles (Figure I-6).⁵³ Lee *et al.* have shown in recent work that SAR mixing can be used to effectively at a wide range of flow rates.⁵⁴ Their mixer incorporated three-dimensional structures in the form of repeated units and a higher number of units was required to achieve mixing at higher flow rates. While lamination mixers have been highly successful, the complex 3-D flow geometries associated with most of these designs require cumbersome fabrication and assembly steps. Moreover, the footprints occupied by these channels do not always make them conducive for integration into “on-chip” systems.

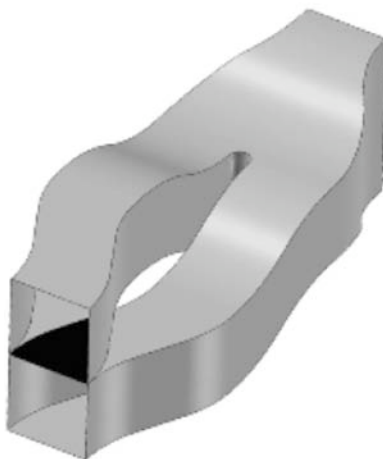


Figure I-6. Example of channel structure used to perform serial lamination mixing. The structure or step has a minimum cross-sectional feature of 1 mm and a length of 6 mm. individual steps were connected in series to form the micromixer. The curved features help in minimizing secondary flow effects that are typically generated in geometries involving sharp turns. Schönfeld, F.; Hessel, V.; Hoffman, C., An optimized split-and-recombine micro-mixer with uniform ‘chaotic’ mixing, *Lab Chip* **2004**, *4*, 65-69 – Reproduced by permission of The Royal Society of Chemistry.

Injection

Injection-type micromixers are similar to parallel lamination mixers, except that only one of the inlet streams is split into multiple streams and then injected into the other flowing stream. Typically, arrays of micro-nozzles are used to inject microplumes of one fluid on top of the other in order to increase the overall contact surface area and consequently increase diffusive mixing. Miyake *et al.* were amongst the first to utilize this concept in a mixer design that had 400 nozzles arranged in a square array (Figure I-7).⁵⁵ Capillary flows have also been used to generate microplumes.⁵⁶ Although these

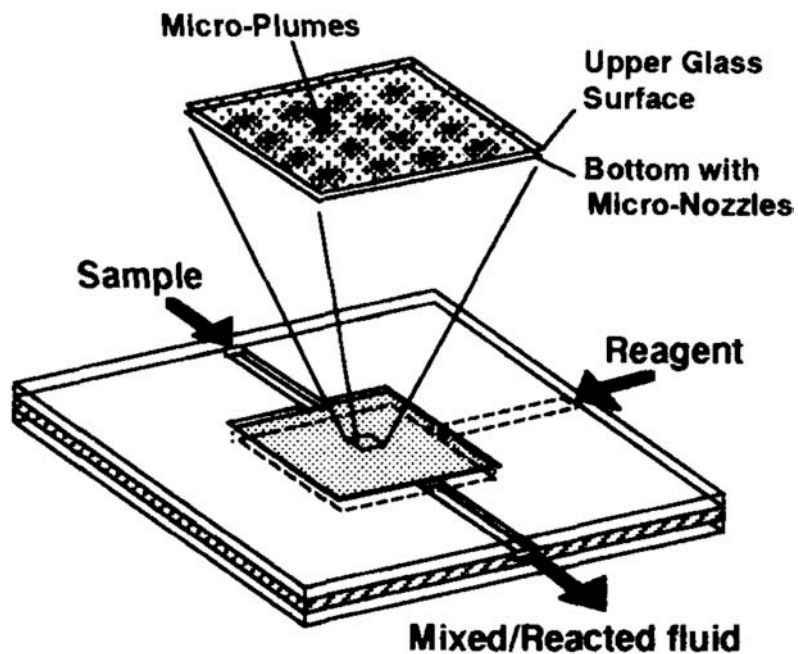


Figure I-7. Example of an injection-type micromixer. The mixing is first filled with one fluid and the second fluid is injected directly into the first fluid via micro-nozzles positioned below. Micro-plumes are generated thereby increasing the overall contact area between the two fluids for rapid diffusive mixing to occur. The micro-nozzles are separated from each other by $100\ \mu\text{m}$ and a mixing area of area $2\ \text{mm} \times 2\ \text{mm}$ accommodates up to 400 nozzles. Reprinted with permission from Miyake, R.; Lammerink, T. S. J.; Elwenspoek, M., Micro mixer with fast diffusion, *Proc. MEMS'93, 6th IEEE Int. Workshop Microelectromechan. Syst.*, San Diego, CA, USA 1993; 248-253. © 2000 IEEE.

mixers are capable of rapidly increasing the contact area between different species, fabrication of the complex setup involved requires a multi-level procedure that can be quite tedious. Moreover, it can be challenging to reproducibly fabricate arrays involving hundreds of micro-nozzles with precision.

Droplet

Micromixers based on droplet mixing offer an attractive approach to overcome many of the complexities associated with fabrication of 3-D structures in lamination and injection type mixers. Fluid elements trapped in droplets get rapidly intermixed due to the presence of an internal flow field that is characteristic of moving droplets. Ismagilov *et al.*^{28, 57} have used this inherent recirculation to mix fluids inside confined droplets that are dispersed in an immiscible liquid (Figure I-8). Günther *et al.*⁵⁸ have shown that liquids can be mixed by recirculation that is associated with the introduction of a gas phase that forms a segmented gas–liquid slug flow. A drawback of droplet micomixing techniques is that since multi-phase or immiscible liquids are often needed to generate droplets, an additional separation step would be required if the mixed elements inside the droplet are to be extracted.

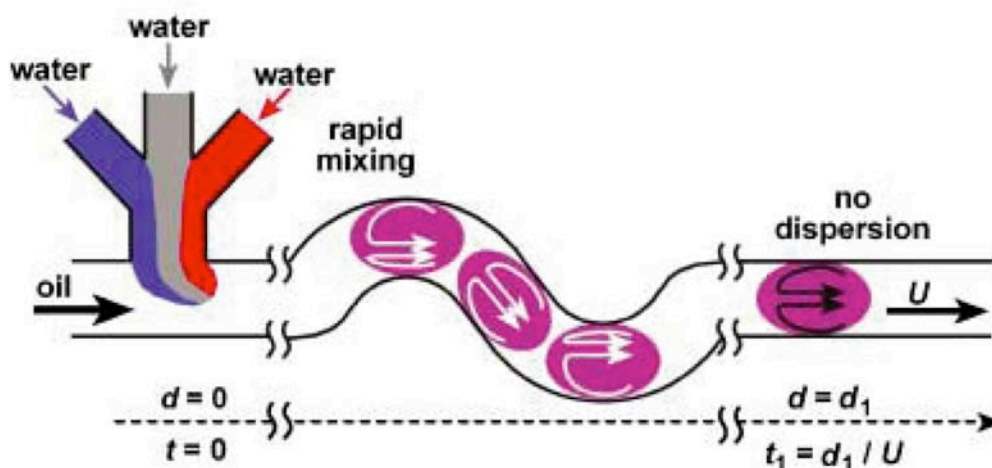


Figure I-8. Example of a droplet-based micromixer. The streams to be mixed flow in a laminar manner before encountering a flowing immiscible liquid to give rise to tiny droplets or plugs. As the droplets flow through varying channel geometries, internal recirculation causes the engulfed streams to get rapidly intermixed. The maximum cross-sectional feature in the mixer was 50 μm . Reprinted with permission from Song, H.; Tice, J. D.; Ismagilov, R. F., A microfluidic system for controlling reaction networks in time, *Angew. Chem. Int. Ed.* **2003**, 42, 768-772. © 2003 Wiley-VCH.

Rotation

Passive rotation mixers that are designed to generate transverse flows across the channel cross-section have also been investigated. Grooves, ridges, projections, obstacles and barriers are examples of features that are patterned inside channels to induce disturbances to the flow pattern. Johnson *et al.*⁵⁹ (Figure I-9) and Stroock *et al.*⁶⁰ (Figure I-10) have demonstrated this by patterning the floor of a microchannel with oblique grooves to generate lateral flows that repeatedly stretch and fold fluid segments

across the channel cross-section. In these designs faster *chaotic* mixing is achieved at lower Re and the mixing length has a logarithmic dependence on Pe .

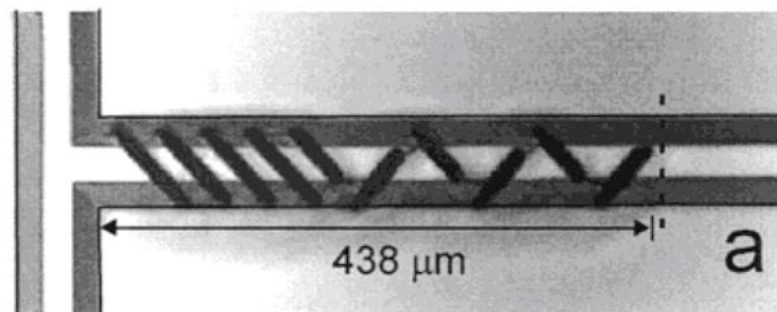


Figure I-9. Slanted wells for chaotic mixing. This mixer was used for mixing under both electroosmotic and pressure driven flows. In the latter case the wells were used to generate transverse flows across the channel. The average depth over the majority of the wells was measured to be 100 μm below the bottom of the channel. Reproduced with permission from Johnson, T. J.; Ross, D.; Locascio, L., Rapid microfluidic mixing, *Anal. Chem.* **2002**, *74*, 45-51. © 2002 American Chemical Society.

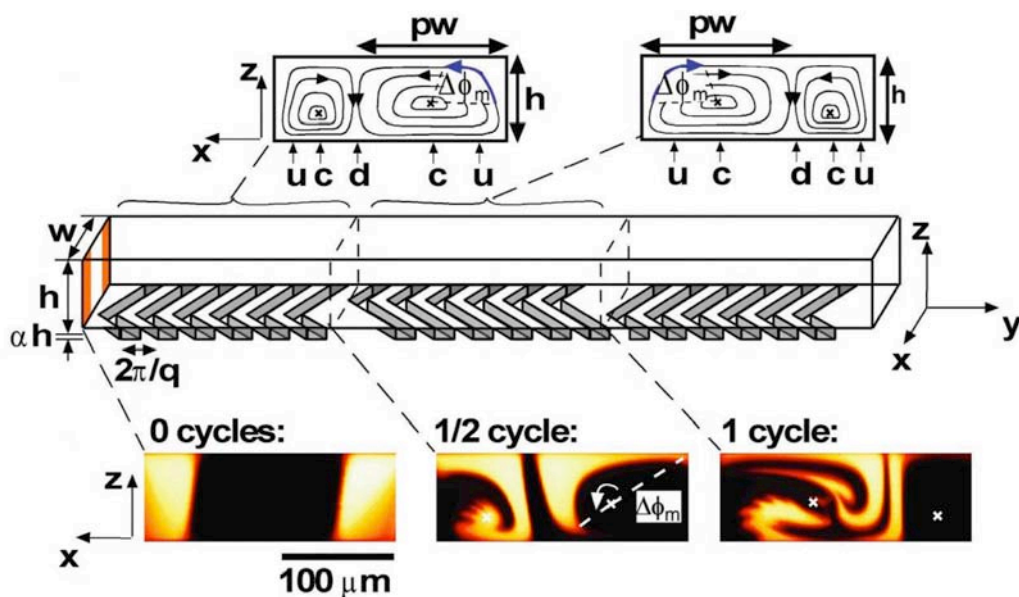


Figure I-10. Staggered herringbone mixer. The herringbones induces transverse rotation to the flow and repeatedly stretches and folds fluid elements across the cross-section as seen from the confocal images (below the channel schematic). The asymmetric nature of the herringbones varies the center of transverse rotation as seen from the flow streamlines (above). The main channel has a cross-section of $200\ \mu\text{m} \times 77\ \mu\text{m}$, and the depth of the grooves is under $18\ \mu\text{m}$. The distance between the start of consecutive grooves is $100\ \mu\text{m}$. Reprinted with permission from Stroock, A. D.; Dertinger, S. K. W.; Ajdari, A.; Mezić, I.; Stone, H. A.; Whitesides, G. M., Chaotic mixer for microchannels, *Science* 2002, 295, 647-651. © 2002 AAAS.

Howell *et al.*⁶¹ showed a modification of this basic design, which involves patterning ridges on the top and bottom of the channel. In this mixer, combined transverse flows generated at the top and bottom of the channel contributed to mixing. Another mixer with patterned features on the top and bottom of the channel has been demonstrated (Figure I-11).⁶² The barriers that were placed on the top wall at regular

intervals induced periodic disturbances to helical flow profile that was generated by the action of slanted grooves patterned along the entire bottom surface.

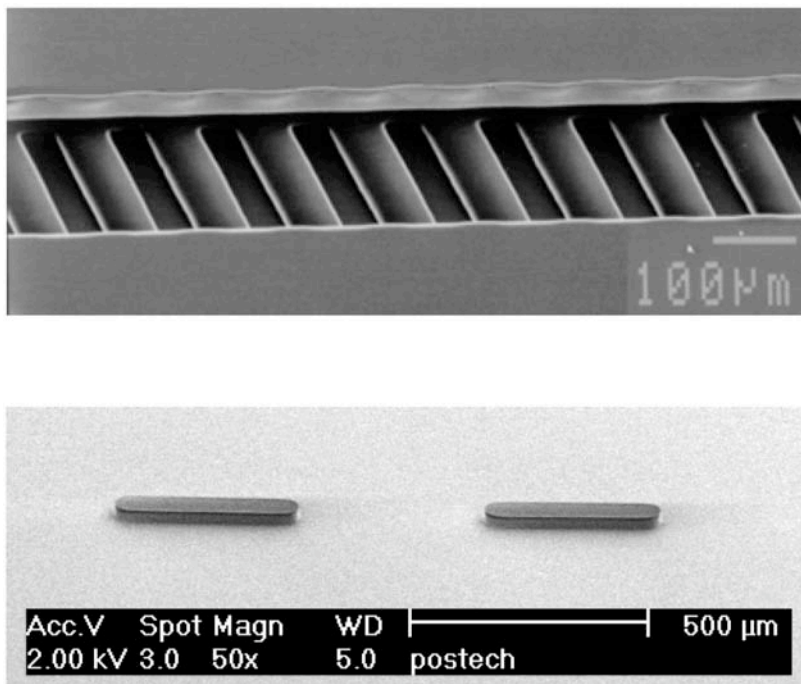


Figure I-11. Barrier embedded micromixer.⁶² The bottom of the mixer is patterned with slanted grooves (above) while the top of the mixer (below) has barriers patterned periodically. The transverse stretching and folding of the fluid by the slanted grooves is further accelerated by the presence of the barriers on the upper surface. The channel cross-section measures $240\ \mu\text{m} \times 60\ \mu\text{m}$. The grooves are slanted at 45° with a depth of $9\ \mu\text{m}$ and the barriers are $30\ \mu\text{m}$ wide and $40\ \mu\text{m}$ tall.

A 3-D serpentine geometry with recurring “C-shaped” units has been demonstrated by Liu *et al* (Figure I-12).⁶³ A similar micromixer with repeated L-shaped units was constructed and used for enhancing the performance of surface-based microfluidic biosensors.³³ The efficiency of this mixer increases with Re due to presence of eddies formed at the channel bends. Kim *et al* demonstrated a mixer having triangular projections on the channel walls that induce stretching and folding of the fluid

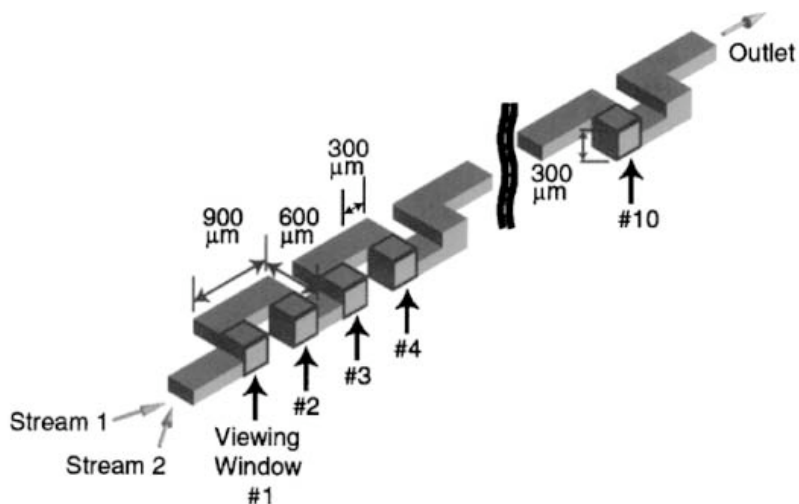


Figure 1-12. Three-dimensional serpentine channel mixer with C-shaped units. Mixing is achieved as a result of eddies formed at the bends. The strength of the eddies increases with flow rate, and consequently faster mixing can be achieved at shorter downstream distances. Reprinted with permission from Liu, R. H.; Stremler, M. A.; Sharp, K. V.; Olsen, M. G.; Santiago, J. G.; Adrian, R. J.; Aref, H.; Beebe, D. J., Passive mixing in a three-dimensional serpentine microchannel, *J. Microelectromechan. Syst.* **2000**, *9*, 190-197. © 2002 IEEE.

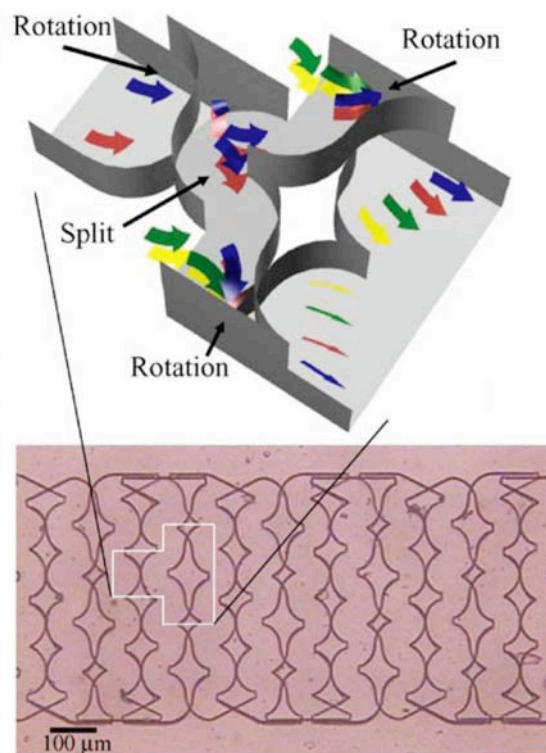


Figure I-13. Micromixer utilizing the breakup process.⁶⁶ Fluid elements undergo specific flow effects as indicated in the schematic of an individual mixer segment (above). An optical micrograph of the mixer is shown below. Mixer segments are 100 μm wide and 50 μm deep.

segments.⁶⁴ A mixer, which can be classified as a SAR mixer also, with combined effects of splitting-and-recombining and advection has been realized in a geometry comprised of a series of “F-shaped” mixing elements.⁶⁵

Three-dimensional passive rotation using a breakup process has also been shown to be efficient for mixing (Figure I-13).⁶⁶ While this mixer design is effective for Re ranging from 1 – 50, its efficiency is highest at $Re = 10$ due to the combined influence of stretching and folding, breakup and diffusion processes. At lower flow rates ($Re = 1$) stretching and folding of the interface is absent and mixing is breakup and diffusion limited. At higher flow rates ($Re = 50$) diffusion is minimal and fluids are mixed via stretching and folding and breakup processes.

Other examples of mixing techniques that have recently been introduced involve self-circulation in a mixing chamber that is efficient at high flow rates ($Re \geq 50$),⁶⁷ an in-plane passive micromixer with modified Telsa structures that employed the “Coanda effect” to improve mixing (Figure 1-14),⁶⁸ and a mixer based on surface tension in a geometrical mixing chamber.⁶⁹

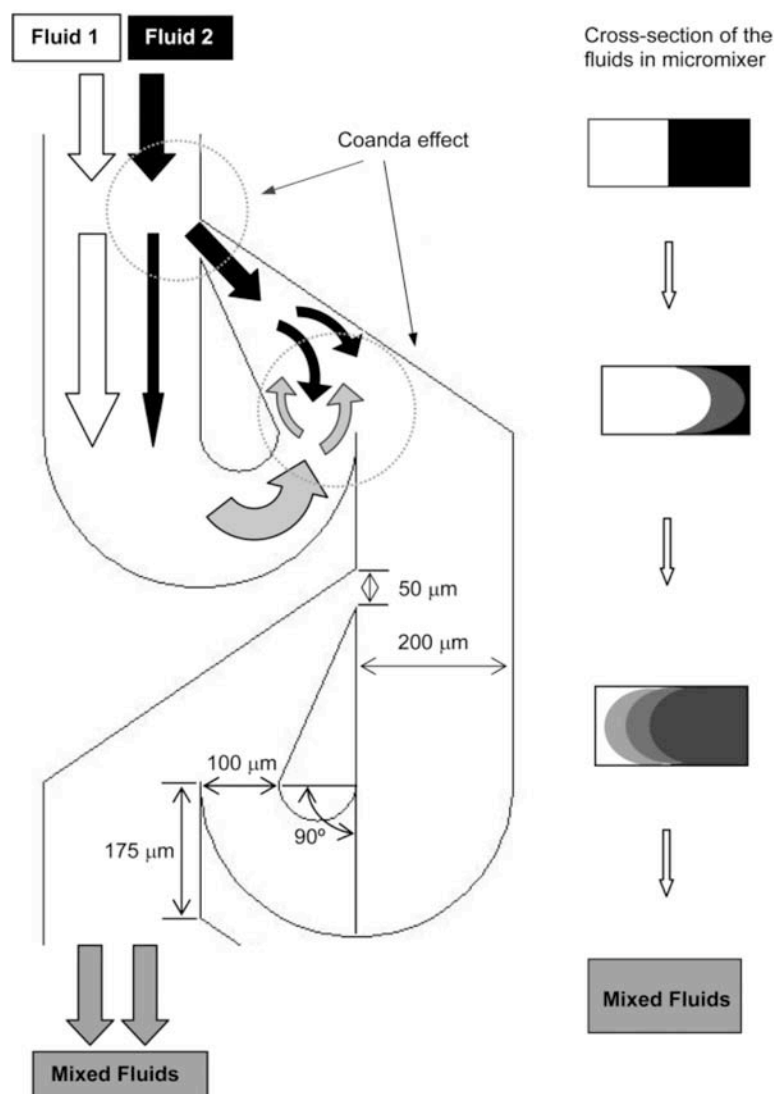


Figure I-14. Schematic of micromixer with Telsa structures. Mixing in this type of mixer is achieved using the “Coanda” effect that causes transverse dispersion with the Telsa structures and consequently impacts the convection of the fluids. This planar micromixer has a uniform height of 110 μm. Hong, C.-C.; Choi, J.-W.; Ahn, C. H., A novel in-plane passive microfluidic mixer with modified Telsa structures, *Lab Chip* **2004**, *4*, 109-113 – Reproduced by permission of The Royal Society of Chemistry.

Mixing in more complex 3-D flow networks has also been investigated. For example, micro-stereolithography has been used to construct mixing geometries mimicking conventional macroscale static mixers.⁷⁰ Another example involves construction of 3-D microvascular networks incorporating arrays of square-spiral towers via direct-write assembly (Figure I-15).⁷¹ The resulting design consisted of square-spiral towers embedded within a 3-D network and promoted fluid mixing through chaotic advection. Mixing efficiency in this case exhibited an exponential dependence on Re . A barrier embedded Kenics micro-mixer that operates using combined stretching/folding and splitting/reorientation processes has also been fabricated using micro-stereolithography (Figure I-16).⁷²

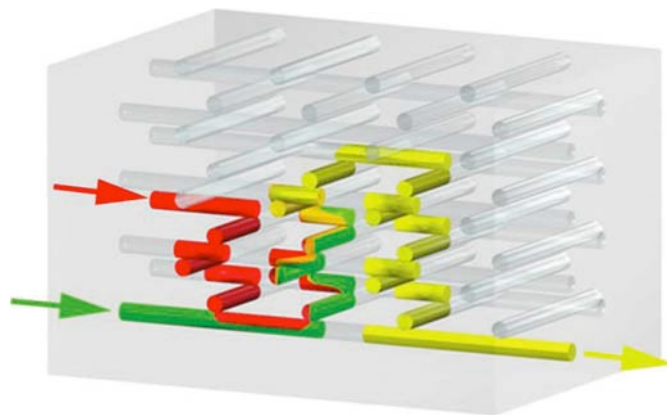


Figure I-15. Schematic of square-spiral tower micromixer. Mixing in this system is due to chaotic advection and the mixing efficiency increases exponentially with Re . The diameter of the channels is around $200\ \mu\text{m}$. Reprinted with permission from Therriault, D.; White, S. R.; Lewis, J. A., Chaotic mixing in three-dimensional microvascular networks fabricated by direct-write assembly, *Nat. Mater.* **2003**, 2, 265-271. © 2003 Nature Publishing Group.

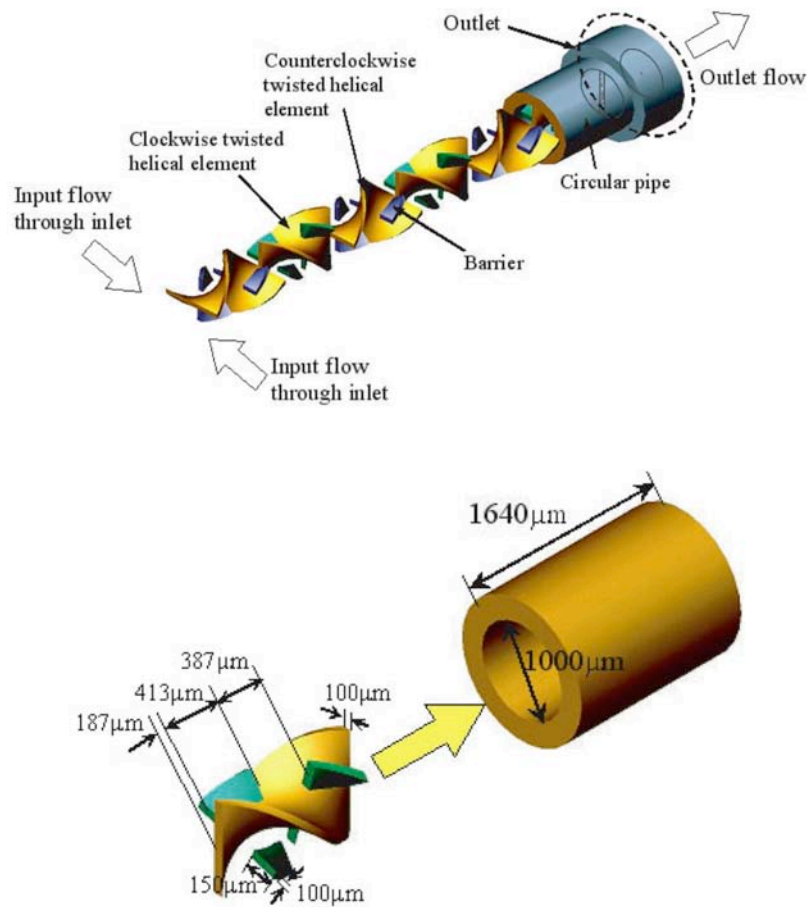


Figure I-16. Barrier embedded Kenics micromixer.⁷² The mixer has a series of alternating helical elements with barriers patterned on them. The helical structures split and reorient the fluid while the barriers induce stretching and folding of the fluid elements.

Table I-1 provides a representative sampling of some of the rotation-based mixers described above. Many of the mixer designs listed incorporate complex 3-D structures that, from a practical standpoint, are difficult or impossible to fabricate in a manner consistent with processes used to construct standard lab-on-a-chip components. The need to incorporate specialized processes and/or precise multilayer alignment steps makes these approaches far less attractive from both economic and process integration perspectives.

Table I-1. Summary of recent micromixer designs.

Source	Re	Mixing length	Effective range
Liu <i>et al.</i> ⁶³	6-70	>90% in ~ 11.7 mm ^a ($Re = 70$)	$Re > 35$ Better at high flow rates
Johnson <i>et al.</i> ⁵⁹	0.03-0.45	>90% in 0.443 mm ($Re \sim 0.033$)	Better at low flow rates
Stroock <i>et al.</i> ⁶⁰	10^{-2} -10	90% in 7 mm ($Re = 10^{-2}$)	$10^{-2} \leq Re \leq 10$ Better at low flow rates
Therriault <i>et al.</i> ⁷¹	0.15 - 70	90% in 6 mm ($Re = 30$)	$Re > 10$ -15 Better at high flow rates
Hong <i>et al.</i> ⁶⁸	0.08-8.31 ^b	90% in 7 mm ($Re = 4.16$) ^b	$4 < Re < 8.3$ ^b Better at high flow rates
Kim <i>et al.</i> ⁶²	0.2-2.28	80% in 13 mm ($Re = 0.2$)	$0.2 < Re < 2.28$ Better at low flow rates
Kim <i>et al.</i> ⁷²	7-28	90% in 5 mm ($Re = 7$)	$7 < Re < 28$ Better at low flow rates
Park <i>et al.</i> ⁶⁶	1-50	85% in 4 mm ($Re = 10$)	$1 < Re < 50$ Best at $Re = 10$

^a Measured using given dimensions.

^b Calculated using 110 μm as the characteristic dimension.

Dean flows

Manipulating the action of transverse vortex phenomena that naturally arise in specific flows offers a promising approach to address some of the drawbacks associated with recent micromixing techniques. For example, fluids traveling through curvilinear channels experience an interplay between inertial forces acting to direct axial motion and centrifugal effects acting along the conduit's radius of curvature. Under appropriate conditions, these effects establish a radial pressure gradient whose magnitude can become sufficient to generate a transverse flow field (Figure I-17). These so-called *Dean flows* occur widely in nature and play an important role in a variety of applications ranging from chemical and mechanical engineering (e.g., heat exchangers, piping systems) to biomedical science (e.g., arterial blood flow, dialysis instruments).⁷³

The concept of using Dean flow for mixing has been explored extensively on the macroscale,⁷⁴⁻⁷⁸ where the use of helical tubes or pipes that extend out of a 2-D plane allows curved flow trajectories to be maintained far downstream. A further adaptation of Dean effects are so-called *twisted pipe* designs (constructed by joining a series of planar curved segments such that each subsequent segment is oriented at a nonzero pitch angle relative to the previous one) in which the inherent symmetry of the secondary flow streamlines is disrupted yielding chaotic particle trajectories.⁷⁹

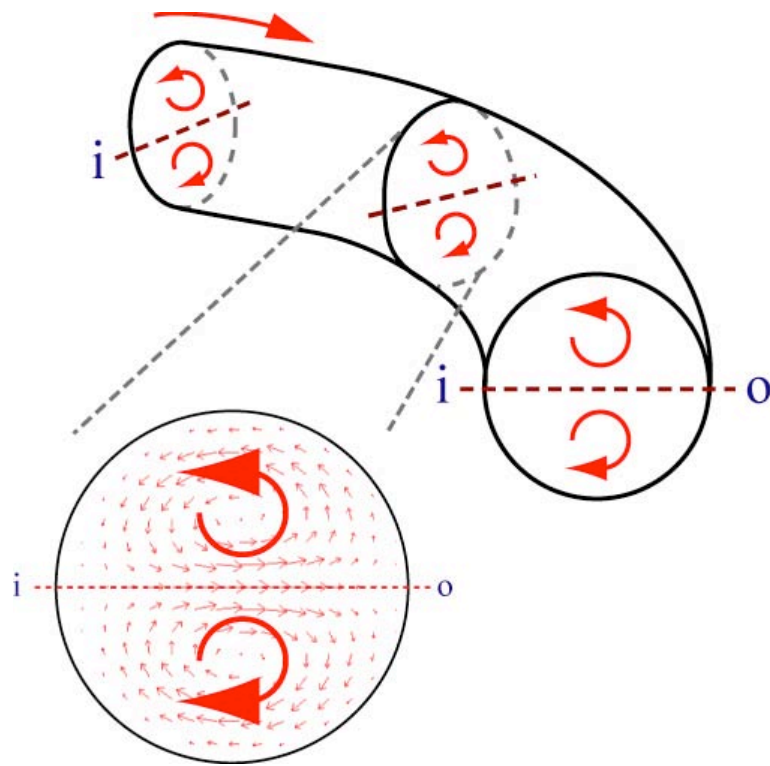


Figure I-17. Transverse Dean flow in a curved pipe. The interplay between inertial and centrifugal effects establish a radial pressure gradient that generates a transverse flow in the form of two counter-rotating vortices above and below the channel midplane (“i” and “o” denote the inner and outer walls of the pipe).

Variations of helical and twisted pipe arrangements at the micro-scale have been previously investigated to enhance mixing in microfluidic systems, however the corresponding non-planar flow geometries often require multi-level or specialized fabrication processes that can introduce added complexity (e.g., see Figure I-18).^{60, 63, 70,}

⁷² Yi and Bau demonstrated secondary flow recirculation in structures composed of 90°

bends (Figure I-19).⁸⁰ They also constructed a 3-D stirrer from a multi-level procedure utilizing ceramic tapes and found the mixer to be effective at $Re > 10$.

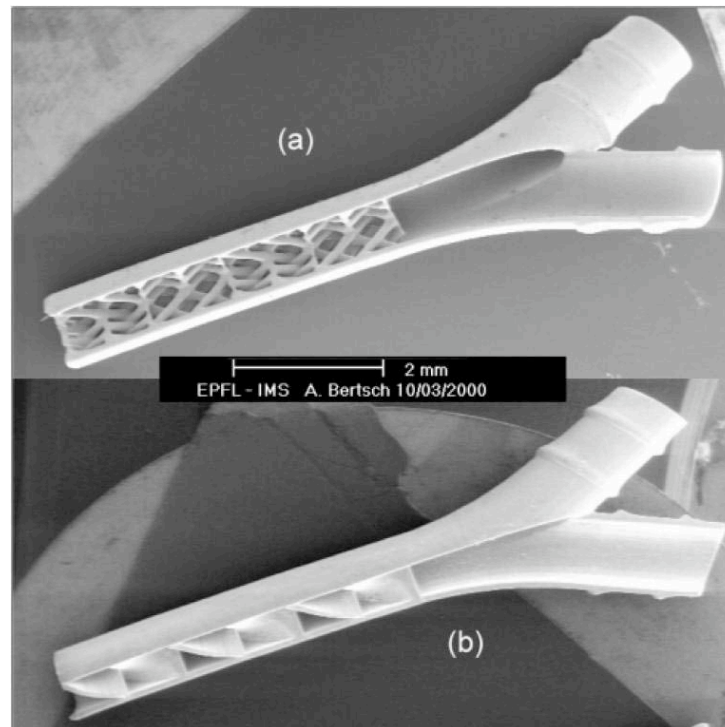


Figure I-18. SEM image of micromixers based on conventional static mixers. Microstereolithography was used to construct mixers comprising of intersecting channels (above) and helical elements (below). Both mixers have a diameter of 1200 μm and an overall length of about 2.48 cm and 2.54 cm respectively. Bertsch, A.; Heimgartner, S.; Cousseau, P.; Renaud, P., Static micromixers based on large-scale industrial geometry, *Lab Chip* 2001, 1, 56-60 – Reproduced by permission of The Royal Society of Chemistry.



Figure I-19. Three-dimensional stirrer comprised of a series of square bends. Reprinted from *International Journal of Heat and Fluid Flow*, 24, Yi, M.; Bau, H. H. The kinematics of bend-induced mixing in micro-conduits, 645-656. © 2003, with permission from Elsevier.

The transverse secondary flow associated with Dean effects can be characterized in terms of a dimensionless *Dean number* κ that expresses the relative magnitudes of inertial and centrifugal forces to viscous forces:

$$\kappa = \delta^{0.5} Re \quad (\text{I-4})$$

where δ is a geometric parameter that relates to the extent of the centrifugal effects and is given by the relation:

$$\delta = d/R \quad (\text{I-5})$$

where d is the characteristic cross-sectional channel dimension, and R is the flow path radius of curvature.⁷³ Here we compute

$$Re = Vd/\nu \quad (\text{I-6})$$

by taking d as the channel hydraulic diameter

$$d = 4A_c/P \quad (\text{I-7})$$

where A_C is the cross-sectional area and P is the wetted perimeter (the trapezoidal microchannel cross-sections were approximated as rectangular). Microchannel Dean flows generally fall in the regime $\kappa \ll 100$, where the secondary flow consists of a pair of counter-rotating vortices positioned symmetrically above and below the channel midplane. At very low flow rates ($\kappa \sim 1$) centrifugal effects are not strong enough to significantly perturb the axial laminar flow profile. As the flow rate is increased ($\kappa \sim 10$) the transverse flow component acts to transport fluid from the inner wall of the channel radially toward the outer wall (Figure I-20).

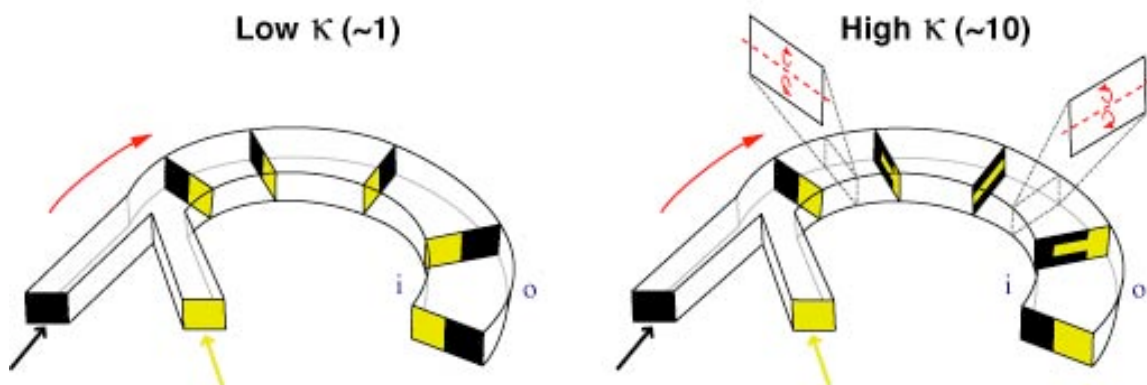


Figure I-20. Idealized Dean flow phenomena in curved microchannels. At low κ (left), two parallel streams of different species (yellow and black) entering a curved microchannel segment experience unperturbed laminar flow. At $\kappa \sim 10$ (right), the transverse flow generated by the counter-rotating Dean vortices transport the inner (yellow) stream toward the outer wall while the outer (black) stream is pulled inward causing the positions of each species to be transposed at the exit. (“i” and “o” denote the inner and outer channel walls).

Under these conditions (low curvature limit ($\delta < 1$), $Re \lesssim 100$), the essential features of the secondary flow field are well-described by Dean's solution to a perturbation analysis of the equations of motion.⁸¹⁻⁸³ The equations of motion are written in the two toroidal local coordinate systems (x, y, θ) and (r, φ, θ) . The flow field is assumed to be steady, incompressible and fully developed in the whole geometry (Figure I-21).

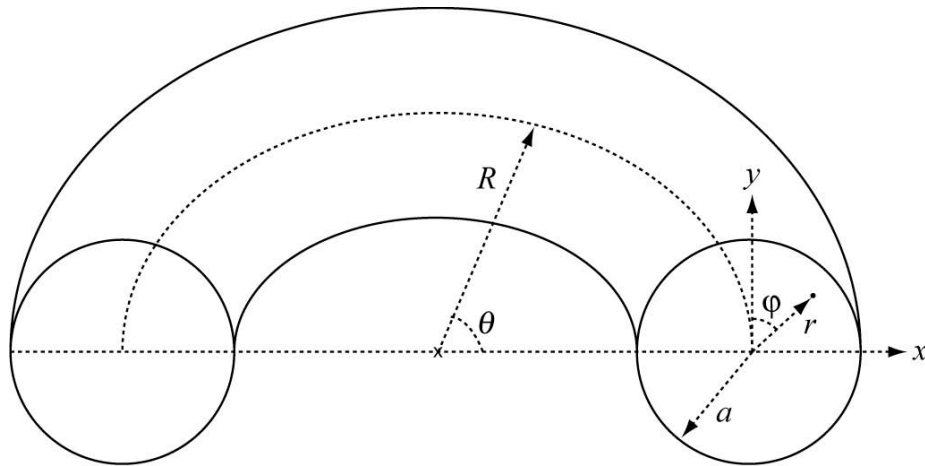


Figure I-21. Toroidal coordinate system.

Dean^{81, 82} showed that the secondary flow velocities are given by the following two equations:

$$u = \frac{A^2 \kappa^2}{4468} (1 - x^2 - y^2)(4 - 5x^2 - 23y^2 + 8x^2y^2 + x^4 + 7y^4)$$

$$v = \frac{A^2 \kappa^2}{1152} (1 - x^2 - y^2)xy(3 - x^2 - y^2) \quad (\text{I-8})$$

where A is a dimensionless parameter expressing the overall pressure gradient driving the flow and is given by:

$$A = \frac{a^2}{\mu V} \frac{\partial P}{R \partial \theta} \quad (\text{I-9})$$

where μ is the dynamic viscosity, V is the average axial velocity and P is the pressure.

The axial velocity component in the local coordinate (x, y, θ) is given by^{81, 82}:

$$w = \frac{2\kappa^2}{\text{Re}} (1 - x^2 - y^2) \quad (\text{I-10})$$

Jones *et al.*⁷⁹ showed that the independent variable can be changed from time t to angular position θ by dividing Equation I-8 by Equation I-10 and Castelain *et al.*⁸⁴ showed that the resulting system of two differential equations defines the cross-sectional mapping of fluid particles for different values of θ :

$$\begin{aligned} \frac{dx}{d\theta} &= \frac{\text{Re}}{144} (4 - 5x^2 - 23y^2 + 8x^2y^2 + x^4 + 7y^4) \\ \frac{dy}{d\theta} &= \frac{\text{Re}}{24} xy(3 - x^2 - y^2) \end{aligned} \quad (\text{I-11})$$

Centrifugal effects are greatest along the channel centerline where the axial velocity is maximum, resulting in outward flow along the midplane while slower moving fluid near the walls is simultaneously swept inward. Ultimately, a nearly complete 180° rotation can be induced causing two parallel fluid streams to almost entirely switch positions inside the channel. Theoretical predictions and experimental results of cross-sectional view show a good agreement in detailing this effect (Figure I-22). The same effect can also be visualized by imaging aqueous streams with different color dyes (Figure I-23).

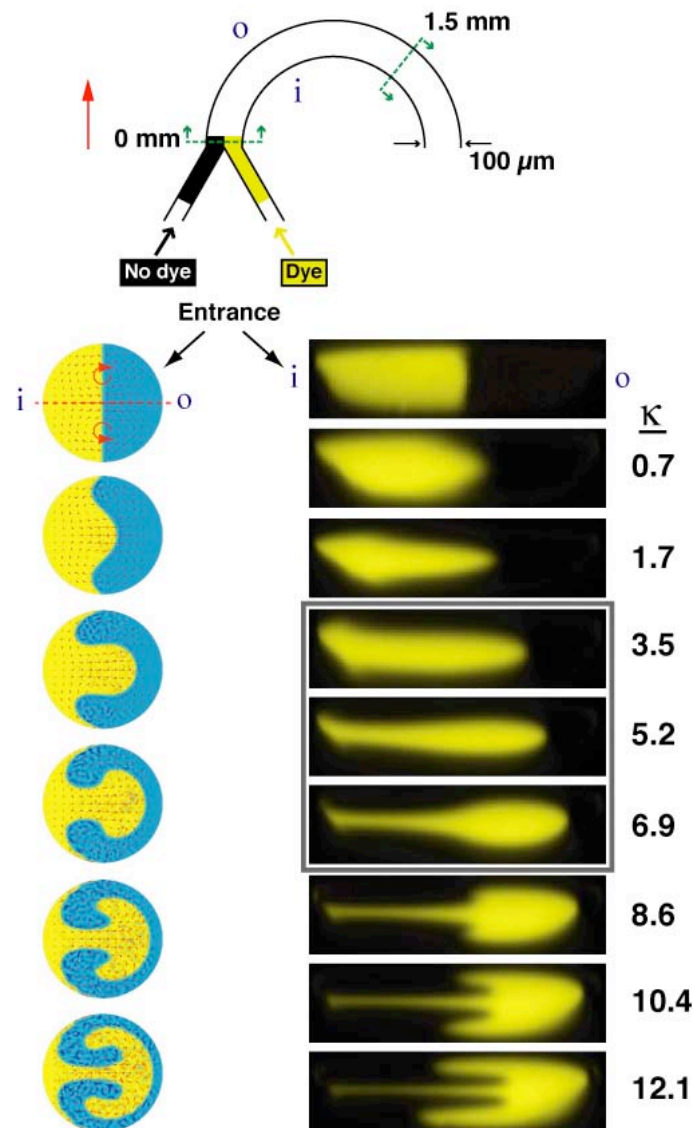


Figure I-22. Cross-sectional investigation of Dean flow in a microchannel. (Upper) Schematic of the curved microchannel geometry investigated (100 μm wide, 29 μm tall, 630 μm radius of curvature, “i” and “o” denote the inner and outer channel walls). The transverse flow field was examined at the entrance to the curved segment and at a location 1.5 mm downstream. Analytically computed velocity and concentration profiles are shown (left lower) beside confocal cross-sectional images of the transverse flow in the microchannel depicted in (right lower) at flow rates ranging from $2.6 < Re < 45.1$ ($0.7 < \kappa < 12.1$). The boxed area represents conditions under which the transverse flow induces $\sim 90^\circ$ rotation in the upper and lower halves of the channel.

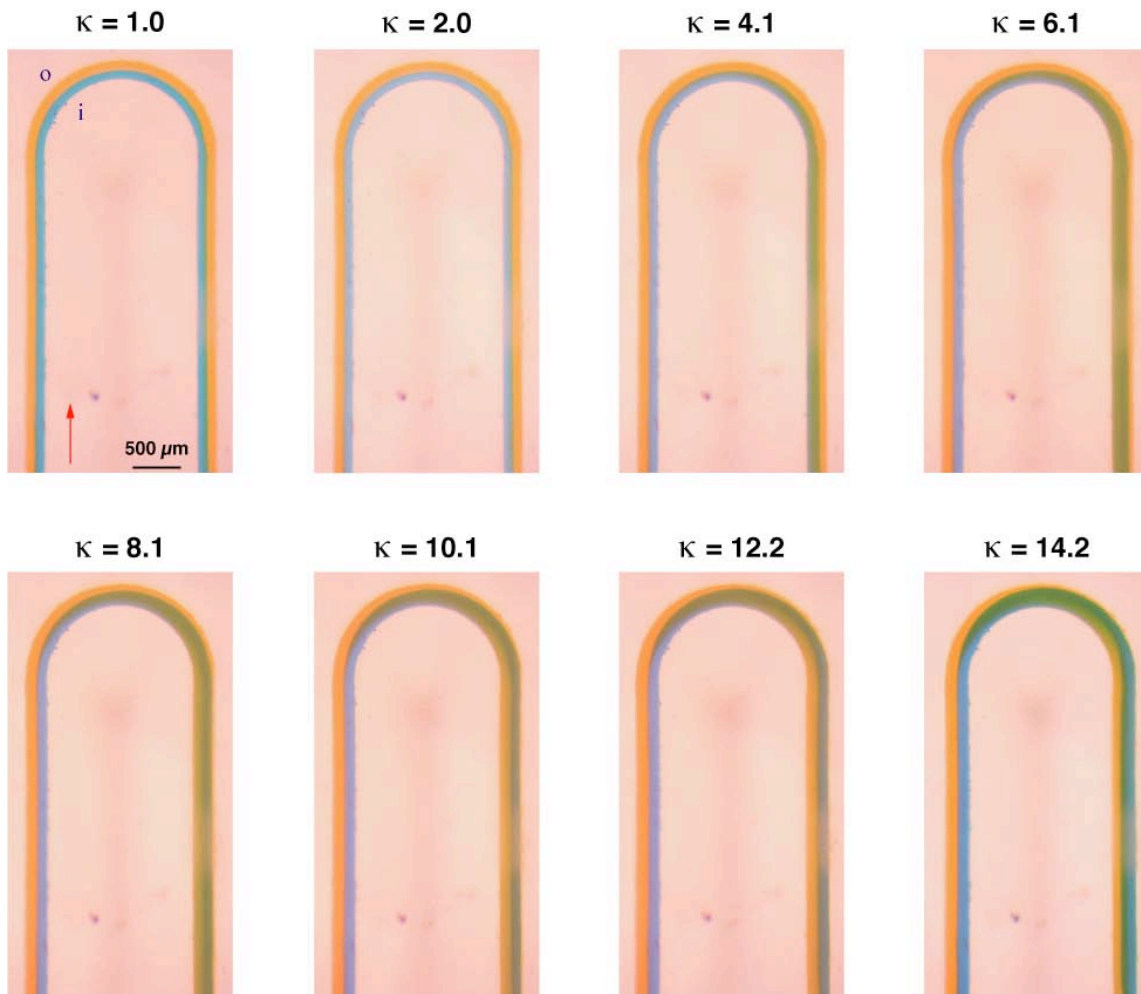


Figure I-23. Top-view imaging of Dean flow in a microchannel. Aqueous streams labeled with blue and yellow food dye in a curved microchannel segment (200 μm wide, 29 μm tall, 630 μm radius of curvature, “i” and “o” denote the inner and outer channel walls) are imaged at flow rates ranging from $3.6 < Re < 50.9$ ($1.0 < \kappa < 14.2$). At $\kappa = 1.0$ the streams flow in parallel along the entire length. As the flow rate is increased the inner blue stream is transported from the inner to the outer channel wall and beyond $\kappa = 10.1$ it appears that the two streams have effectively switched positions inside the channel.

An additional pair of vortices is known to appear at higher Dean numbers, and recent studies have shown that enhanced micromixing can occur in these flows (Figure I-24).^{85, 86} However, the corresponding Re in these experiments is fairly large ($Re \gg 100$) and outside the range of conditions that are realistically achievable in most microfluidic systems.

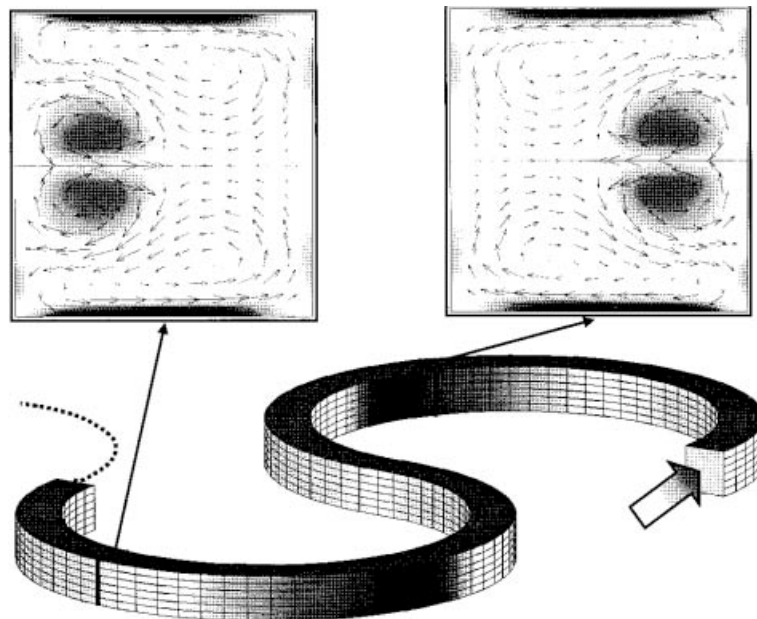


Figure I-24. Dean flow mixing at high flow rates.⁸⁶ Meandering channel showing the presence of a second pair of Dean vortices at flow rates corresponding to $\kappa > 200$.

Dean effects in planar 2-D configurations

Dean effects have been investigated to study mixing in serpentine-like microchannels.^{71, 87, 88} Unfortunately, in these channels that are made up of opposing curved segments, the effects caused by Dean rotation get reversed as the fluids flow from one bend to the other, and this cycle continues along the entire length of the channel. Consequently the interface between the two fluids simply undulates between the channel walls and the little mixing that occurs is attributed to molecular diffusion at the interface between the two streams. One way of overcoming this flow reversal problem is to design a channel in a spiral format such that the transverse secondary flows are sustained over longer distances. Howell *et al.*⁸⁹ have shown this to be possible in large (cross-sectional dimensions > 1 mm) circular channels (Figure I-25) and Vanka *et al.*³⁰ have studied this effect in a spiral channel (793 μm wide and 397 μm tall) at a flow rate corresponding to $Re = 6.8$. In such channels the fluid experiences a reduction in the channel radius of curvature as it flows downstream, accompanied by a corresponding increase in the strength of the transverse secondary flow.⁹⁰ Mengeaud *et al.* performed finite element simulations in a 100 μm wide zigzag microchannel.⁹¹ They found that below a critical $Re \sim 80$, mixing was achieved by molecular diffusion alone. At higher Re , mixing was attributed to recirculation in the laminar flow that induced a transverse component to the flow velocity. Table I-2 provides some recent examples of work involving secondary flow effects in planar microchannel configurations.

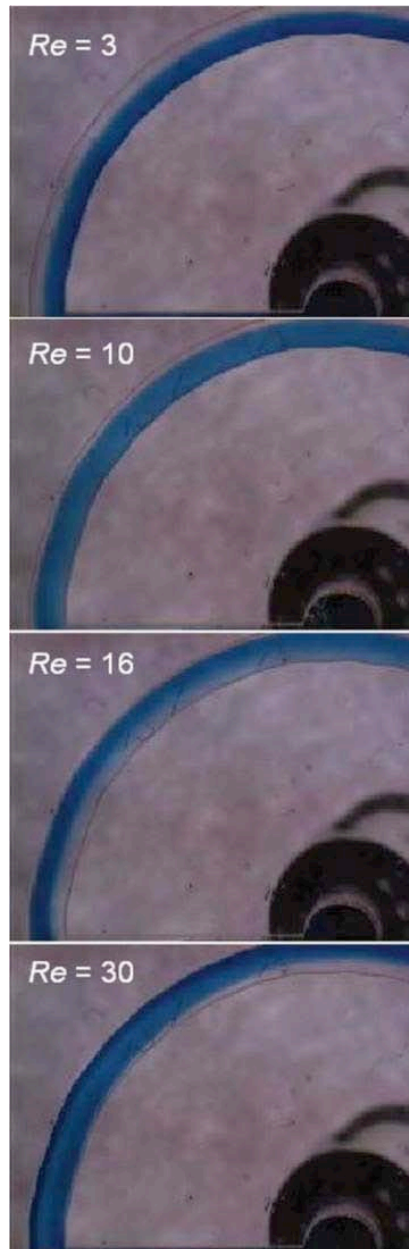


Figure I-25. Dean effects in a circular microchannel. The channel has a cross-section of $1.27 \text{ mm} \times 1.27 \text{ mm}$ and a uniform radius of curvature of 5 mm . Transverse secondary flows are effective from $Re = 10$. Howell, P. B.; Mott, D. R.; Golden, J. P.; Ligler, F. S., Design and evaluation of a Dean-vortex based micromixer, *Lab Chip* 2004, 4, 663-669 – Reproduced by permission of The Royal Society of Chemistry.

Table I-2. Examples of work involving secondary flows in planar microchannels.

Source	Design	Dimensions ^a	Flow rate	Result
Liu <i>et al.</i> ⁶³	Square-wave	w = 300 μm h = 150 μm	$Re = 6 - 140$	Chaotic advection: $Re > 70$
Mengeaud <i>et al.</i> ⁹¹	Zig-zag	w = 100 μm h = 48 μm	$Re = 1 - 800$	Laminar recirculations: $Re > \sim 80$
Yi <i>et al.</i> ⁸⁰	Square bends		$Re = 1 - 80$	Secondary flow effectiveness: $Re > 10$
Therriault <i>et al.</i> ⁷¹	Serpentine	d = 150 μm R = 500 μm	$Re = 0.15 - 70$ $\kappa = 0.08 - 38.3^b$	Linear dependence on effectiveness: $Re > 10$
Yamaguchi <i>et al.</i> ⁸⁸	Serpentine	w = 210 μm h = 205 μm R = 500 μm	$Re = 5 - 26^b$ $\kappa = 3.22 - 16.73$	Permanent distortion of interface: $Re = 26$
Vanka <i>et al.</i> ³⁰	Spiral Concentric	w = 793 μm h = 397 μm Max. R = 9.398 mm R = 6.096, 4.826, 3.556 mm	$Re = 6.8$ $\kappa = 1.98 - 13.8$ $\kappa = 2.4 - 3.2$	Significantly better mixing than straight channel geometries at $Re = 6.8$
Vanka <i>et al.</i> ⁹⁰	Curved duct		$Re = 0.1 - 10$	Enhanced mixing at $Re > 10$ for $Sc = 1000$
Howell <i>et al.</i> ⁸⁹	Circular (Figure 4)	w = 1.27 mm h = 1.27 mm R = 5 mm	$Re = 3 - 30$ $\kappa = 1.5 - 15.1^b$	Onset of secondary flow: $Re > 10$
Schönfeld <i>et al.</i> ⁸⁶	Meandering	w = 0.2 mm R = 1.0 mm	$Re = 2 - 2012$ $\kappa = 1 - 900$	Additional pair of vortices: $\kappa > 200$
Jiang <i>et al.</i> ⁸⁵	Meandering (Figure 8)	w = 1 mm h = 1 mm	$\kappa = 35 - 351$	Additional vortex pair: $\kappa > 140$

^a w = width; h = height; d = diameter; R = radius of curvature.

^b The hydraulic diameter was calculated from given dimensions and then used to compute Re and κ for aqueous systems.

Summary and motivation

In a majority of micromixer designs, efficiency is characterized by the introduction of two parallel liquid streams and observing the minimum distance over which they become intermixed. Upon closer inspection, however, it is also evident that the process of evaluating and drawing comparisons between performances of different designs is less than straightforward. For example, different research groups employ different experimental techniques to determine when the fluid streams become mixed. These experiments range from observing color changes at the interface between streams of different dyes to introducing reagents (e.g. phenolphthalein and sodium hydroxide) that react to form a visible interfacial front between streams. In addition to these “top view” measurement techniques, some groups have employed confocal microscopy in order to image cross sectional slices of the flow field. The situation becomes even more complex when this variety of experimental characterization techniques is further combined with the use of different working fluids and different data analysis algorithms (Tables I-3 and I-4). This lack of a common set of experimental and analysis protocols makes it nearly impossible to meaningfully compare different designs. However this is precisely the data needed in order to develop advanced mixers to satisfy the demands of future miniaturized analysis systems. An equally important factor that is often overlooked is the ease with which a particular design can be fabricated. Many of the mixer designs so far incorporate complex 3-D structures that, from a practical standpoint, are difficult or impossible to fabricate in a manner consistent with processes used to construct standard lab-on-a-chip components. The need to incorporate

specialized processes and/or precise multilayer alignment steps makes these approaches far less attractive from both economic and process integration perspectives. Some of them even require timescales on the order of hours to days to construct.

Table I-3. Summary of techniques used to image and characterize mixing.

Source	Fluid system	Dye/indicator	Imaging	Intensity
Liu <i>et al.</i> ⁶³	Ethyl alcohol	Phenolphthalein, NaOH pellets	Top view	Normalized
Johnson <i>et al.</i> ⁵⁹	Carbonate buffer	Rhodamine B	Top view	Normalized
Stroock <i>et al.</i> ⁶⁰	Glycerol/water	Fluorescein- labeled polymer	Cross-section	σ
Therriault <i>et al.</i> ⁷¹	Water	Fluorescent red or green	Top view	Normalized
Hong <i>et al.</i> ⁶⁸	Aqueous sodium morpholine propane sulfonate buffer Perfluorodecaline/ C ₆ F ₁₁ C ₂ H ₄ OH	Fluo-4 and CaCl ₂ [Fe(SCN) _x] ^{(3-x)+}	Top view	Color
Kim <i>et al.</i> ⁶²	Ethanol	Phenolphthalein, NaOH, Rhodamine B	Top view	Normalized
Kim <i>et al.</i> ⁷²	Ethanol	Phenolphthalein, NaOH	Top view	Normalized
Park <i>et al.</i> ⁶⁶	Water	Fluorescein	Cross-section	σ

Table I-4. Mixing characterization techniques in planar secondary flow systems.

Source	Fluid system	Dye/indicator	Imaging	Intensity
Liu <i>et al.</i> ⁶³	Ethyl alcohol	Phenolphthalein, NaOH pellets	Top view	Normalized
Mengeaud <i>et al.</i> ⁹¹	Phosphate buffer	Fluorescein	Top	c_{\min}/c_{\max}
Yi <i>et al.</i> ⁸⁰	Water	Dye	Top	
Therriault <i>et al.</i> ⁷¹	Water	Fluorescent red or green	Top	Normalized
Yamaguchi <i>et al.</i> ⁸⁸	Water	Red, green	Top	
Vanka <i>et al.</i> ³⁰	Sucrose solution	Rhodamine 6G	Top ^a	Color
Howell <i>et al.</i> ⁸⁹	Water	Blue food	Top	
Jiang <i>et al.</i> ⁸⁵	Water	NaSCN, Fe(NO ₃) ₃	Top	

^a A software was used to generate cross-sectional intensity profiles.

The motivation behind this work is to overcome many of these limitations associated with the above-mentioned micromixers. Microfluidics is in a desperate need of techniques wherein gentle passive micromixing can be achieved in the shortest possible distances by using simplified microchannels (ideally, planar 2-D smooth-walled) that can be easily constructed (ideally, in a single lithography step) in time scales on the order of minutes. Naturally occurring Dean flow effects that arise in curved conduits offer a tremendous opportunity of building such micromixers and helping microfluidic technology to live up to its expected potential.

Objectives

While current generation micromixing techniques have made useful contributions to the field of microfluidics, many of them require channel geometries that utilize complex fabrication techniques. Although patterning surfaces with intricate features is becoming straightforward, the problem arises when two patterned surfaces need to be aligned, assembled, and bonded with accurate precision. In cases where the bonding is irreversible, the opportunity to realign in case of initial error is nonexistent and many of the fabrication steps have to be repeated. Creating features using specialized techniques (e.g., stereolithography) is not only time consuming but also expensive to perform for most research laboratories. Moreover, such techniques are impractical when the research is still in exploratory or fundamental stages and a number of experiments need to be performed to obtain robust and consistent results. Considering all these factors and looking at the enormous amount of micromixers in literature, both active and passive, there still exists the need to build mixers that achieve gentle passive micromixing in the shortest possible distances by using simplified microchannels (ideally, planar 2-D smooth-walled) that can be easily constructed (ideally, in a single lithography step) in time scales on the order of minutes.

The purpose of this research is to achieve these goals by exploiting and manipulating Dean flows in simple 2-D microchannels that are fabricated in minutes from a single lithography step. With clever variations of channel curvature and width, mixing levels comparable to chaotic mixers are achieved. The following micromixer designs are investigated and characterized:

- Spiral micromixing geometries with spiral sections arrayed along the flow path. Adding more turns to the spiral increases the overall contour length of the channel but keeps the footprint area occupied by the channel at a minimum. Curvature-induced vortices contribute to mixing at high flow rates, while the fairly large channel lengths provide for diffusive mixing at lower flow rates.
- Planar split-and-recombine (P-SAR) curved micromixing geometries in which the main flow channel is split into multiple narrow streams and then realigned at precise locations downstream. By the action of counter-rotating Dean vortices over the entire length of the channel two reagent streams entering the mixer are multiplied and arranged as alternating lamellae so as to increase overall interfacial area for diffusive mixing.
- Asymmetric serpentine mixer (ASM) geometries in which conventional serpentine-like channels are patterned with abrupt expansions at periodic locations. The expansions introduce a vortex system in the horizontal plane which acts in harmony with the pre-existing Dean induced vortex pair in the vertical plane to rapidly mix fluid streams with increasing flow rates.
- *Hybrid* micromixer configurations based on combining distinct mixing elements such as transverse Dean flows, expansion vortex effects or chaotic effects to design micromixers effective over a greatly expanded Re number range than has been previously demonstrated. An example of a straightforward process to improve micromixer efficiency involves implementing a *hybrid* approach, whereby the elements designed in preliminary studies, effective at $Re \geq 1$, will be

combined (either in series or in parallel) with elements effective at $Re \leq 1$. One technique would be to integrate chaotic effects with the basic ASM design by patterning grooved or herringbone structures in the floor of the channel. Another technique involves combination of efficiencies of the spiral and ASM designs such that rapid micromixing can be achieved at a wide range of Re in a channel structure constructed from a single lithography step.

CHAPTER II

EXPERIMENTAL PROCEDURES*

This chapter details all the experimentation techniques used in this research. The fabrication techniques are simple and do not require specialized equipment and laboratory techniques. The procedures can be easily performed in any research laboratory. Flow experiments were carried out using a standard syringe pump and both top-view and cross-sectional imaging techniques were obtained. The extent of mixing was quantified from these images by simple and straightforward methods.

Design and photomasks

All the microchannels in this work were designed using Adobe Illustrator 10 (Adobe Systems Incorporated; San Jose, CA) and then printed on transparency films with a 3,166 dpi printer (Mika Color; Los Angeles, CA) to produce clear-field photomasks. Features as small as 25 μm with minimal distortion on transparency films have been resolved by using a 5,080 dpi printer.⁹² Channels designed in this work employ a minimum width of 80 μm that can be routinely resolved with almost negligible distortion using the 3,166 dpi printer.

* Some of the figures used in this chapter are reprinted with permission from:

1. Printed circuit technology for fabrication of plastic-based microfluidic devices by Sudarsan, A.P.; Ugaz, V. M., *Anal. Chem.* **2004**, *76*, 3229-3235. © 2004 American Chemical Society.
2. Thermoplastic elastomer gels: an advanced substrate for microfluidic chemical analysis systems by Sudarsan, A. P.; Wang, J.; Ugaz, V. M. *Anal. Chem.* **2005**, *77*, 5167-5173. © 2005 American Chemical Society.

Master mold fabrication using printed-circuit technology

Master molds incorporating microchannel structures were fabricated using a previously reported method involving printed circuit technology (Figure II-1).⁹³ Printed circuit boards (PCB's) were purchased pre-coated with a positive tone photoresist (1-oz copper foil: Circuit Specialists Inc.; Mesa, AZ; 0.5-, 2-, and 4-oz copper foil: Injectorall Electronics Corp.; Bohemia, NY) and exposed to UV illumination through the photomask for 90 s (approximate flux 4.5 mW/cm²) to transfer the pattern onto the PC board. Note that in circuit board nomenclature, copper foil thicknesses are typically specified in units of *oz/ft²*, or more commonly just *oz*, representing the weight of copper foil per square foot of base material. Following exposure, the PC boards were immersed for 90 – 120 s under gentle agitation in a developer solution prepared by mixing 3.5 mL of a 50% w/w aqueous sodium hydroxide solution (Fisher Scientific; Hampton, NH) with 500 mL of deionized (DI) water.

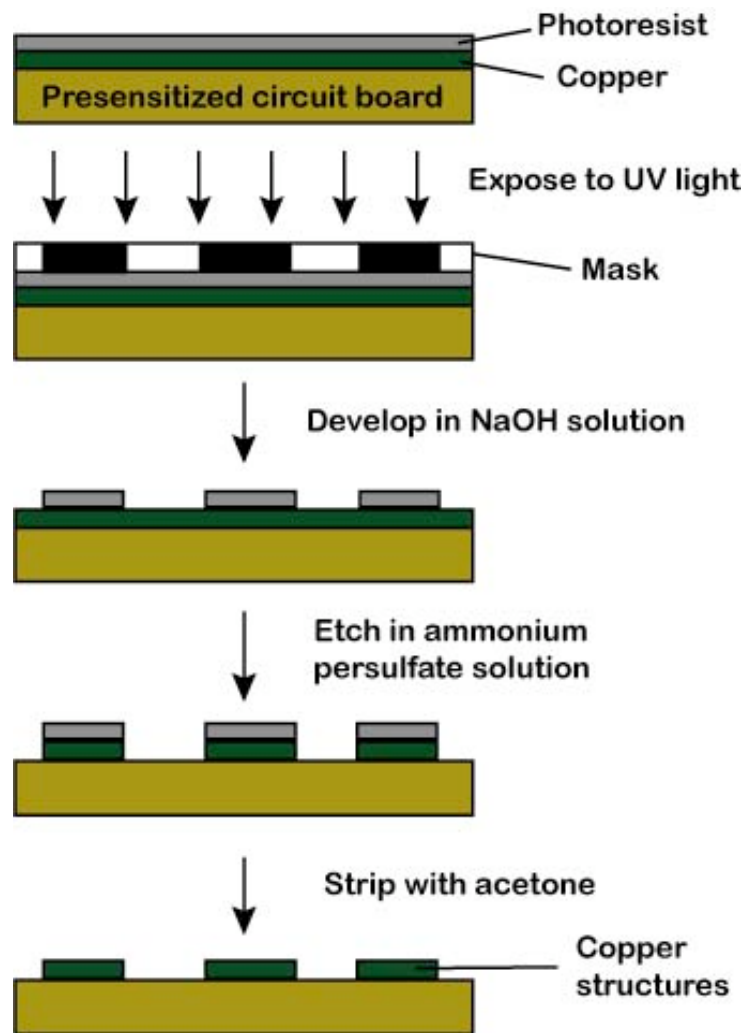
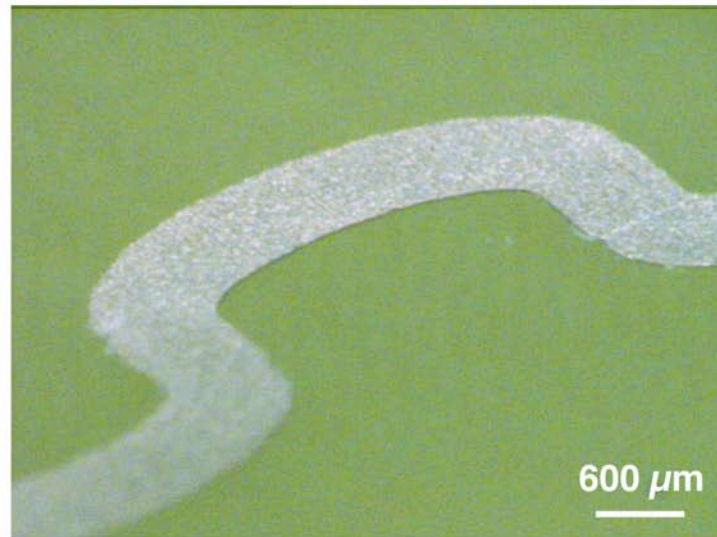


Figure II-1. Overview of the printed-circuit board master fabrication process. The entire process takes about 20 minutes to perform for a 1-oz PC board.

Once the exposed areas were completely developed, the PC board surface was rinsed with DI water. Next, the PC boards were transferred to a vertical glass tank or beaker containing an etching solution prepared by dissolving 150 g of ammonium peroxydisulfate crystals (certified ACS grade; Fisher Scientific; Hampton, NH) in 1 L of DI water to etch away the underlying copper foil in the exposed areas. The etching tank was mounted on a hot plate in order to maintain the solution at a temperature of ~ 45 °C, and a stirrer bar at the bottom of the tank was used to provide continuous agitation. After the etching process was completed, the remaining photoresist masking the channel structures was stripped with acetone from a squirt bottle and the PC boards were rinsed completely once again in DI water. This entire fabrication process can be completed in about 20 minutes for a 1 oz PC board once the transparency photomask is ready. Figure II-2 shows a PC board with an etched copper structure and a typical surface profilometry scan.

a.



b.

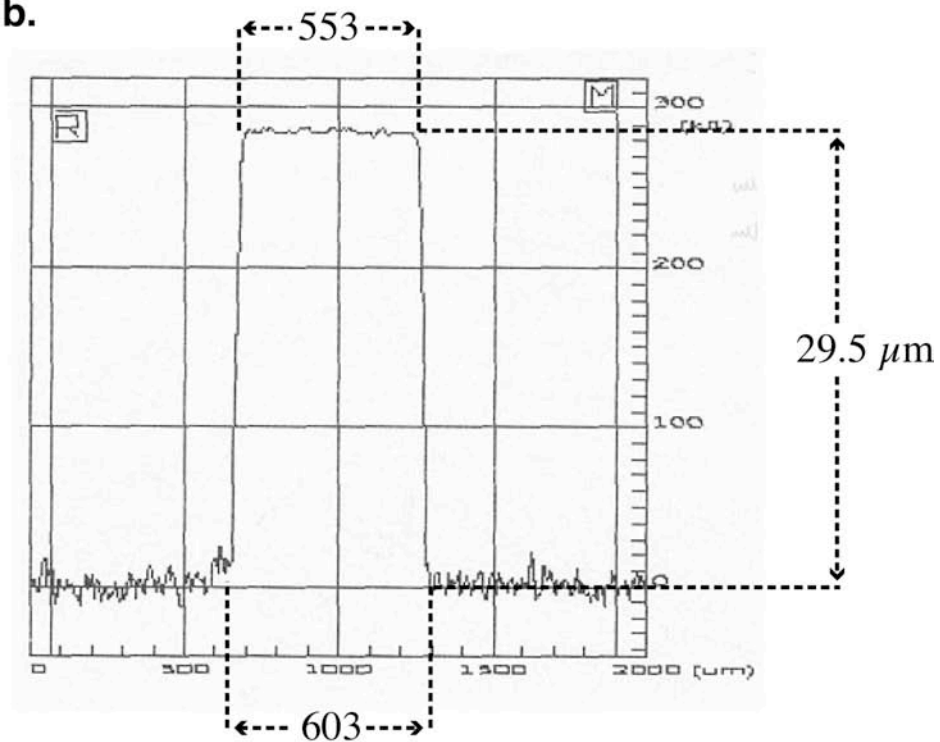


Figure II-2. Profile of etched structures on a PC board. (a) Photograph of a 600 μm wide copper channel on a 1 oz PC board. The image was taken using a Hirox 3-D microscope. (b) Surface profile of a 600 μm wide channel patterned on the surface of a 1-oz PC board.

The dimensions of the channel features on the PC boards were characterized using a stylus profilometer (Dektak 3; Veeco Instruments; Woodbury, NY). Due to the isotropic nature of the etching, channel structures have a trapezoidal cross-sectional profile. For flow measurements, the cross-section was approximated to be circular and the hydraulic diameter

$$d = 4A_C/P \quad (\text{II-1})$$

where A_C is the cross-sectional area and P is the wetted perimeter, was used as the characteristic cross-sectional dimension. The average height of the channel structures (equivalent to the thickness of the copper foil) from a number of 1-oz PC boards was measured to be 29 μm .

Thermoplastic elastomer gels for device fabrication

Thermoplastic elastomer gels were used as the material of construction for making microchannels.⁹⁴ Slabs of elastomers were synthesized by combining commercially available polystyrene–(polyethylene/polybutylene)–polystyrene (SEBS) triblock copolymer resins in hydrocarbon extender oils for which the ethylene/butylenes midblocks are selectively miscible. The thermodynamic incompatibility between blocks induces microphase separations and self-assembly of the insoluble styrenic end blocks into distinct domains with characteristic size scales on the order of 10–20 nm.⁹⁵⁻¹⁰⁷ The soluble midblocks emanating from these nanodomains penetrate into the oil producing arrays of loops (beginning and terminating within a single nanodomain) and bridges (joining adjacent nanodomains) resulting in the formation of a long-range viscoelastic

gel network in which the polystyrene domains act as physical cross-link junctions (Figure II-3). Like PDMS, this gel network is optically transparent, viscoelastic, and biocompatible but also possesses the further advantage of being melt processed at temperatures in the vicinity of 100 °C. Other examples of thermoplastic elastomers used for micromolding include polystyrene–(polyisoprene)–polystyrene¹⁰⁸ (SIS) and polystyrene–(polybutadiene)–polystyrene¹⁰⁹ (SBS) block copolymers.

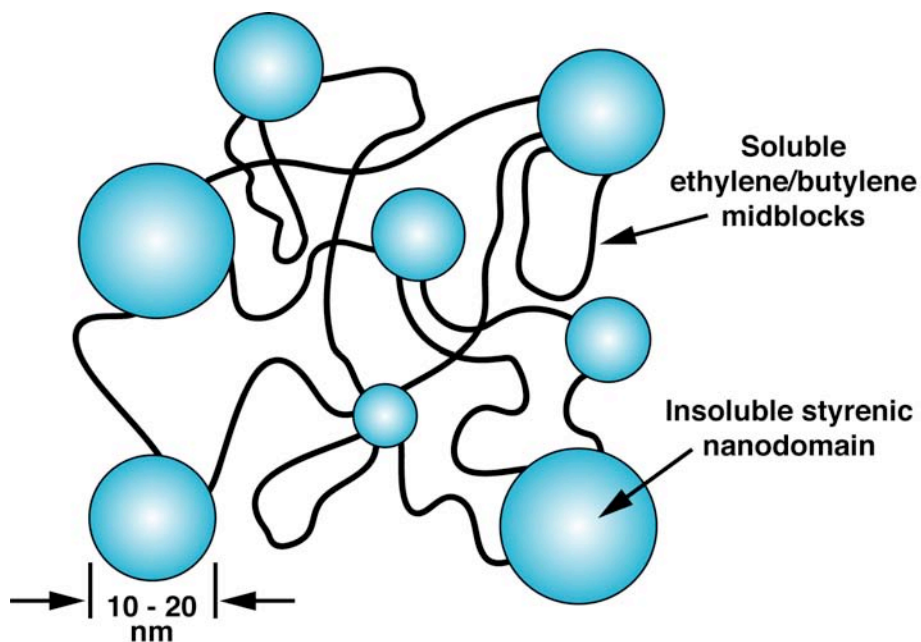


Figure II-3. Gel network formed by microphase separated SEBS triblock copolymers. The immiscible styrene end blocks associate into nanodomains that act as physical cross-link junctions for the viscoelastic network.

Synthesis

SEBS resins are available as commodity materials (e.g., CP-9000, Kraton-G series), and the gels are typically used in the production of transparent candles¹¹⁰⁻¹¹² and in the health and beauty industries.¹¹³ CP-9000 can be purchased in small amounts from hobby stores or candle suppliers for approximately \$5-7/lb with lower pricing available for larger quantities. Resin (CP-9000 purchased from www.candlefactoryco.com and www.craftlobby.com) and mineral oil (light mineral oil; Fisher Scientific; Hampton, NH) were mixed (33 wt% copolymer) and placed under vacuum overnight at room temperature in order to allow the oil to uniformly coat the resin surface. The mixture was then heated to 170 °C under vacuum for 4 h to allow the resin and oil to intermix and to remove any residual air pockets. Finally, the mixture was cooled to room temperature to form a hardened slab of elastomer.

Microchannel fabrication

The solidify gel was cut into smaller pieces and placed on top of the PC board master mold that had been preheated to 120 °C on a hot plate (Figure II-4). Once the elastomer began to soften, a glass plate was placed on top of the slab and gentle pressure was applied by hand to ensure complete contact with the structures on the PC board master mold. After cooling and release, the solidified gel incorporates the shape of the structures on the master. Fluidic access holes were made using a syringe needle, and the molded slab was thermally bonded to a flat surface of the elastomer to form enclosed channel networks (Figure II-5).

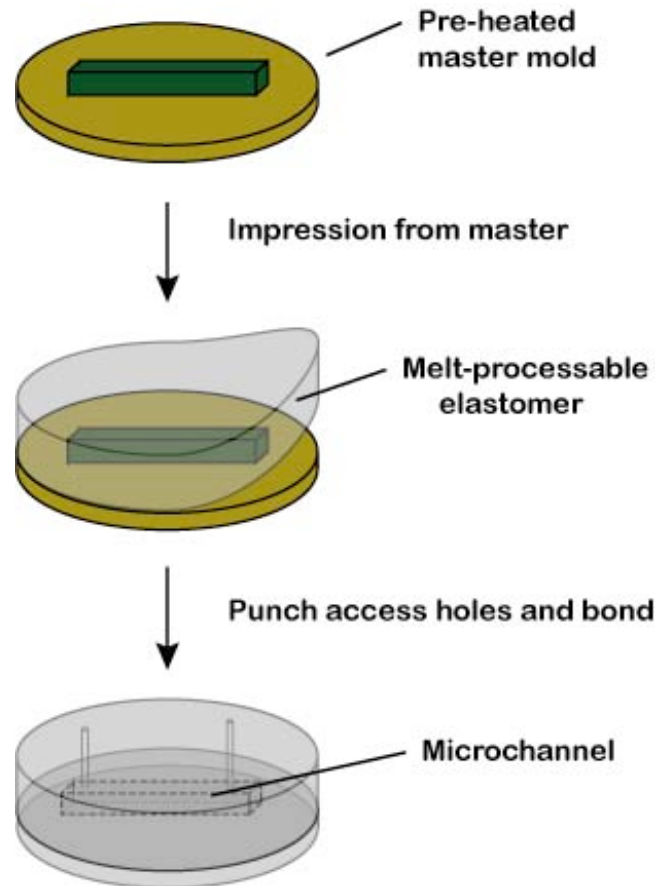


Figure II-4. Soft lithography using thermoplastic elastomer gels. Impressions were taken from PC boards that were pre-heated to 120 °C. The channel making process can be completed in about 5 minutes when using a hot plate for bonding.

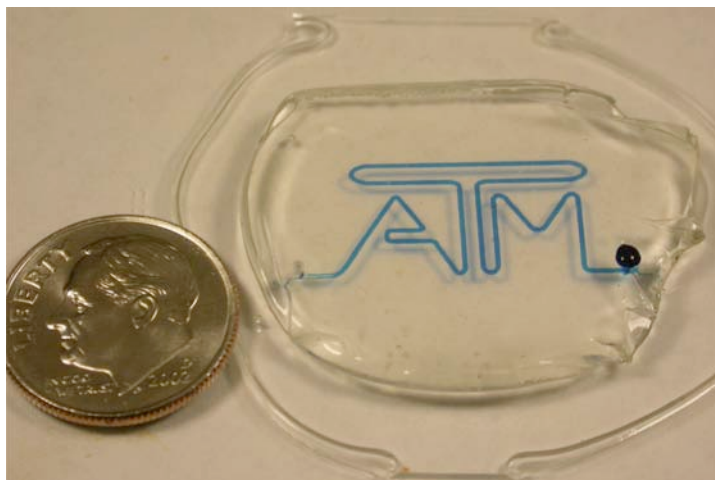


Figure II-5. Microfluidic channel structure constructed from SEBS gels. The channel is molded from a 1-oz PC board and has a cross-section of $400\ \mu\text{m} \times 29.5\ \mu\text{m}$.

The gel material naturally adheres to any smooth elastomer, glass, or plastic surfaces, allowing static or low-pressure fluidic networks to be easily assembled. Additionally, stronger bonds can be achieved either with elastomer or glass surfaces by briefly heating the material at the bond interface to a temperature just below its softening point either by placing the molded slab and the flat layer on a pre-heated hot plate at $120\ ^\circ\text{C}$ for about 10-15 s or by annealing the two surfaces in pre-heated oven at $70\ ^\circ\text{C}$ for about 10 – 15 minutes. A handheld heat gun can also be used for bonding purposes. Bonds to glass surfaces are reversible, while bonds between elastomer layers can be made seamless and essentially permanent. The characteristic trapezoidal profile of channel structures on the PC board as a result of the etching process is evident from cross-sectional SEM images of molded thermoplastic elastomer microchannels (Figure II-6).

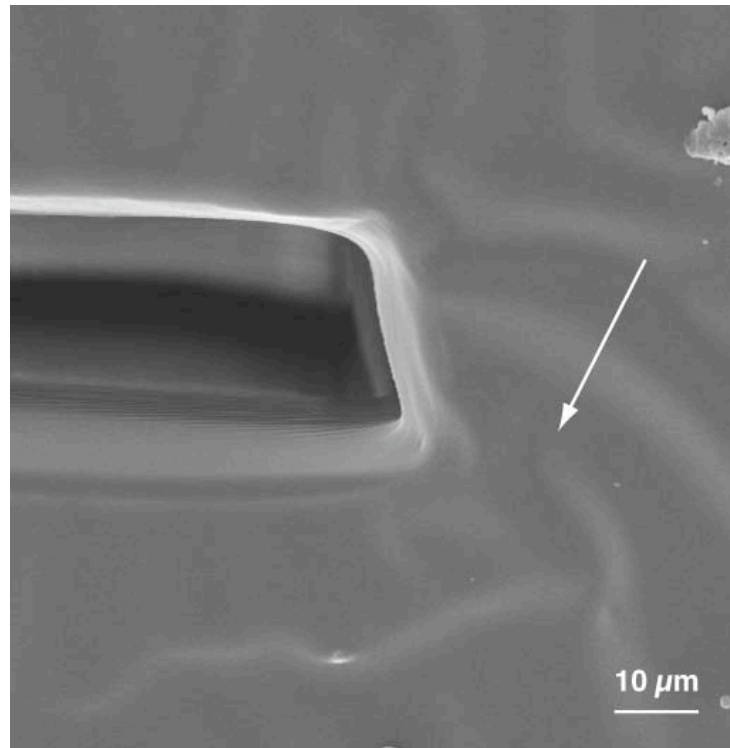


Figure II-6. Cross-sectional SEM image of a bonded microchannel. A scissor-cut was made across the microchannel before imaging using scanning electron microscopy (SEM). The sidewall clearly shows the trapezoidal profile that is replicated from the PC board master mold. The arrow indicates the original position of the bond interface between the two layers, which is essentially seamless upon bonding. The scale bar is 10 μm in length.

Fabrication of complex microstructures

A direct casting procedure can also be used to create complex 3-D structures, whereby an object is embedded in molten elastomer and later released upon cooling (Figure II-7). Another fabrication approach, similar to that reported for PDMS,¹¹⁴ involves directly embedding an entangled collection of fluidic channels within a bulk

elastomer slab by immersing the channels into the molten elastomer. Upon cooling, the channels become seamlessly entrenched in the bulk gel, allowing the fabrication of braided or knotted flow structures (Figure II-8). Selecting a lower wt% gel composition for the bulk material ensures the channels will remain intact during the embedding process.

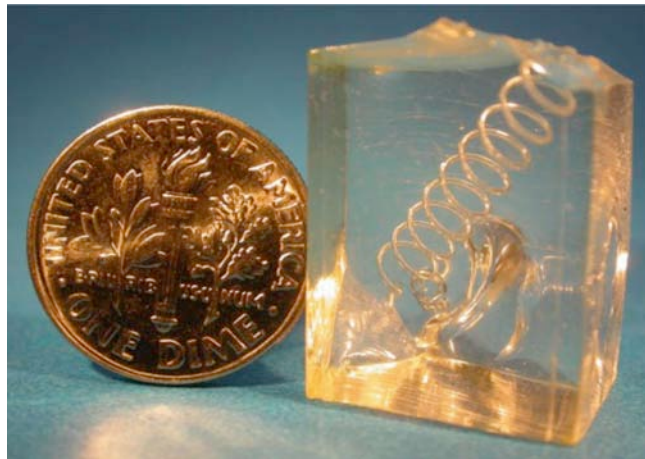


Figure II-7. Direct casting procedure to construct helical 3-D structures. Helical microchannel created by direct casting of a spring with a diameter of 580 μm into molten elastomer and then released from the solidified gel upon cooling.

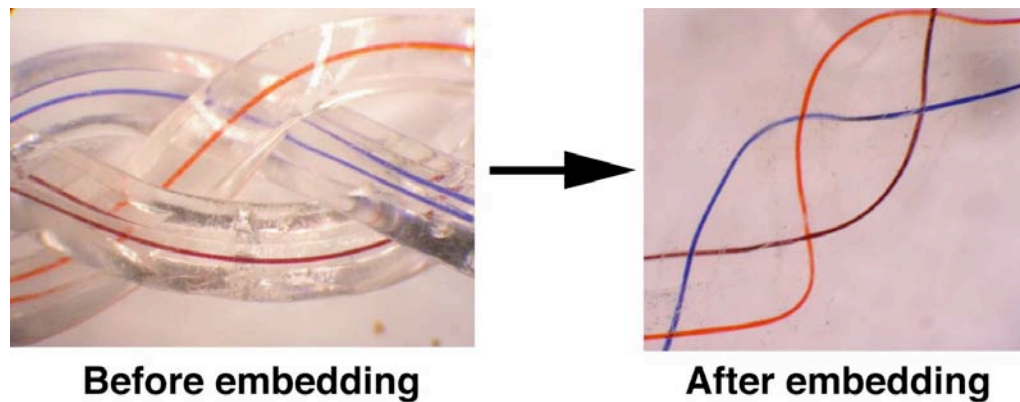


Figure II-8. Fabrication of an entangled bundle of microchannels. Braided microfluidic channel structure constructed by direct casting of 200 μm diameter wires in 33 wt% elastomer gel. Individual channels are cut out, filled with dye, and knotted together before embedding in a 9 wt% elastomer slab.

Multilevel microfluidic structures can be easily fabricated by simply stacking individual patterned layers on top each other (Figure II-9). Any number of layers can be used to build such structures and permanent bonding between layers can be achieved by the annealing process mentioned above. The layers are can be repositioned prior to bonding thereby allowing subsequent layers to be precisely aligned.

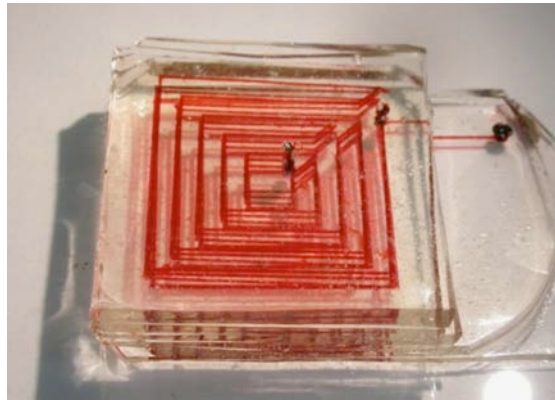


Figure II-9. Fabrication of multilevel microstructures. Five Individual layers of channel networks (400 μm wide and 30 μm tall) are molded from a 1-oz PC board master and stacked on top of each other. The channels are filled with a dye to enable visualization of the interconnected fluidic network.

A tremendous advantage of using elastomer gel substrates is that, unlike PDMS, multiple impressions can be made against different masters to easily and rapidly construct complex microchannel geometries incorporating multiple-height features within the same fluidic network. After an initial impression is made using the first master, any number of subsequent impressions can be made in the same elastomer slab using different masters containing features with distinct heights and/or shapes (Figure II-10). Techniques to create multilevel structures in PDMS are less straightforward and usually require multiple steps of spin coating photoresist and exposure through a series of photomasks.¹¹⁴ If the channels are misaligned after exposure the entire process has to be repeated, whereas, in using thermoplastic elastomers against PC board master molds, impressions are made only after ensuring precise alignment.

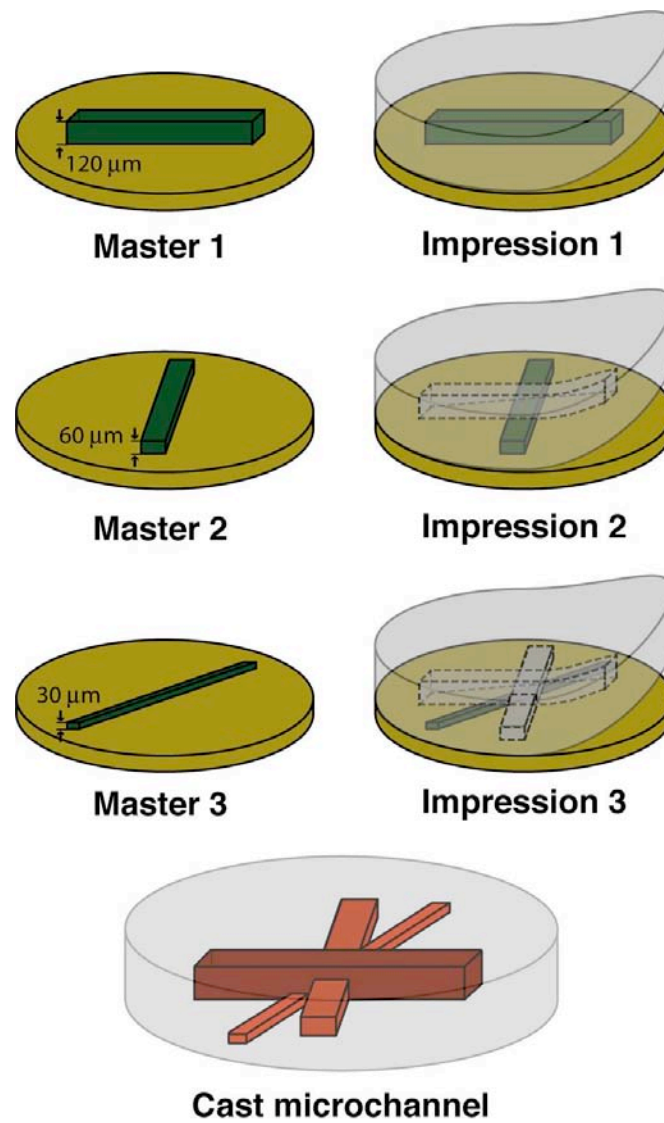


Figure II-10. Procedure used to generate multi-height channel structures.

Maintaining the master mold temperature at a level well below the point where bulk flow of the elastomer occurs ensures that subsequent impressions will not distort

the previously patterned structures. This procedure can be used to generate channel networks consisting of intersecting and/or non-intersecting channels of varying height (Figure II-11), as well as more complex structures containing multi-height ridges or grooves on the top and/or bottom surfaces of the channel (similar to patterns employed for generating chaotic mixing patterns⁶⁰) (Figure I-12). Substrate alignment can be done prior to heating the master mold to ensure accurate pattern registry with each impression. The simplicity with which these multi-height channel structures can be fabricated using SEBS elastomer gels is a unique quality not readily available in conventional soft lithography substrates like PDMS.

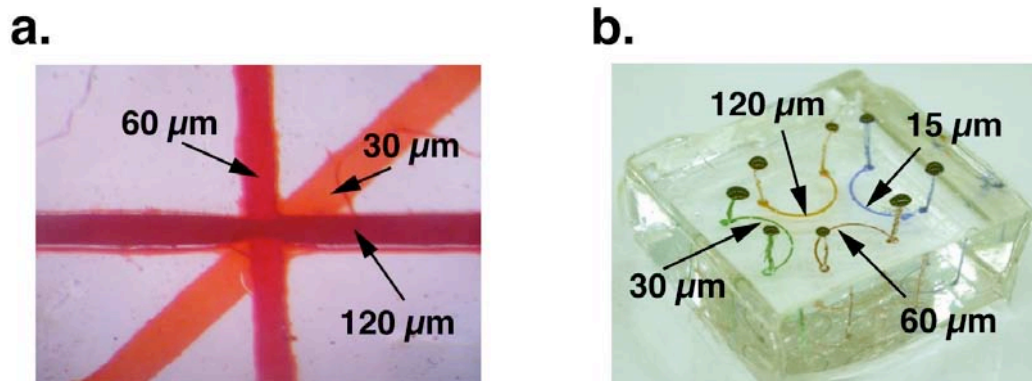


Figure II-11. Examples of variable height features. (a) Microfluidic junction formed by intersecting channels of three different heights (30, 60, and 120 μm; as indicated on figure). Channel cross-sectional dimensions are as follows: horizontal 300 μm × 120 μm; vertical 200 μm × 60 μm; diagonal 400 μm × 30 μm. (b) Four nonintersecting semicircular 250 μm wide channels of different heights (15, 30, 60, and 120 μm; as indicated on figure).

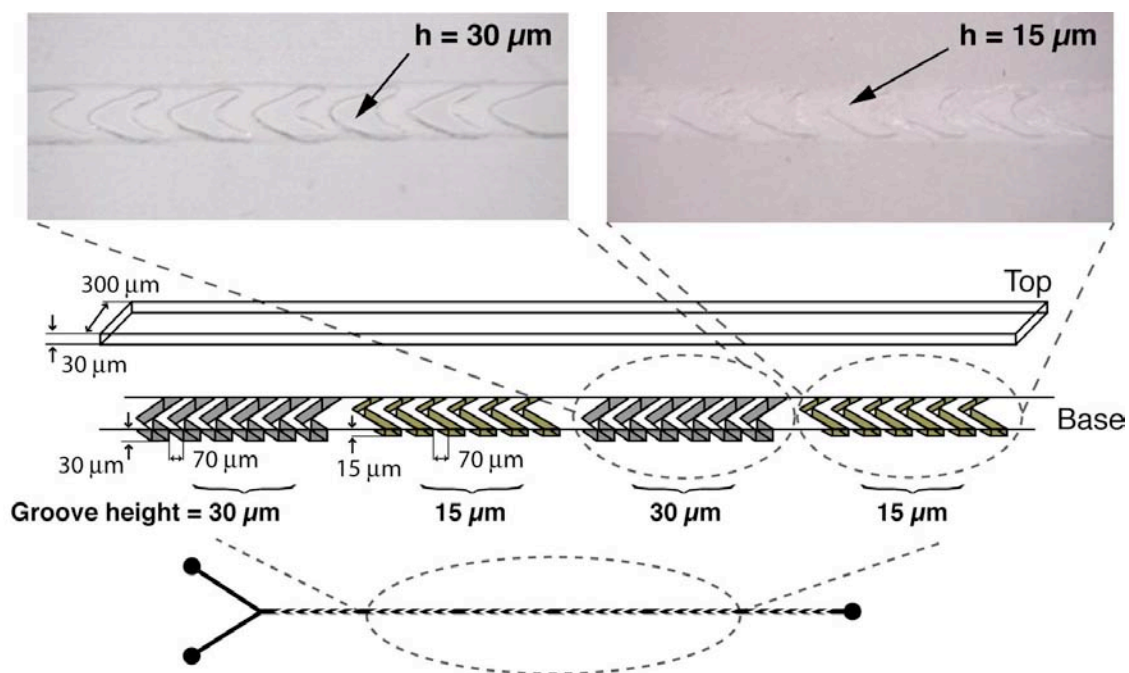


Figure II-12. Fabrication of multi-height structures with herringbone patterns. Multiheight herringbone channel structure incorporating a series of alternating 15 μm and 30 μm tall grooved structures bonded with a 300 μm wide by 30 μm tall top channel.

Solvent compatibility

Solvent compatibility of SEBS gels was characterized by measuring swelling ratios of elastomer samples after immersion in different solvents at room temperature, similar to procedures previously employed for PDMS.¹¹⁵ Dimensions of rectangular pieces were measured using precision calipers and placed in the solvents for 24 h, after which their lengths were measured again while still in the solvent. Swelling ratios were determined as the ratio of the final to initial lengths. Measurements were made from

five separate pieces and then averaged to compute the final swelling ratio. These results (Table II-1) indicate that SEBS gels are compatible with a wide range of solvents.

Table II-1. Swelling ratios for SEBS gels ranging from 9 – 33 wt% copolymer.

Solvent	Swelling ratio
Acetone	1.02 – 1.15
2-propanol	0.86 – 0.94
Methanol	1.00
Ethanol	1.00
Water	1.00
Sodium hydroxide solution (aq. 50% w/w)	1.02 – 1.07
Sulfuric acid	1.00*
Toluene	Incompatible
Chloroform	Incompatible

* Only 33 wt% gel composition was tested.

Biocompatibility

Biocompatibility of SEBS elastomer materials was tested by performing an *Eco* RI restriction digestion reaction on a lambda phage DNA target. The experiment was performed by first preparing a 100 μ L master mix containing 48 μ L DDH₂O, 10 μ L 10x NEBuffer, 40 μ L lambda phage DNA (500 μ g/mL), and 2 μ L *Eco* RI (20 U/ μ L). Enzyme, buffer, and DNA were obtained from New England BioLabs (Ipswich, MA). 20 μ L aliquots were placed in 0.2 mL reaction tubes whose inner surface was coated with 23 wt% elastomer. A parallel reaction in an uncoated tube was performed as a control. The tubes were then incubated at 37 °C in a thermocycler for one hour. Products were heated to 65 °C for 10 minutes prior to analysis by electrophoresis with a 1 kb sizing ladder (Bio-Rad Inc.; Hercules, CA) on a 0.5 % agarose gel (1 μ L product volume loaded in each lane; running conditions: 60 Volts for one hour). Bands were visualized by post-staining the gel with SYBR-Green 1 (Molecular Probes; Eugene, OR). All five digested bands were visible after 1 h of incubation at 37 °C in both the untreated and elastomer coated tubes, thereby demonstrating a high degree of compatibility with standard biochemical reagents and protocols (Figure II-13).

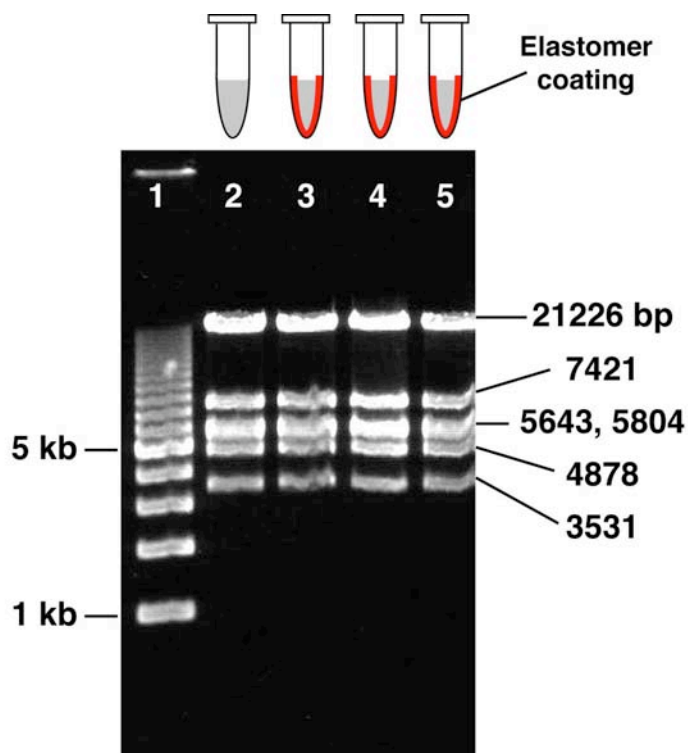


Figure II-13. Biocompatibility of SEBS elastomers. Agarose gel electrophoresis of products from *Eco* RI restriction enzyme digestion of lambda phage DNA performed in reaction tubes coated with 23 wt% elastomer gel. Lane 1: 1 kb sizing ladder, lane 2: control reaction performed in uncoated reaction tube, lanes 3-5: reactions performed in elastomer-coated tubes. The expected fragment sizes are produced in all cases.

SEM sample preparation and imaging

Bonded microchannels from SEBS gels were imaged using Scanning Electron Microscopy (SEM). Cross-sectional profiles were obtained by making a scissor-cut across the channels and then mounted onto 1-inch diameter stub or holder that was coated with silver paint. The samples were positioned firmly on the stub by using

double-sided conductive carbon tape. Since the gel was originally synthesized under vacuum conditions, the samples did not require an additional drying process. The stub was then placed in an enclosed plastic container that contained osmium for about 20 minutes. A beaker containing hot water from the tap was placed on top of the plastic container to assist vaporization of the osmium. The osmium coating procedure was modified from previously employed procedures.^{116, 117} The samples were then sputter coated with a 50%-Au 50%-Pd mixture for 6 minutes using a Hummer I sputter coater (TECHNICS Inc.; Alexandria, VA). The coating was carried out in a vacuum of 200 millitorr and 10 DC milliamperes under automatic mode to form a uniform coating of about 300 Å above the osmium layer. Since the temperature generated in the sputtering chamber is about 60 °C and the osmium coating was first performed to prevent any deformation of the elastomer surfaces during the sputtering process. For gels with higher service temperatures, the osmium coating step can be eliminated and sputtering could be done for 10 minutes under the same conditions mentioned. However, it should be noted that the osmium process is required when specimen sidewalls need to be coated and it also appears that the dual coating procedure with osmium followed by sputtering tends to form a more uniform coat than what is obtained purely by sputtering. The samples were then imaged using an SEM (JEOL JSM – 6400 Scanning Microscope) at a working distance of 48 mm and an accelerating voltage of 15 kV. Samples were magnified 100 – 800 times its original size depending on the amount of detail required. Figure II-14 shows SEM images of microchannels molded from thermoplastic elastomer gels before and after bonding.

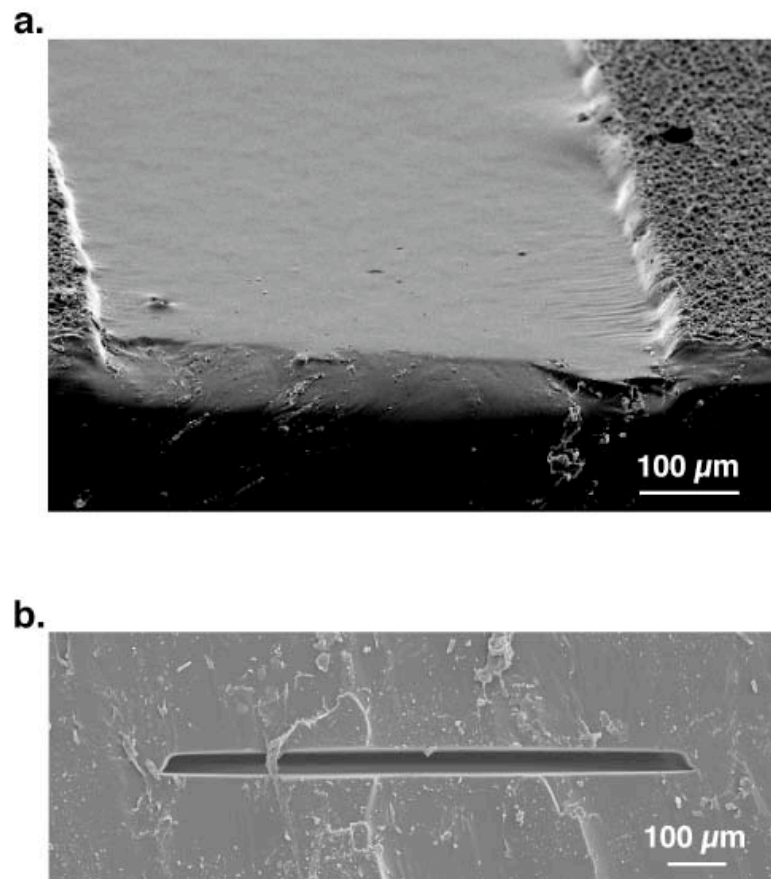


Figure II-14. SEM images of channels before and after bonding. (a) Image of a 600 μm wide by 29 μm tall microchannel before bonding. The inherent surface roughness on the surface of the PC board is clearly reproduced on the surface of the elastomer as seen on either side of the channel. (B) Image of a 1000 μm wide by 29 μm tall microchannel after bonding.

Flow visualization and mixing characterization

All flow and mixing experiments were performed using aqueous systems. Two different imaging mechanisms were performed.

Top-view imaging

Digital images of the flow were obtained using a MZ 8 microscope (Leica Microsystems Inc.; Bannockburn, IL) interfaced with a Coolpix 4500 digital camera (Nikon). The interface between the camera and the microscope was achieved using a digital camera C-mount coupler (Thales Optem Inc.; Fairport, NY). This technique was used for imaging parallel aqueous streams labeled with blue and yellow food dyes (Adams Extract; Austin, TX) diluted to 0.01 g/mL of water. Flow rates were controlled using multi-feed syringe pumps either from Harvard Apparatus (Holliston, MA) or KD Scientific Inc. (Holliston, MA). The devices were interfaced with the syringe pump using Teflon tubing (Small Parts Inc.; Miami Lakes, FL). Pipette tips attached to the Teflon tubing were inserted into the fluidic access holes of the devices to complete the flow network. Care was taken to ensure that the outer diameter of the pipette tips was larger than the diameter of the access holes. Due to the relatively soft nature of the thermoplastic elastomer, the pipette tips were forced into the access holes to make a hermetically sealed connection. Figure II-15 shows the setup that was used.



Figure II-15. Top-view imaging setup.

The extent of mixing in the microchannels was determined by the amount of green color that was generated when the blue and yellow streams mixed at the interface. The digital images were imported into Adobe Photoshop (Adobe Systems Inc., San Jose, CA) where the green color was filtered out and the images were converted to gray-scale and inverted (Figure II-16). Mixing intensity was then calculated using the following equation:

$$\text{Mixing Intensity} = \frac{\text{Width of Mixed Interface}}{\text{Width of Channel}} \quad (\text{II-2})$$

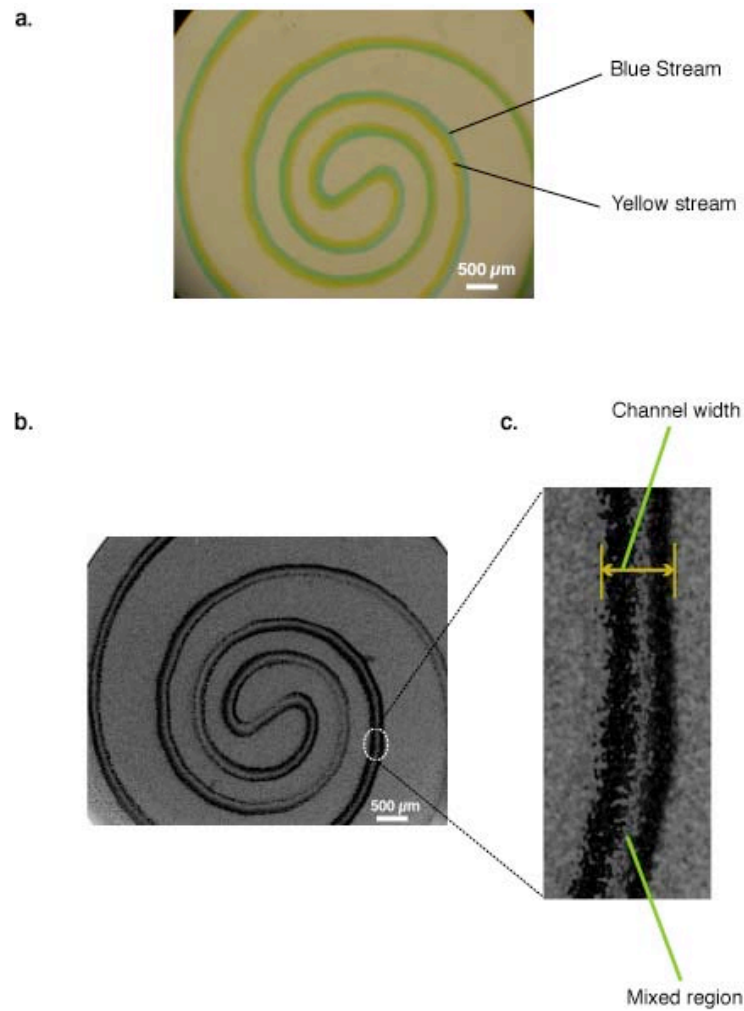


Figure II-16. Image processing using the top-view technique. (a) Digital image displaying the flow of blue and yellow aqueous streams in a spiral microchannel. (b) Gray-scale image depicting the green mixed interface. (c) Close-up view showing the measurement of the channel width and the width of the mixed interface between the two streams.

Cross-sectional imaging

Cross-sectional images of flow in the microchannels were obtained by using LSM 5 PASCAL (Figure II-17; Carl Zeiss MicroImaging, Inc.; Thornwood, NY) and Leica TCS SP5 (Figure II-18; Leica Microsystems, Inc.; Bannockburn, IL) confocal scanning microscopes. The excitation wavelengths were 543 nm from a He/Ne laser and 488 nm from an Ar laser for the Zeiss and Leica microscopes respectively. In both cases a 40 \times , 0.6 NA objective was used. Flow images of two aqueous streams, one of which was labeled with fluorescent Rhodamine 6G (Sigma-Aldrich; St. Louis, MO), were obtained.



Figure II-17. Cross-sectional imaging using a LSM 5 PASCAL confocal microscope.



Figure II-18. Cross-sectional imaging using a Leica TCS SP5 confocal microscope.

Mixing efficiency was quantified by computing the standard deviation of the intensity distribution over each image by using

$$\sigma = \langle (I - \langle I \rangle)^2 \rangle \quad (\text{II-3})$$

where I is the grayscale value of each pixel (scaled between 0 and 1) and $\langle \cdot \rangle$ denotes an average over all the pixels in the image. Thus, $\sigma = 0.5$ corresponds to two completely unmixed regions while $\sigma = 0$ corresponds to complete mixing. As was the case with the top-view imaging a syringe pump, interfaced with the microchannels using Teflon tubing, was used to control the flow rate in the microchannels. A typical cross-sectional image from confocal laser scanning is shown in Figure II-19.



Figure II-19. Typical cross-sectional image obtained from confocal laser scanning.

Binding experiments

Binding experiments were carried out between two aqueous streams, one containing 50 $\mu\text{g/mL}$ calf thymus DNA (Sigma-Aldrich; St. Louis, MO) and the other containing 2.5 $\mu\text{g/mL}$ ethidium bromide (Maxim Biotech, Inc.; Rockville, MD). Fluorescence in the micromixer was detected using an Olympus SZX-12 fluorescence stereoscope with a mercury arc illumination source and GFP filter set (Olympus America, Inc.; Melville, NY), and imaged using a CCD-300 camera with Geniisys intensifier (DAGE-MTI; Michigan City, IN).

Summary

The main thing to note from this chapter is the ease with which experimental procedures are carried out. By using conventional printed-circuit technology to make master molds, a number of different designs can be etched on the same PC board, allowing for extremely high parallel fabrication capabilities. The melt-processable elastomer allows for devices to be molded in a few minutes. A big advantage is that the resin required to make this elastomer is relatively inexpensive and devices can be used and disposed without having to consider about cost. Additionally, devices could be

cleaned after use and re-melted for future molding. Finally, it is important to mention that the mixer geometries fabricated in this work require a single lithography step and the channels are 2-D smooth-walled. Design to device can be achieved consistently in about thirty minutes to one hour.

CHAPTER III

SPIRAL MICROMIXERS*

In this chapter, we explore the use of compact spiral-shaped flow geometries designed to achieve efficient mixing in a format that can be constructed using a single planar soft lithography step without the need for multilayer alignment. A series of 150 μm wide by 29 μm tall channels were constructed, each of which incorporated a series of spiral shaped sections arrayed along the flow path. Five spiral designs with varying channel lengths were investigated, and mixing studies were carried out at flow rates corresponding to Re ranging from 0.02 to 18.6. Under the right conditions, transverse Dean flows are induced that augment diffusive transport and promote enhanced mixing in considerably shorter downstream distances as compared with conventional planar straight channel designs.

Naturally occurring Dean flows offer a promising approach to overcome many of the limitations associated with micromixing in 2-D planar microchannels. Fluids traveling through curvilinear channels experience an interplay between inertial forces acting to direct axial motion and centrifugal effects acting along the conduit's radius of curvature. Under appropriate conditions, these effects establish a radial pressure gradient whose magnitude can become sufficient to generate a transverse flow field.

* Part of the data reported in this chapter is reprinted with permission from: Fluid mixing in planar spiral microchannels by Sudarsan, A.P.; Ugaz, V. M., *Lab Chip* **2006** 6, 74-82. © 2006 by The Royal Society of Chemistry.

Manipulating the action of this passively generated transverse vortex phenomena makes it possible to design an entirely new class of mixers in planar microchannels. Ultimately, it would be desirable to achieve gentle passive micromixing in the shortest possible downstream distance by using simplified microchannels (ideally, planar 2-D smooth-walled) that can be easily constructed (ideally, in a single lithography step) without the need for complex and specialized instrumentation and techniques.

Initial work with Dean effects has involved investigation of mixing in serpentine-like microchannels.^{71, 87, 88} Unfortunately, in these channels that are made up of opposing curved segments, the effects caused by Dean rotation are mostly reversed as the fluids flow from one bend to the other, and this cycle continues along the entire length of the channel (Figure III-1). Consequently the interface between the two fluids simply undulates between the channel walls and the little mixing that occurs is attributed to diffusion at the interface between the two fluids. One way of overcoming this flow reversal problem is to design a channel in a coiled or spiral format such that the transverse secondary flows are sustained over longer distances.

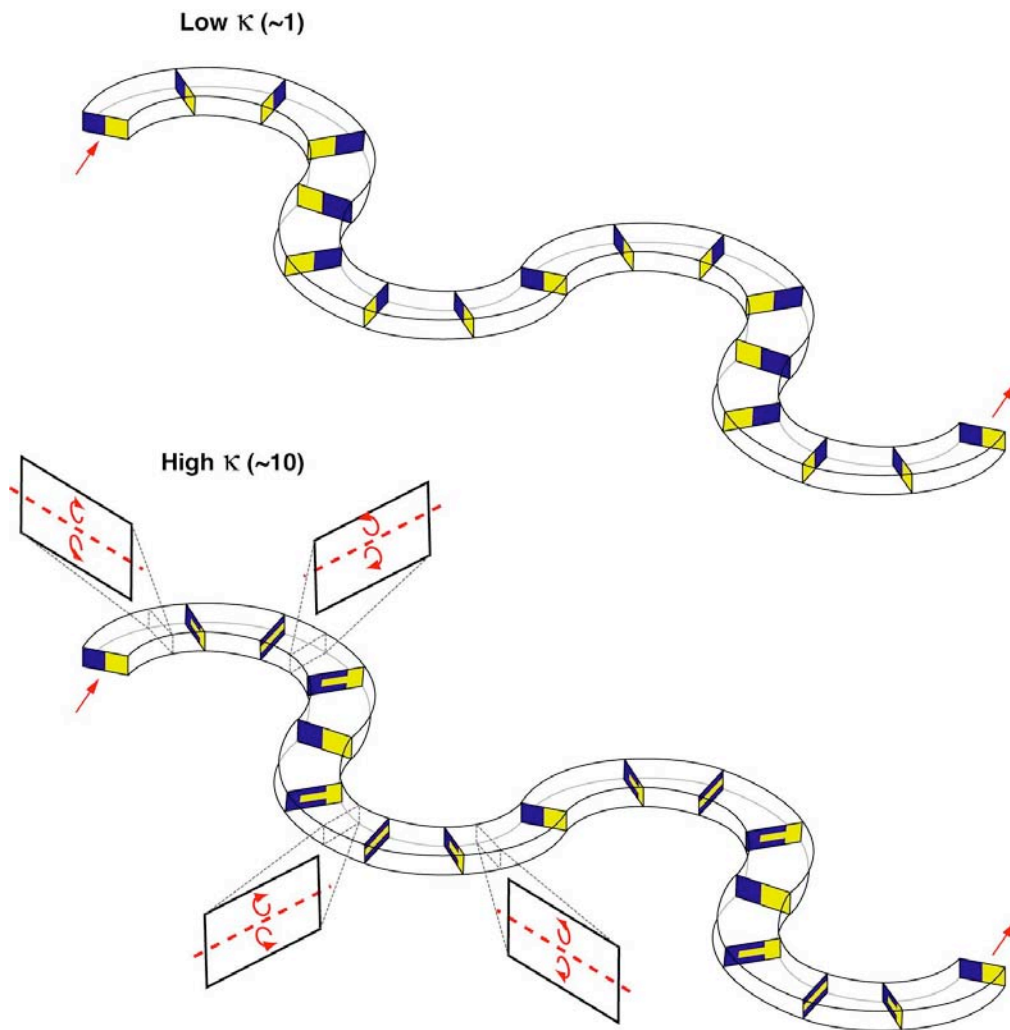


Figure III-1. Idealized Dean flow phenomena in a serpentine microchannel. At low κ (above), two parallel streams of different species (yellow and blue) entering a curved microchannel segment experience unperturbed laminar flow. At $\kappa \sim 10$ (below), the transverse flow generated by the counter-rotating Dean vortices transport the inner (yellow) stream toward the outer wall while the outer (blue) stream is pulled inward causing the positions of each species to be transposed at the end of each semi-circular arc causing the interface between the two fluids to undulate between the channel walls and the little mixing that occurs is attributed to diffusion at the interface between the two fluids.

Concept

Spiral-shaped microchannels offer the advantage of being able to sustain the direction of transverse Dean rotation over longer periods of time. The effect of reverse transverse rotation that is prevalent in serpentine geometries can be significantly reduced. Moreover, the coiled geometry required to build these microchannels occupies fairly little footprint area when incorporated into lab-on-a-chip microsystems. In such channels the fluid experiences a reduction in the channel radius of curvature as it flows downstream, accompanied by a corresponding increase in the strength of the transverse secondary flow.

Design

A variety of spiral channels were designed, each incorporating three individual *spiral mixing sections* connected in series. Each section was composed of an inlet and outlet spiral connected by a central 'S'-section of length 1.0 mm (Figure III-2). The inlet and outlet spirals were designed by joining circular arcs whose radius of curvature decayed by 80% every 90°.

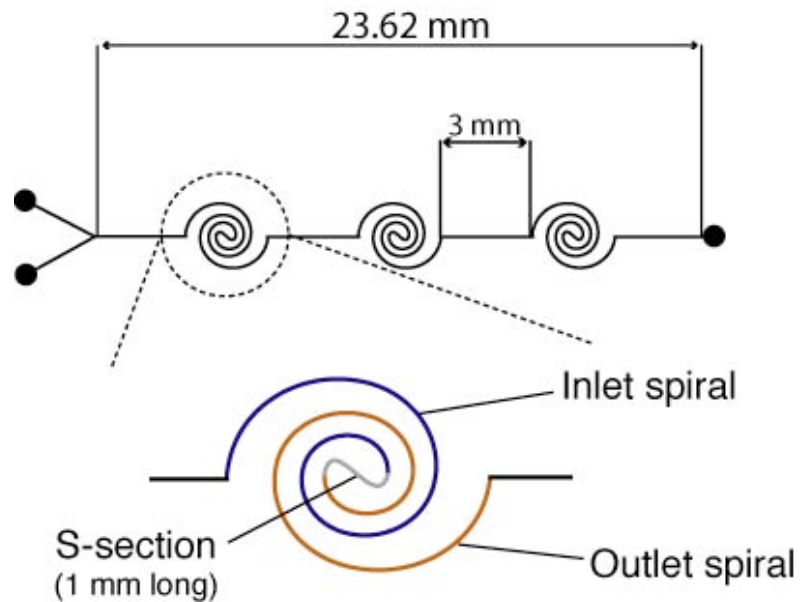


Figure III-2. Schematic of the spiral network incorporating three mixing sections. Each section consists of an inlet and outlet spiral joined by a central ‘S’-section.

The longest arc had a radius of curvature of 3.1 mm and the shortest arc had a radius of curvature 420 μm . Spiral sections of five different lengths were designed; the longest incorporated ten arcs on each spiral and the shortest section had two arcs on each spiral (Table III-1).

Table III-1. Dimensions of the five different spiral channel designs investigated.

All quantities are measured in units of mm.

Spiral design	Arcs on spiral	Max. radius of curvature	Length of inlet/outlet spiral	Length of mixing section	Footprint of mixing section
1	2	0.52	1.47	3.97	1.2 × 1.0
2	4	0.81	3.77	8.57	1.7 × 1.5
3	6	1.27	7.35	15.73	2.9 × 2.3
4	8	1.98	12.96	26.95	4.4 × 3.6
5	10	3.10	21.73	44.49	6.9 × 5.5

All channels are 29 μm tall

Individual spiral sections were connected by straight segments of length 3.0 mm. All spiral channels were 150 μm wide and 29 μm tall. Due to the isotropic nature of the copper etching used to create the PC board master molds, channel structures have a trapezoidal cross-section profile. The hydraulic diameter of the channel is calculated to be 49 μm and is taken as the characteristic cross-sectional dimension. Figure III-3 shows the Dean numbers along the spiral contours for $Re = 0.19$ to 18.6. As the radius of curvature decreases, the Dean number increases due to a corresponding increase in the value of δ .

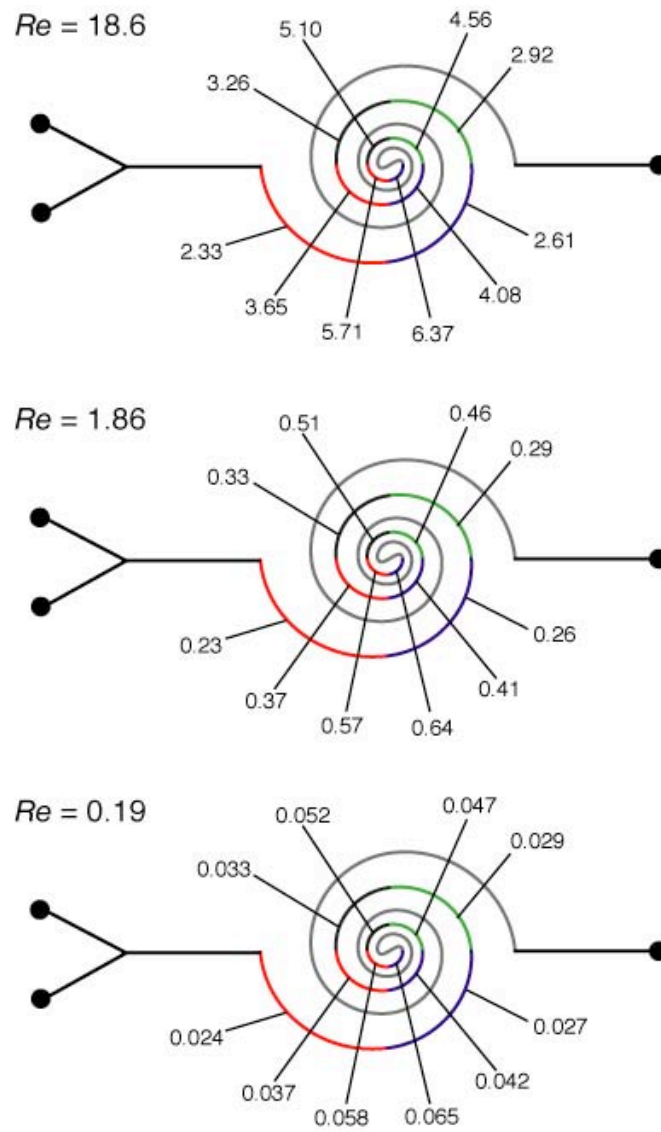


Figure III-3. Dean number along the spiral contour at different Re .

Flow visualization

In conventional planar straight microchannel geometries, any mixing that occurs is purely by diffusion. In curved channels, transverse secondary Dean flows arise as a result of the interplay between inertial and centrifugal forces. By designing curved channels in spiral formats, the strength of these secondary flows increases as the fluid travels from the outer to the inner regions of the spiral path where the radius of curvature is smallest. Moreover, the direction of rotation of the secondary flows is sustained over the entire length of the spiral, as compared to designs incorporating alternating segments of opposing curvature (e.g., serpentine channels). At low flow rates ($Re < 1$), the strength of these secondary flows is not sufficient to significantly perturb the laminar flow profile, and mixing between two parallel streams is primarily by diffusion. Nevertheless, since these channels are in a spiral format, the necessary length required to achieve appreciable levels of mixing by diffusion can be increased, while at the same time keeping the overall footprint of the channel at a minimum (see Table IV-1). With increasing flow rate ($Re > 1$), the secondary flows become stronger and greatly increase the extent of mixing. Thus, spiral geometries offer advantages under both low and high flow rate conditions.

The first channel design we tested consisted of spiral sections made of two up of two arcs in each of the inlet and outlet spirals, with the longer arc having a 520 μm radius of curvature. Figure III-4 shows the mixing intensity for this channel at flow rates corresponding to $Re = 0.02 - 18.6$, as compared with straight channels of the same length. At the lowest flow rate, mixing levels of up to 80% can be achieved in under 19

mm. At the highest flow rate investigated, mixing levels of 90% can be achieved at the same distance. Unlike straight channels, the mixing length becomes shorter with increasing Re , as expected based on the fact that the Dean number (and hence the strength of the secondary flow promoting mixing) is directly proportional to Re .

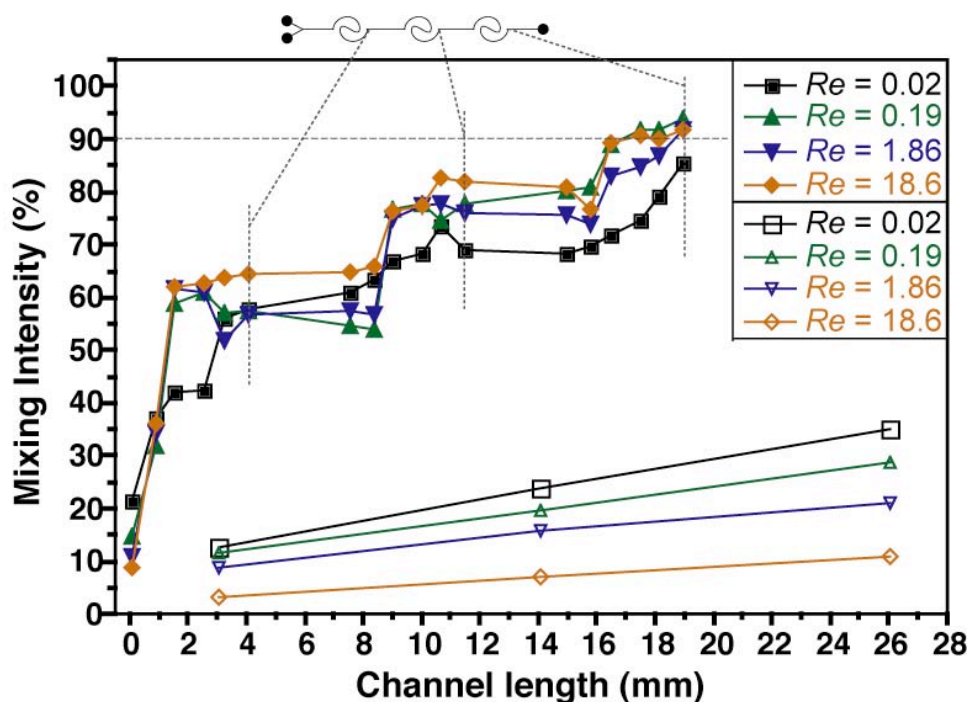


Figure III-4. Mixing intensity comparison between a spiral and straight channel. Mixing intensity within a two-arc, three-section spiral channel as a function of Re (filled symbols). The mixing intensity for a straight channel of equal length is also shown for comparison (open symbols).

By increasing the length of individual spiral contours, higher levels of mixing can be achieved within the first spiral section (Figure III-5). The increased length not only provides a longer time for diffusion at slow flow rates, but also helps in sustaining the transverse secondary flow. The strength of the transverse secondary flows is at a maximum in the arcs with the smallest radius of curvature (i.e., in the central region of the spiral), and hence at higher flow rates most mixing is expected to occur in these segments.

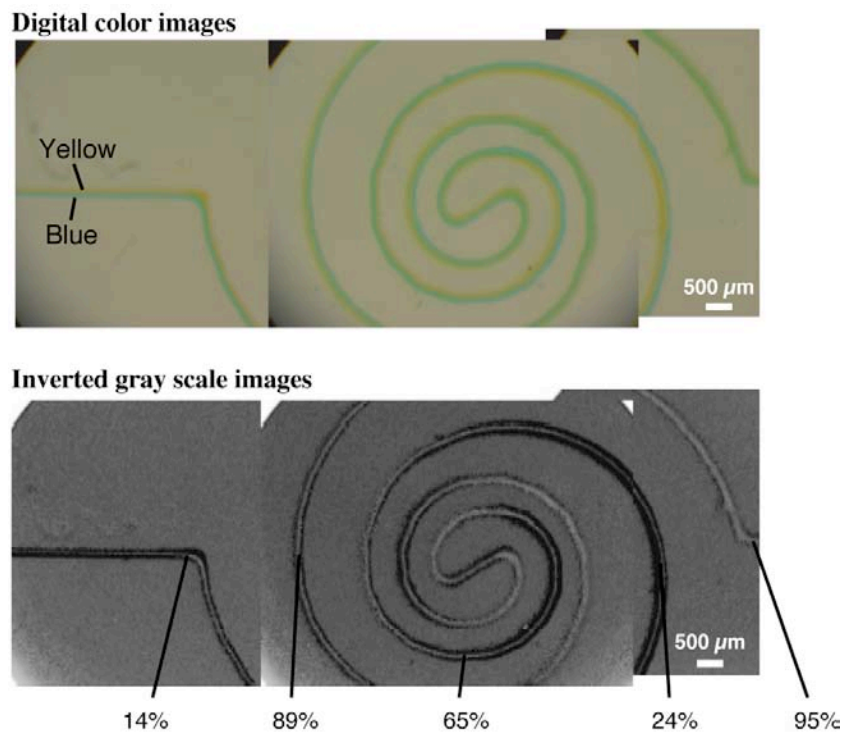


Figure III-5. Images of spiral mixing. Digital color images of parallel blue and yellow streams entering the first section of an eight-arc spiral and corresponding gray-scale images depicting the evolution of the green mixed interface. Mixing intensity values as a function of Re along the contour of the section is indicated on the image.

Figure III-6 gives a measure of the mixing intensity along the contour of the first section of the channels (for a four-arc, six-arc, eight-arc and ten-arc designs) and it is observed that most mixing occurs at the innermost region of the spiral flow path. Figure III-7 shows the mixing intensity at the end of each section for the four-arc, six-arc, eight-arc and ten-arc spiral channels. In the four-arc channel, mixing levels of 90% are achieved at the end of the second section, whereas in the eight- and ten-arc channels 90% mixing is obtained at the end of the first section.

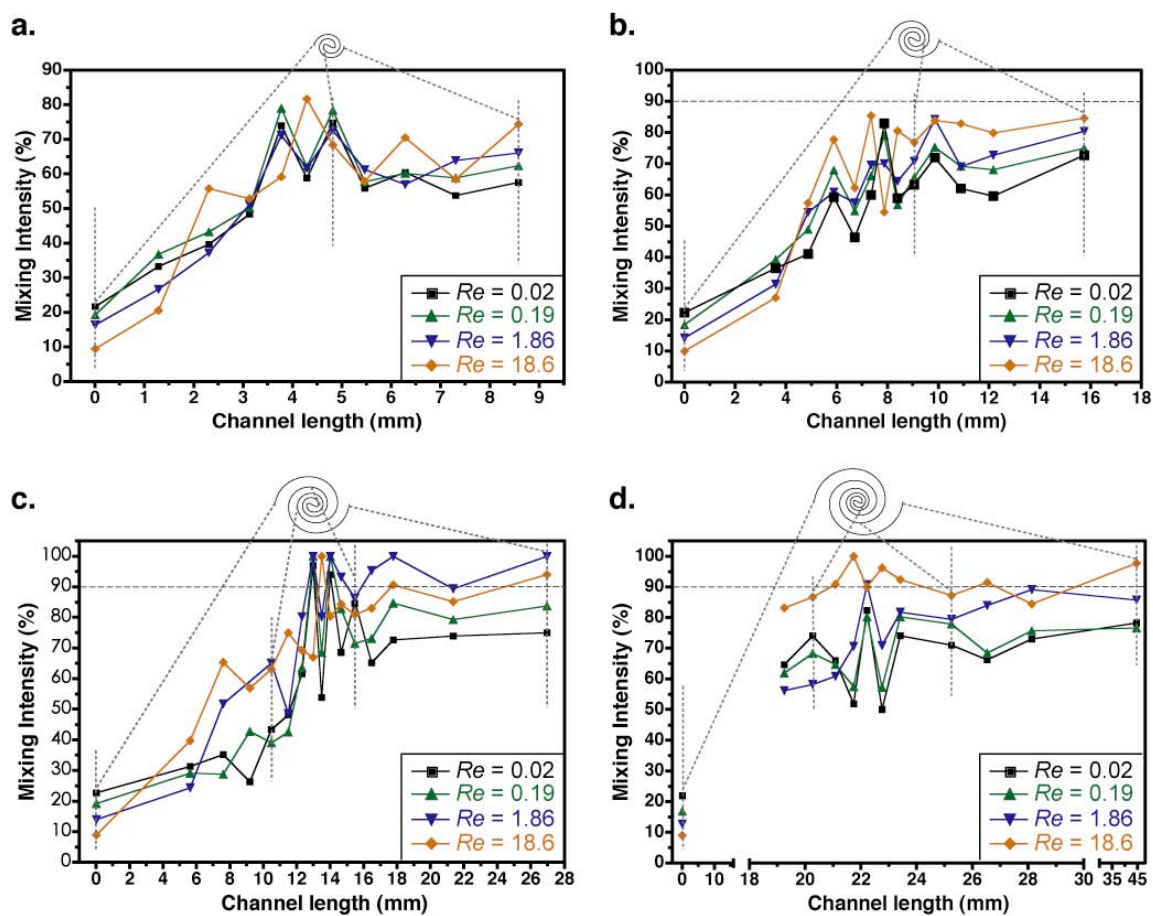


Figure III-6. Mixing intensity along the flow path of the first spiral section. Data shown are for four-arc (a), six-arc (b), eight-arc (c) and ten-arc (d) spiral channels.

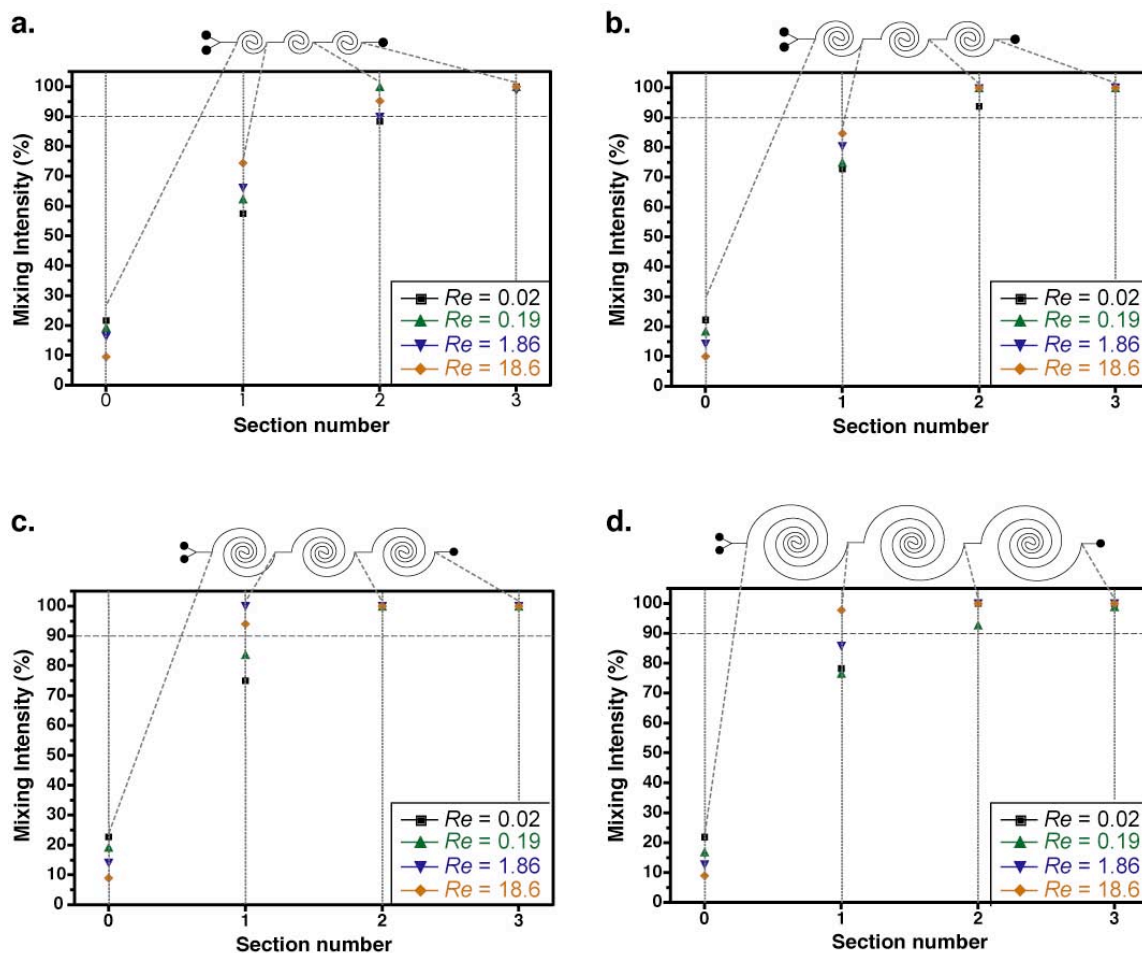


Figure III-7. Mixing intensity at the end of each spiral section. Data are taken as a function of Re at the end of each section for the four-arc (a), six-arc (b), eight-arc (c) and ten-arc (d) spiral channels.

Summary

In this chapter, a comprehensive study of fluid mixing in spiral microchannels was presented. Five different spiral designs incorporating variable lengths of spiral contours were tested and flow studies were carried out for a wide range of flow rates ($Re = 0.02 - 18.6$). At lower flow rates, diffusion is the primary mechanism by which

mixing occurs. At higher flow rates, secondary Dean effects come into play and contribute to increased levels of mixing. As fluid travels downstream inside the spiral contours, it experiences an increase in the magnitude of centrifugal forces accompanied by a corresponding enhancement in mixing performance. The lengths of the spiral contours can be increased within individual spiral sections to achieve additional mixing in one section. Alternatively, multiple sections of spirals with fewer arcs can be designed to achieve mixing at higher flow rates since centrifugal effects are strongest at the innermost regions of the spiral. In either case, considerable flexibility is available to design channels on the basis of flow rates and available device footprint area. The 3 mm-long straight section connecting successive spiral segments can also be shortened or eliminated.

All spiral designs in this work chapter fabricated in a single lithography step without the need for complex three-dimensional structures and cumbersome multi-layer alignment. No specialized laboratory equipment was used and the channels were fabricated in less than 30 min. The micromixer designs can be readily integrated into most microfluidic systems that require simple planar geometries and efficient fluid mixing. Incorporating abrupt expansions at appropriate locations along the channel length can further enhance the efficiency of these spiral mixer designs. The expansions induce a transverse vortex pair in the horizontal plane on either side of the entrance to the expansion. When coupled with Dean induced vortices that exist in the vertical plane, fluid species can be rapidly intermixed by the action of this multivortex system. Utility of incorporating expansions are first discussed in Chapter V, which describes the

functionality of a novel Asymmetric Serpentine Mixer (ASM). Here, the expansions are patterned at appropriate locations along a serpentine channel. Chapter VI describes the functionality of a hybrid micromixer that is a combination of the ASM and spiral designs.

CHAPTER IV

PLANAR SPLIT-AND-RECOMBINE MIXING*

A novel planar split-and-recombine (P-SAR) micromixer is described in this chapter. The mixer demonstrates how split-and-recombine micromixing can be achieved in planar 2-D microchannel geometries. The intrinsic rotational characteristics of Dean flows in curved channels are exploited here. A short background into SAR mixing is first given, before going into the concept behind this unique mixer design.

Split-and-recombine mixing is a passive micromixing technique that involves the generation of multiple alternating lamellae of the fluids to be mixed, thereby creating an increased interfacial area across which diffusive transport can take place. By using this approach, exponential reductions in mixing lengths are capable of being achieved. Conventional SAR mixers rely on complex fabrication techniques to accommodate the number of basic processes necessary to generate the lamellae. For example, the design of a serial lamination mixer involves a multi-step fabrication process beginning with separation of the two streams, where one stream is usually directed orthogonal to the other stream, then the two individual streams are split into multiple narrower streams and then redirected in such a manner that alternating lamellae of the two streams are generated in a single flow channel.

* Part of the data reported in this chapter is reprinted with permission from: Multivortex micromixing by Sudarsan, A.P.; Ugaz, V. M., *Proc. Natl. Acad. Sci. U. S. A.* **2006** *103*, 7228-7233. © 2006 by The National Academy of Sciences of the USA.

Parallel lamination mixers usually involve splitting the individual inlet streams into multiple streams before assembling them in an alternating manner. A few examples of recent SAR mixers are shown in Figure IV-1. Fabrication of such systems usually requires specialized equipment or techniques to realize these complex 3-D structures. Moreover, if such mixers are to be made on a routine basis, fabrication costs are an important factor to consider.

Dean flow phenomena offer a promising approach to design SAR mixers in planar 2-D geometries. The mixers are fabricated from a single lithography step without the need for specialized equipment and techniques. A linear relationship between timescales associated with axial and transverse components of fluid motion enable for relatively easy scaling and optimization of these designs. An added advantage of P-SAR micromixers is that the mixing time is independent of the number of split streams employed. Conventional SAR mixers have an optimum number of split streams whereas,

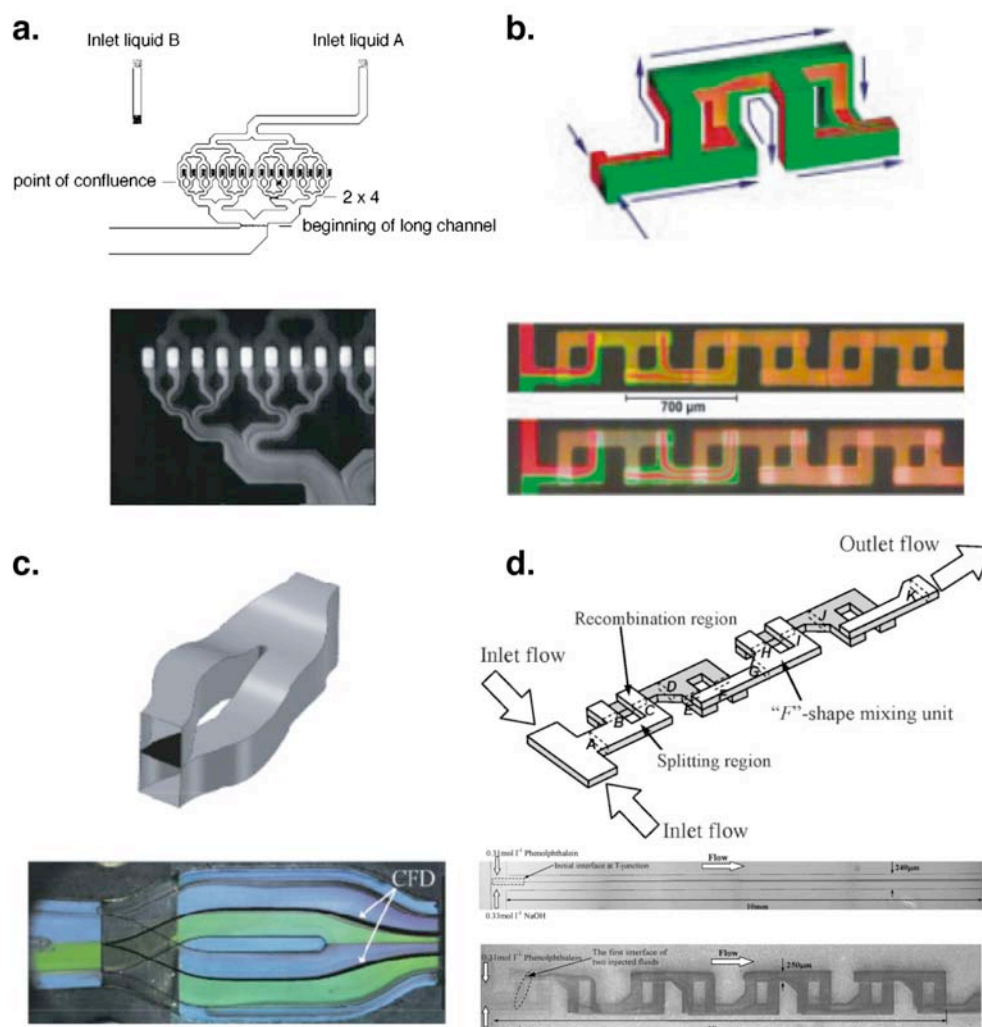


Figure IV-1. Examples of selected SAR mixers from literature. A schematic of the geometry incorporated along with a flow image are shown. (a) Parallel lamination mixer by Bessoth, F. G.; deMello, A. J.; Manz, A., Microstructure for efficient continuous flow mixing, *Anal. Commun.* **1999**, *36*, 213-215 – Reproduced by permission of The Royal Society of Chemistry. (b) Serial lamination mixer. Reprinted with permission from Chen, H.; Meiners, J.-C., Topological mixing on a microfluidic chip, *Appl. Phys. Lett.* **2004**, *84*, 2193-2195. © 2004 American Institute of Physics. (c) Optimized SAR mixer by Schönfeld, F.; Hessel, V.; Hoffman, C., An optimized split-and-recombine micro-mixer with uniform ‘chaotic’ mixing, *Lab Chip* **2004**, *4*, 65-69 – Reproduced by permission of The Royal Society of Chemistry. (d) Second generation mixer by Kim, D. S.; Lee, S. H.; Kwon, T. H.; Ahn, C. H., A serpentine laminating micromixer combining splitting/recombination and advection, *Lab Chip* **2005**, *5*, 739-747 – Reproduced by permission of The Royal Society of Chemistry.

P-SAR mixers function better with increases number of split-streams and the mixing time continually decreases with increasing number of split streams.

Concept

The intrinsic rotational character of Dean flows can be harnessed in combination with a simple 2-D microchannel design to increase interfacial area between species without the need to construct intricate 3-D geometries (e.g., Figure IV-1). In this planar split-and-recombine (P-SAR) design, parallel liquid streams first travel through a curved segment that induces simultaneous $\sim 90^\circ$ rotations in the upper and lower halves of the channel (e.g., the boxed images in Figure I-22), at which point the flow is split into multiple streams that continue along curved trajectories such that each individual split stream experiences a second pair of $\sim 90^\circ$ rotations. These successive rotation steps transpose the position of each species such that alternating lamellae are formed when the streams are rejoined. Illustration of an idealized Dean flow mediated split-and-recombine mixing is shown in Figure IV-2.

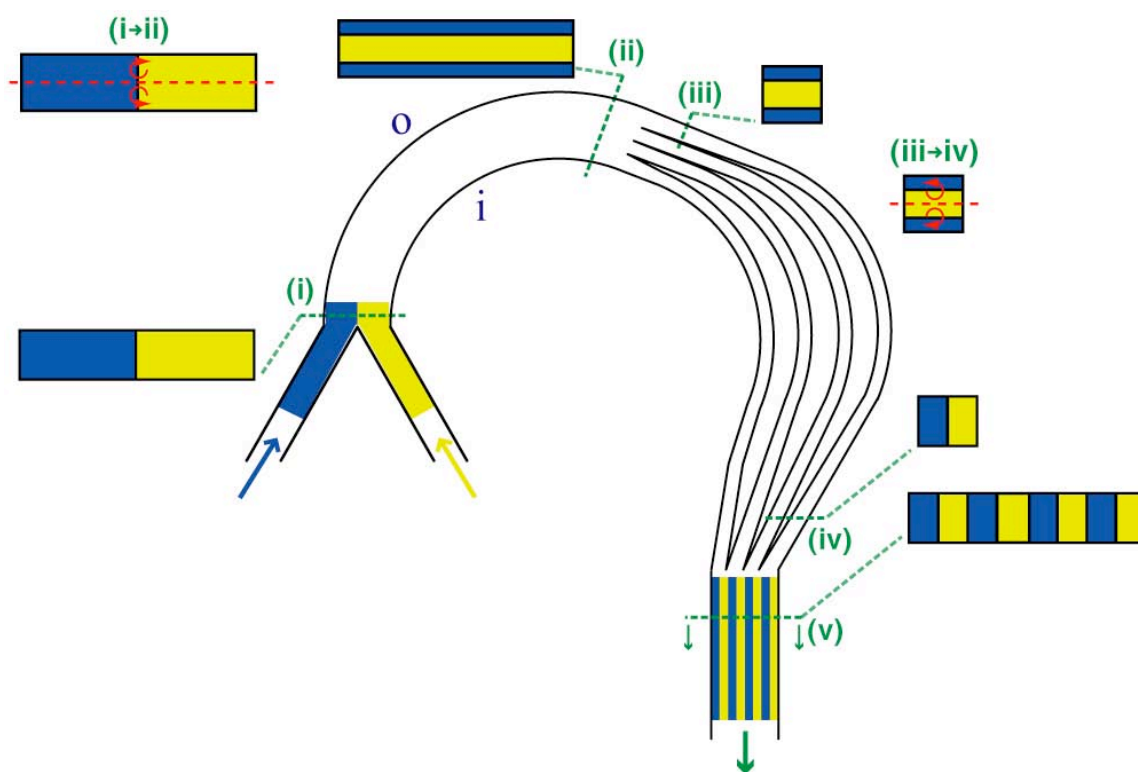


Figure IV-2. Concept of Dean induced planar split-and-recombine lamination. Parallel liquid streams enter a curved microchannel (position i) and travel through a curved segment that induces simultaneous $\sim 90^\circ$ rotations in the upper and lower halves of the channel (between positions i and ii), at which point (position iii) the flow is split into multiple streams that continue along curved trajectories such that each individual split stream experiences a second pair of $\sim 90^\circ$ rotations (between positions iii and iv). These successive rotation steps transpose the position of each species such that alternating lamellae are formed when the streams are rejoined (position v). In the figure “i” and “o” denote inner and outer channels walls respectively.

Flow visualization in a two-split microchannel

We first visualized this Dean induced lamination effect by performing top-view and confocal cross-sectional imaging experiments in a microchannel that is split into two streams at a distance of 1.5 mm from the entrance and subsequently rejoined at a downstream distance of 3.8 mm (Figure IV-3).

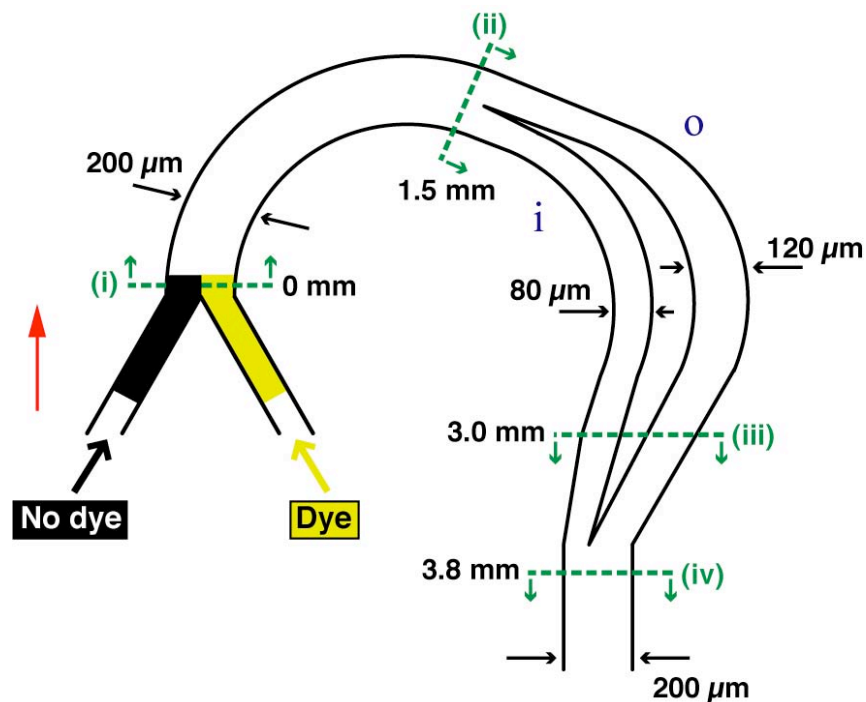


Figure IV-3. P-SAR micromixer incorporating two split streams. Schematic of the microchannel geometry investigated (200 μm wide; 29 mm tall; 630 μm radius of curvature; Re and κ computed based the 200 μm wide segment; widths of the two split streams are chosen to maintain an equal pressure drop in each leg by compensating for their difference in length; “i” and “o” denote inner and outer channels walls respectively).

At low flow rates, the secondary flow is not strong enough to induce sufficient rotation and the stream flowing along the inner wall of the channel exhibits minimal deviation or attraction towards the outer wall. This is evident from confocal images obtained from inside the split streams at a distance of 3.0 mm downstream (Figure IV-4).

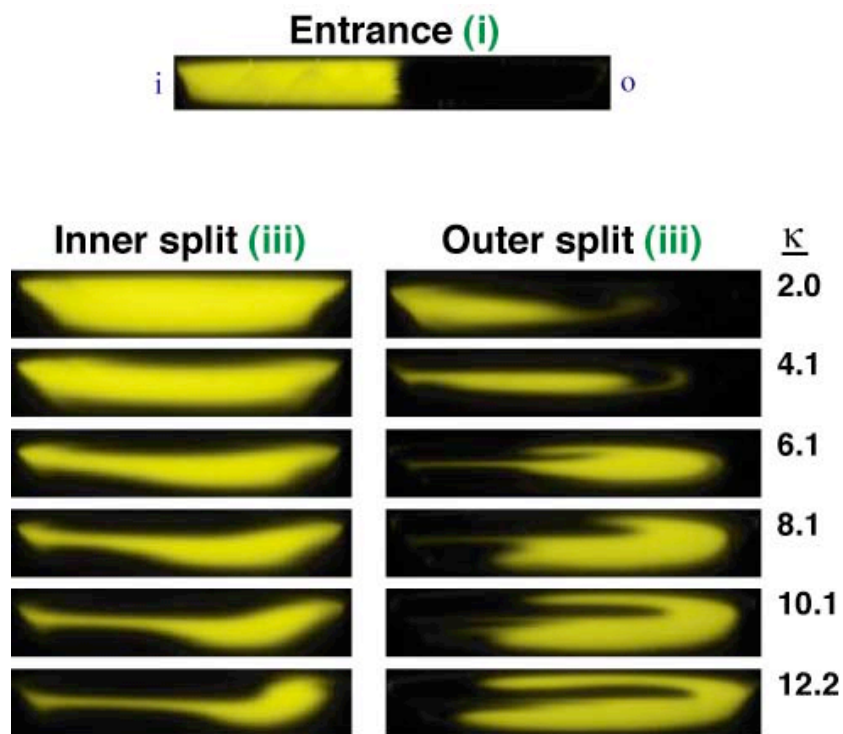


Figure IV-4. Evolution of lamellar structure in a two-split microchannel. The top image is taken at the entrance to the first curved channel segment (position i in Figure IV-3). The lower sets of images are of the flow inside each of the split microchannels taken at flow rates ranging from $7.3 < Re < 43.6$ ($2.0 < \kappa < 12.2$) at a distance of 3 mm downstream from the channel entrance (position iii in Figure IV-3).

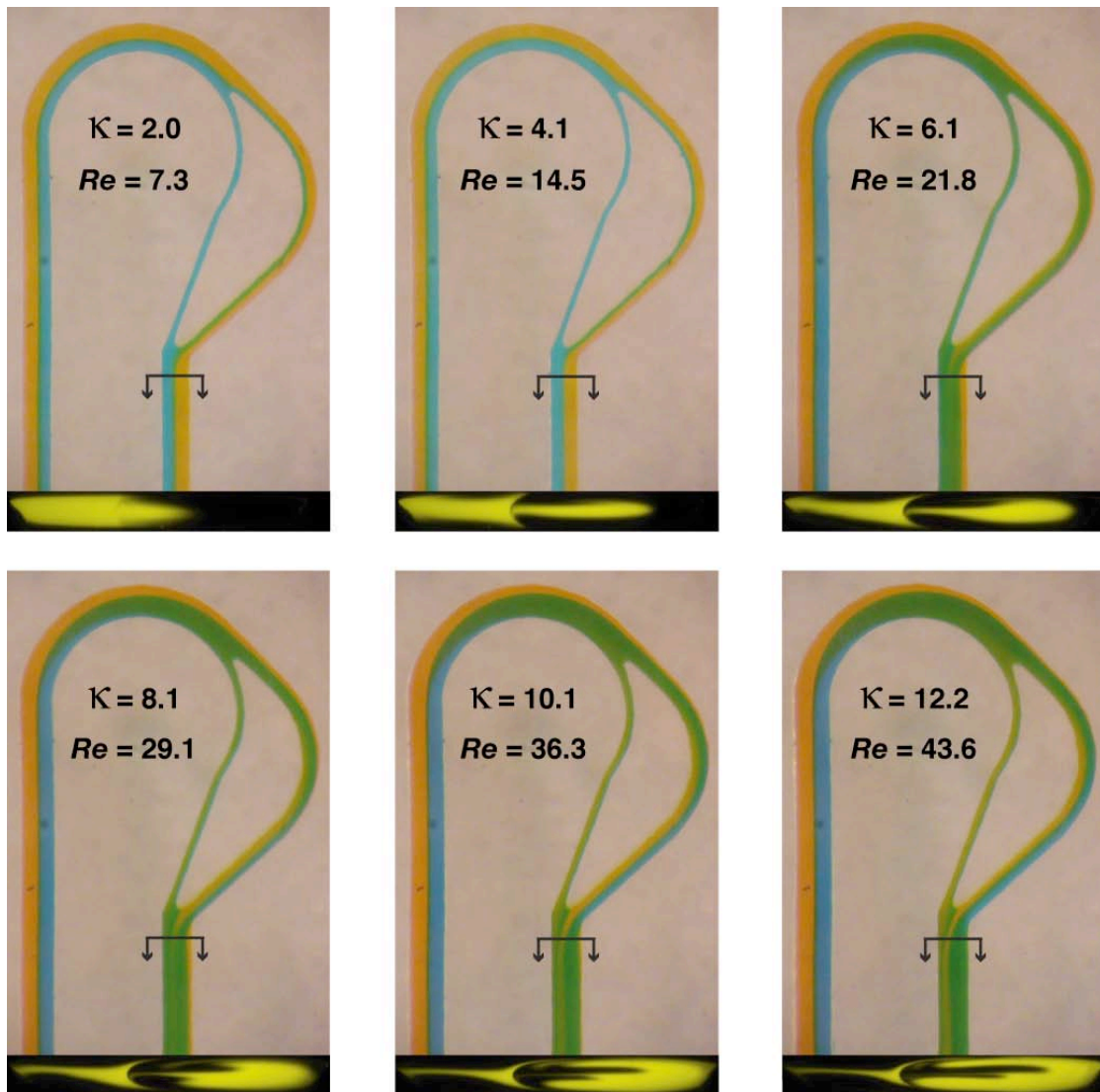


Figure IV-5. Dean induced lamination is a microchannel with two split streams. Confocal images (lower image in each tile) are taken at the location where the two split streams have rejoined (position iv in Figure IV-3). Distinct lamellar zones are observed in the vicinity of $4.1 < \kappa < 12.2$. The top view images (upper image in each tile) of two aqueous streams labeled with blue and yellow food dye. At $\kappa = 2.0$ the streams flow in parallel along the entire length of the channel, whereas at $\kappa = 12.2$ the blue stream is transported from the inner to the outer wall, as indicated by the green color immediately upstream of the split followed by the reemergence of a blue layer at the outer wall within each individual split stream. Alternating blue, blue/green, and yellow striations are visible in the flow after the streams have rejoined, in agreement with the confocal images.

At higher flow rates, however, the fluid species undergo a sequence of rotations as a result of the increased strength of the transverse secondary flows such that upon rejoining, alternating lamellae of each species appear accompanied by a corresponding increase in interfacial area. We visualized this by obtaining confocal images at a position where the split streams rejoined (Figure IV-5). The corresponding top-view images with aqueous streams of blue and yellow tracer dye are also shown.

Planar split-and-recombine mixer (P-SAR)

Design

A planar split-and-recombine micromixer incorporating a series of four successive P-SAR elements arranged in a serpentine-like manner was designed (Figure IV-6). Each P-SAR element incorporated four individual split streams. In the first P-SAR element, the split occurred at a distance of 1.2 mm downstream and then rejoined at a distance of 4.0 mm downstream distance. The contour length of the outer-most split stream was used in making this measurement. The remaining P-SAR elements were designed in a similar way and connected in an opposing manner to each other by a straight segment of width 400 μm and length 500 μm . The individual split streams had a width of 100 μm while the rest of the channel had a width of 400 μm . The radius of curvature was 630 μm for the 400 μm wider segment and as close to 630 μm for the individual split streams. This deviation is required to enable fabrication of these closely separated channels. The micromixer had a uniform height of 29 μm over its entire length.

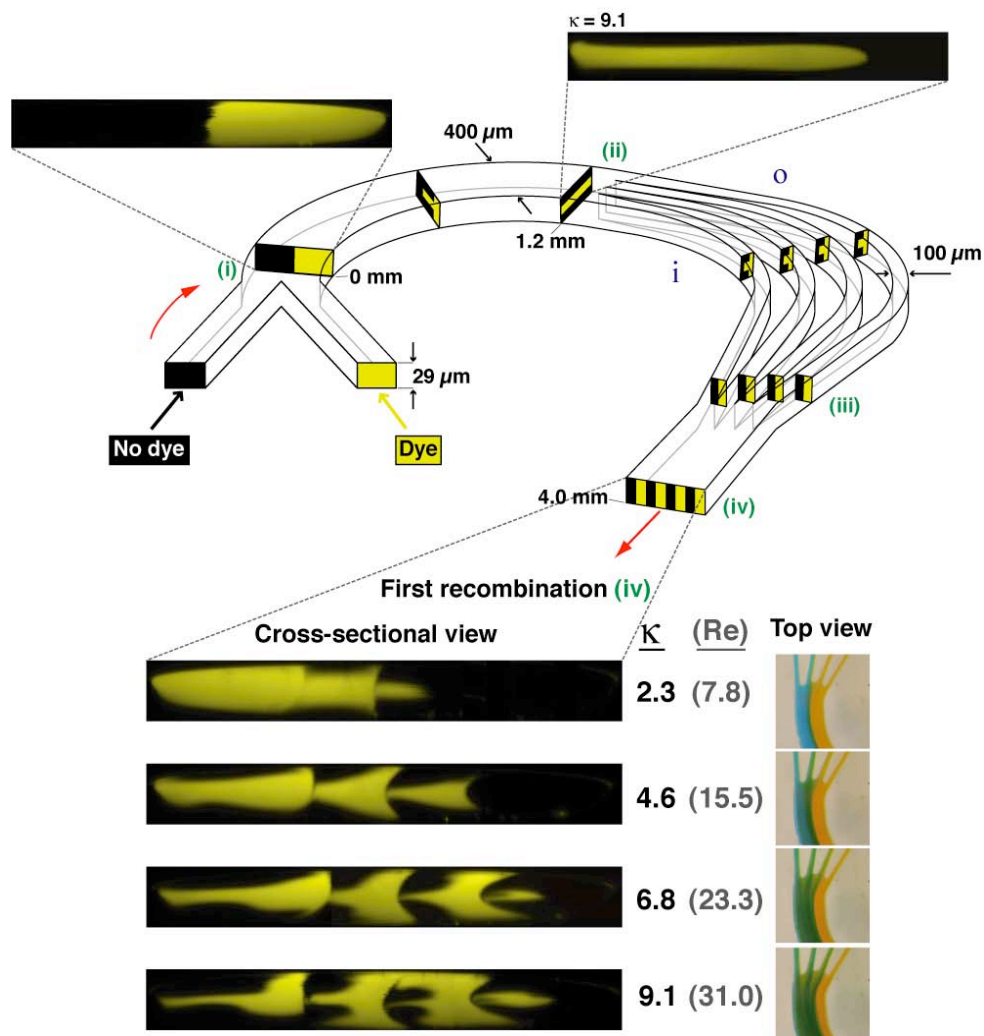


Figure IV-7. Flow visualization in the first P-SAR element. Schematics are shown inside the channel (400 μm wide; 29 μm tall; 630 μm radius of curvature; Re and κ are computed based on the 400 μm wide segment; “i” and “o” denote the inner and outer channel walls respectively); corresponding confocal images are shown outside. Parallel streams of different species enter the curved microchannel (i) and experience a transverse flow generated by the counter rotating vortices above and below the channel midplane that induce a corresponding pair of 90° rotations in the fluid (ii). At this point (1.2 mm downstream from entrance), the flow is split into four parallel streams that proceed along curved trajectories inducing a second pair of 90° fluid rotations in each stream (between ii and iii). Alternating lamellae of the two species are generated when the streams are rejoined 4 mm downstream from the entrance (iv). Cross-sectional the corresponding top-view images taken after the first recombination are shown.

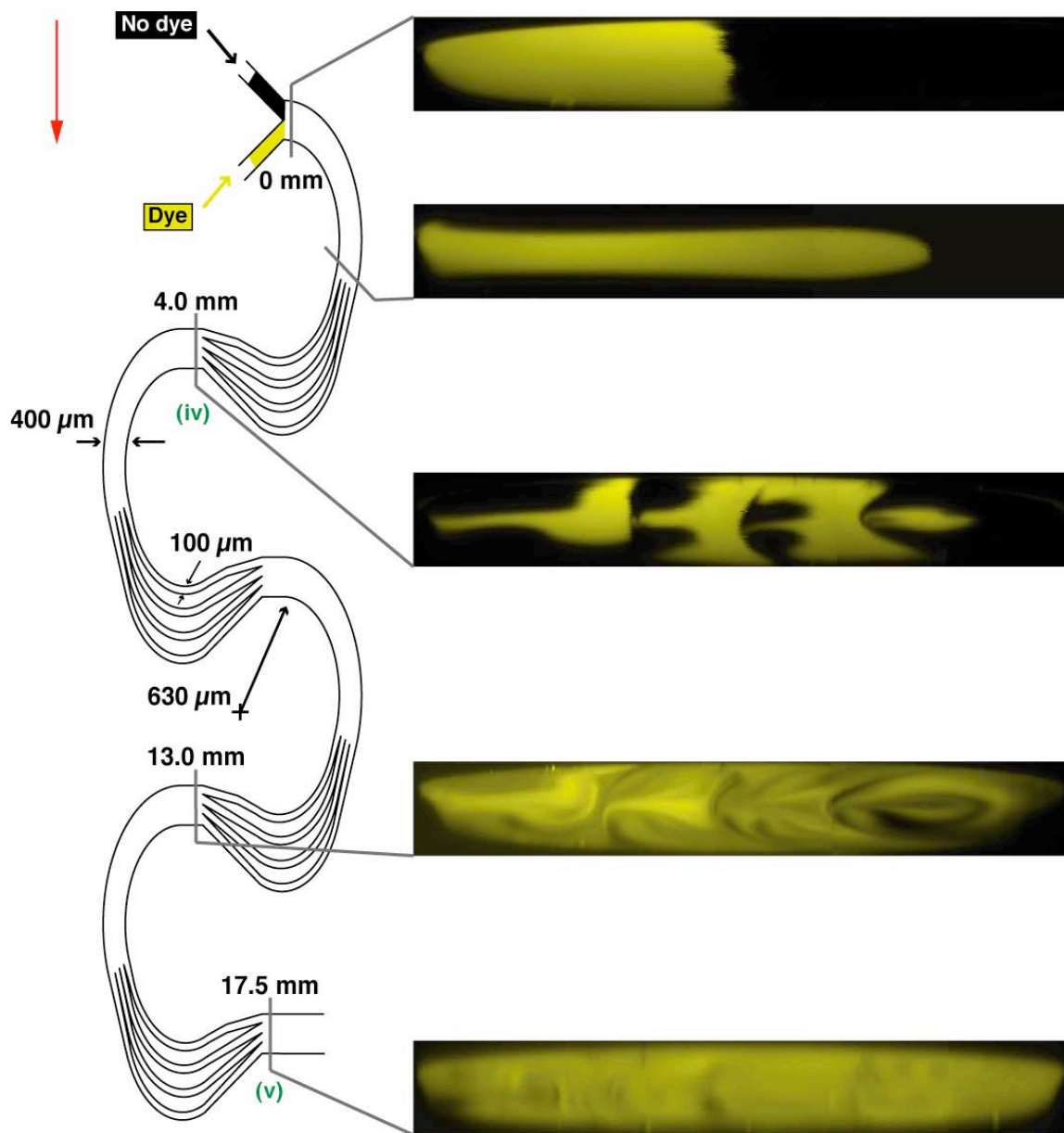


Figure IV-8. Cross-sectional images at $\kappa = 9.1$ images along the P-SAR micromixer. Confocal images were obtained at κ corresponding to $Re = 31.0$. Distinct alternating lamellae of the two aqueous streams appear at the end of the first P-SAR element (position iv). The streams are almost fully mixed at the end of the fourth P-SAR element (position v) as indicated by the uniform fluorescence across the entire image.

Figure IV-8 shows cross-sectional confocal images obtained at different downstream locations along the channel at $\kappa = 9.1$ ($Re = 31.0$). Confocal images taken at different flow rates ($2.3 \leq \kappa \leq 9.1$) at the end of the recombination junction of the fourth P-SAR element (Figure IV-9) indicate that a level of 90% mixing was achieved at the highest flow rate investigated (Figure IV-10).

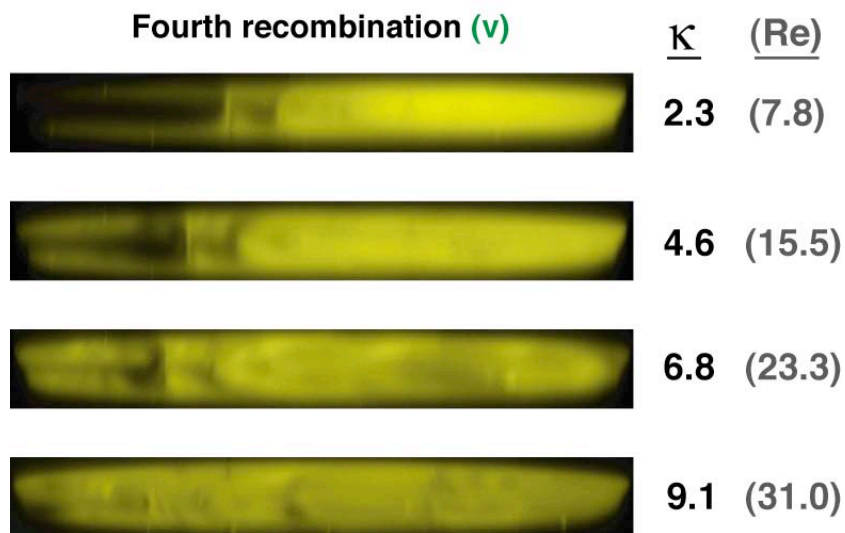


Figure IV-9. Confocal cross-sectional images taken at the fourth recombination. The images correspond to position iv in Figures IV-6 and IV-7. As κ is increased the two species become almost completely intermixed, as indicated by uniform fluorescence over the channel cross-section.

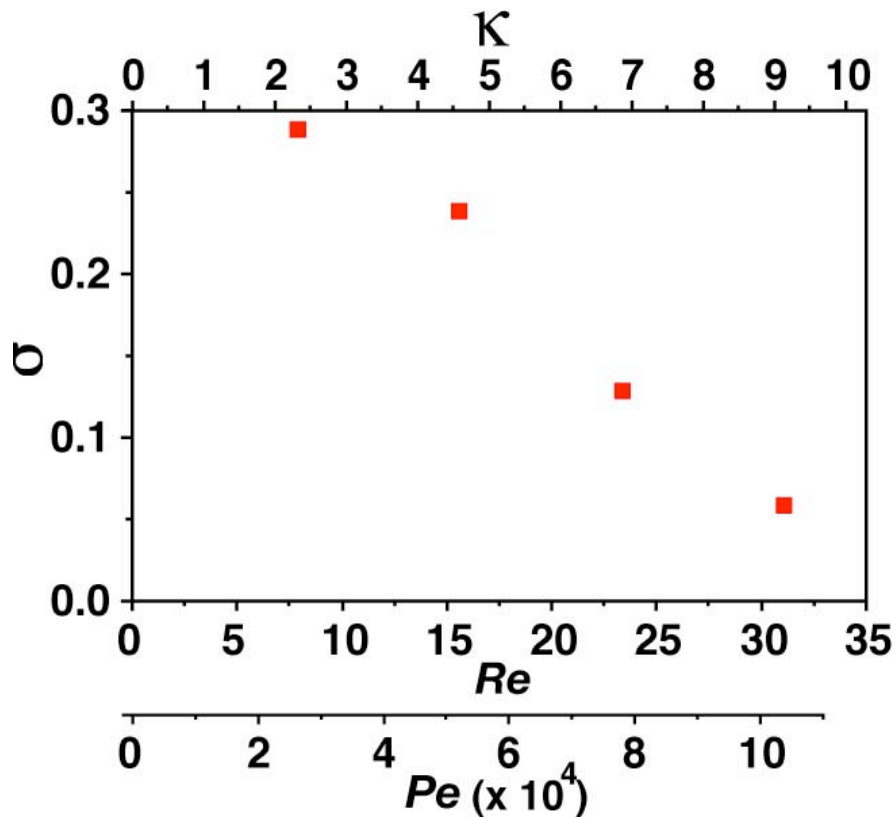


Figure IV-10. Mixing performance of P-SAR micromixer. Plot of σ computed from the confocal image sequence in (Figure V-7) as a function of the Dean, Reynolds, and Péclet numbers (Pe was computed using $D = 3 \times 10^{-6} \text{ cm}^2/\text{s}$ for Rhodamine 6G).

Optimal P-SAR design

Optimal P-SAR design involves splitting the microchannel into multiple streams at a downstream location where the transverse flow has induced simultaneous $\sim 90^\circ$ counter-rotations in the upper and lower halves of the cross-section. The manner in which this location depends on channel geometry and flow conditions can be inferred by considering the relative timescales associated with the axial and transverse components

of fluid motion. Axial transport can be approximated as laminar Poiseuille flow with characteristic velocity⁷⁵

$$u_A \sim U_0 \quad (\text{IV-1})$$

which is the maximum centerline velocity, while the transverse (Dean flow) velocity scales as⁸

$$u_D \sim Re(d/R)U_0 \quad (\text{IV-2})$$

A ratio of corresponding timescales is then

$$t_A/t_D \sim (L_A/u_A)/(L_D/u_D) = (L_A/R)Re \quad (\text{IV-3})$$

where L_A and L_D are characteristic axial and transverse length scales, respectively, and L_D is taken to be the hydraulic diameter d . The downstream location at which a fluid element is transported across the width of the microchannel can then be estimated by setting

$$t_A/t_D \sim 1 \quad (\text{IV-4})$$

suggesting a linear scaling:

$$(R/L_A) \sim Re \quad (\text{IV-5})$$

This relationship is consistent with analysis of flow in macroscale helical pipes⁷⁵, and is experimentally confirmed by visualization of colored dye streams (Figure IV-11). Arbitrarily assigning L_A as the downstream location where transverse rotation effects pull the inner dye stream outward to occupy 80% of the channel width (L_{80}), image analysis of data from over 50 experiments performed using various combinations of R , Re , and cross-sectional dimensions superimpose and exhibit behavior consistent with a linear Re dependence (Figure IV-12). Deviations from the linear trend at high Re are

likely a consequence of slight but visible bulging deformations induced in the channel due to the increased pressure required to impose high flow rate conditions.

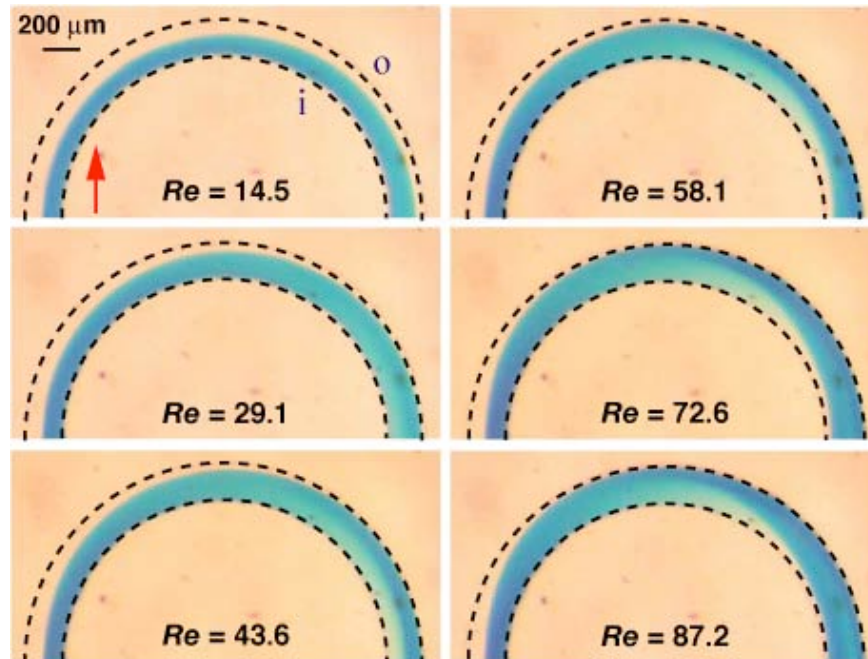


Figure IV-11. Images for optimal P-SAR design. Top view image sequence of aqueous streams (the inner stream is labeled with blue tracer dye) flowing through a curved microchannel segment (200 μm wide; 29 μm tall; 937 μm radius of curvature; “i” and “o” denote the inner and outer channel walls, respectively). The blue stream initially occupies 50% of the cross-section upon entering the curved segment, and the downstream distance where transverse Dean effects pull the blue stream outward to occupy 80% of the channel cross section (L_{80}) is determined at each value of U_0 (and Re) by analysis of digitized images.

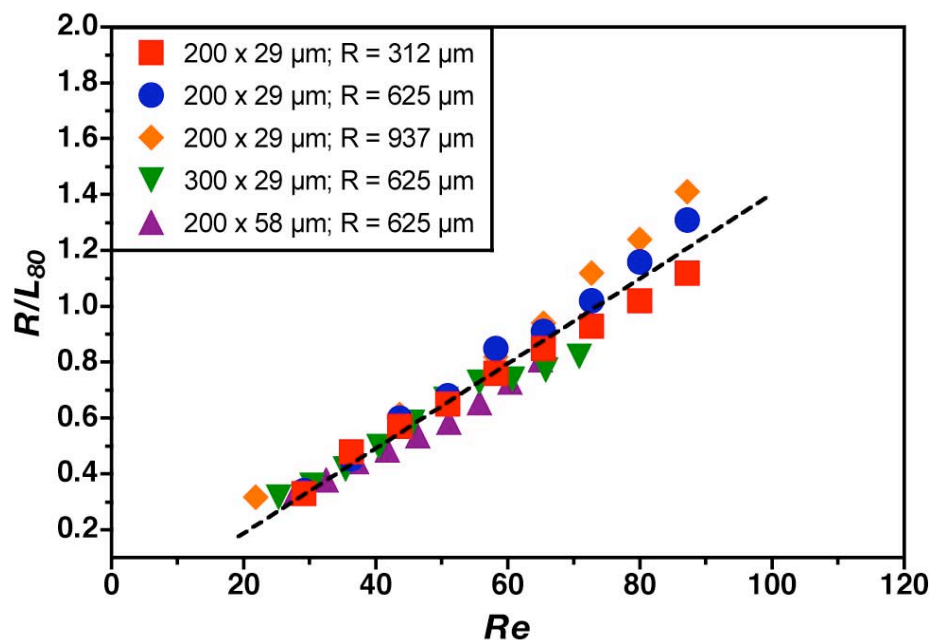


Figure IV-12. Influence of flow and microchannel geometry on transverse rotation. The graph depicts the evolution of the parameter R/L_{80} with Re in microchannel geometries incorporating multiple combinations of cross-sectional area and radius of curvature. The dashed line depicts a linear regression fit to the ensemble of over 50 data points.

Mixing time

Conventional split-and-recombine (SAR) micromixers typically rely on 3-D microchannel networks to divide (split), redirect, and subsequently reassemble liquid streams to generate lamellae of alternating species (Figure IV-1). In these configurations, the total time t , required to mix two inlet streams can be expressed by an equation of the form:

$$t = \frac{nL_b}{2u} + \frac{d_c^2}{2n^2D} \quad (\text{IV-6})$$

where, n is the number of split streams produced from each primary inlet stream, L_b is the length required for branching (Figure IV-13), d_c is the diameter of the channel before and after the branching, and D is the diffusion coefficient.¹¹⁸ The first term on the right hand side of the equation represents the time required for redirecting the fluid flow from the point where the primary stream is split to the point where the individual split streams recombine. The second term on the right hand side corresponds to the time associated with diffusive interspecies transport across lamellae upon recombination. In a conventional SAR micromixer (Figure IV-13a) the time associated with fluid branching increases linearly with the number of splits due to the corresponding increase in total cross-sectional area. In the P-SAR design (Figure IV-13b), however, the branching time is essentially independent of the number of splits (we say “essentially” because there is some variation in path length between the outermost and innermost split streams; we have used the contour length of the outermost split stream in calculations to be conservative).

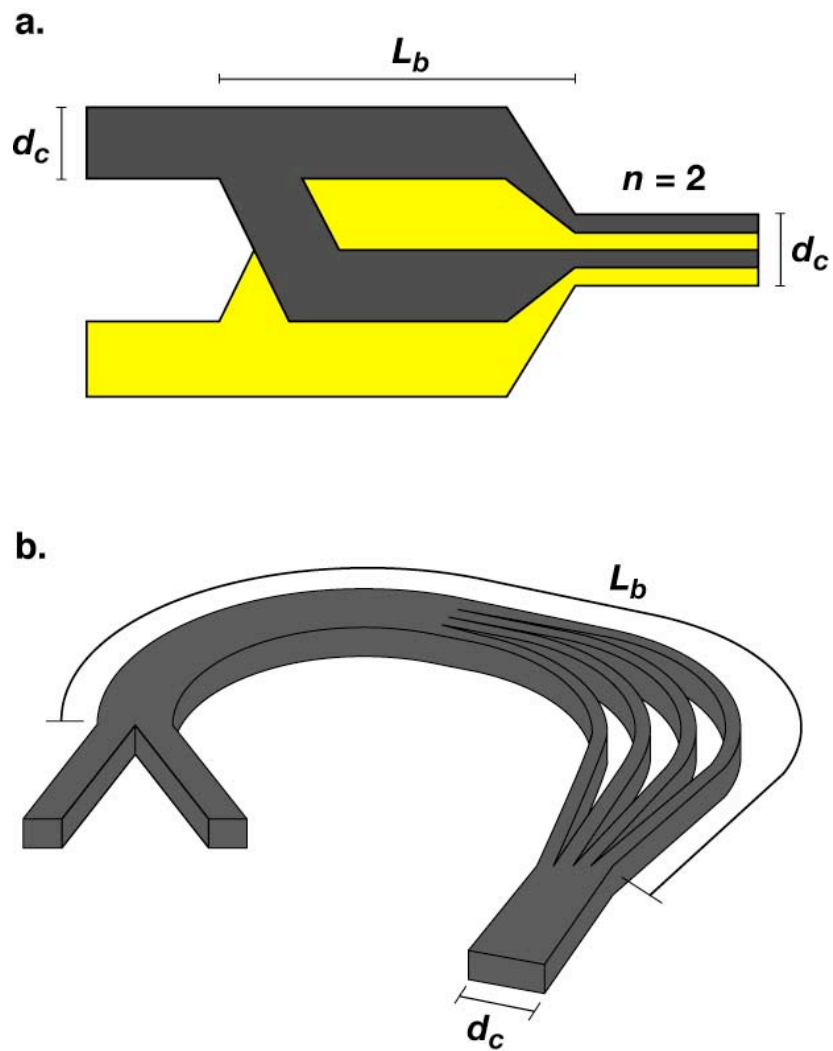


Figure IV-13. Comparison of conventional SAR and P-SAR mixer designs. (a) Illustration of microchannel geometry required to generate alternating lamellae of fluid species using a conventional 3-D SAR micromixer design (adapted from Erbacher *et al.*¹¹⁸). (b) Schematic of 2-D P-SAR microchannel geometry with corresponding branching length L_b is indicated.

Based on this analysis, a comparison of total mixing time as a function of the number of splits shows that there is an optimal number of splits in the conventional SAR design reflecting the balance between branching and diffusive timescales, whereas in the P-SAR design the mixing time continuously decreases with increasing number of splits (Figure IV-14).

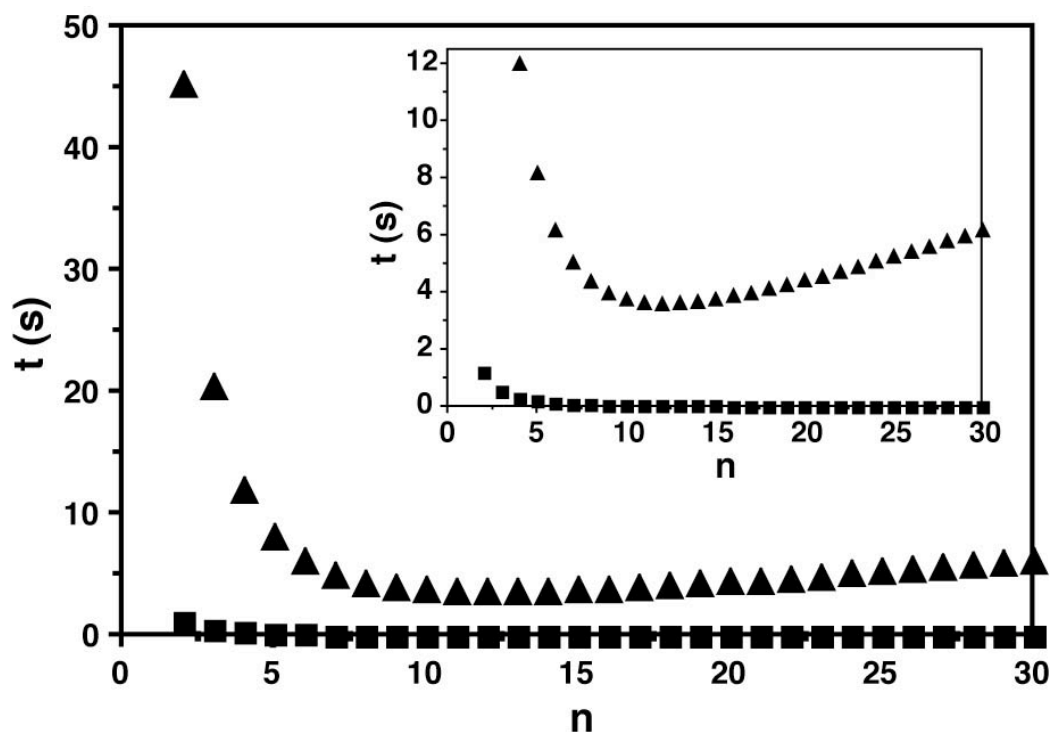


Figure IV-14. Mixing time for conventional SAR and P-SAR mixer designs. Comparison of total mixing time versus number of splits for the conventional SAR [▲] and P-SAR [■] micromixer designs shown in (Figure IV-13a) and (Figure IV-13b), respectively. For the P-SAR design, d_c is taken as the hydraulic diameter (54 μm) and $L_b = 4$ mm. For the conventional SAR design $d_c = 600$ μm and $L_b = 10$ mm as given in Erbacher *et al.*¹¹⁸ The diffusion coefficient is taken to be $D = 10^{-5}$ cm^2/s .

Recently work has shown that analogous lamination flow phenomena can arise in conduits subjected to spanwise rotation where microchannels are constructed on a rotating platform.^{119, 120} Here, transverse flows are generated by Coriolis effects and the Rossby number plays a comparable role to the Dean number.^{121, 122}

Summary

The concept of split-and-recombine mixing in a planar format via a novel P-SAR micromixer has been discussed in this chapter. The mixer is capable at efficient mixing levels without the need for employing complex 3-D channel structures. As is the case with the spiral mixers, fabrication can be routinely achieved in about thirty minutes. An increase in the number of split streams would result in a corresponding increase in the number of lamellae generated. Consequently, efficiency can be enhanced and mixing would be achieved in considerably shorter downstream distances. The relatively linear scaling between timescales associated with axial and transverse components of fluid motion suggest that these geometries can be easily scaled and optimized, and readily integrated in a broad range of lab-on-a-chip systems. An important aspect of the P-SAR design is that the overall mixing time continually decreases with increasing the number of split streams. Unlike conventional SAR mixers where the mixing time increases with increased amount of branching networks, the mixing time here is more or less independent of the number of individual split streams employed.

CHAPTER V

ASYMMETRIC SERPENTINE MIXING*

In this chapter, a second novel micromixer called Asymmetric Serpentine Mixer (ASM) is described. By patterning a serpentine channel with an abrupt expansion, a vortex pair on either side of the expansion is generated. The combined effects of Dean vortices in the horizontal plane and expansion vortices in the vertical plane are used to rapidly intermix fluid streams to achieve efficient mixing levels comparable to mixers based on chaotic advection. In tune with the rest of this research, the ASM requires simple 2-D channels and can be fabricated from a single lithography step. Practical utility of the ASM design is demonstrated by observing its influence on binding interactions between a fluorescent intercalating dye and double-stranded DNA. Factors required to be considered in order to design optimal ASM designs are also discussed in this chapter.

The idea of using eddies formed at bends of microchannels is an effective way to achieve high levels of passive micromixing. For example, Liu *et al.* designed a 3-D serpentine mixer comprising of repeated “C-shaped” elements arrayed along the flow path.⁶³ The mixer was fabricated by double-sided etching on a silicon wafer to realize the required three-dimensional structure. Therriault *et al.* designed a 3-D micromixer in the form of square spiral towers.⁷¹ Direct-write assembly of a fugitive organic ink was

* Part of the data reported in this chapter is reprinted with permission from: Multivortex micromixing by Sudarsan, A.P.; Ugaz, V. M., *Proc. Natl. Acad. Sci. U. S. A.* **2006** *103*, 7228-7233. © 2006 by The National Academy of Sciences of the USA.

used to create this complex microstructure. In both these cases, higher levels of mixing were achieved at increasing flow rates as a result of the increased strength of the eddies formed at the sharp $\sim 90^\circ$ bends. Although these techniques are highly effective, the corresponding non-planar flow geometries often require multi-level or specialized fabrication processes that sometimes involve timescales on the order of several hours to days to fabricate. In the ASM design two systems of vortices, one in the horizontal plane and the other in the vertical plane, are generated and act in harmony to perform rapid and efficient micromixing.

Concept

Beyond a critical Re , fluid encountering a sudden increase in a conduit's cross-sectional area undergoes local separation from the wall in response to the adverse pressure gradient resulting in the formation of a vortex pair bracketing the entrance to the expansion.^{123, 124} When these expansion phenomena in the horizontal plane are coupled with Dean effects in the vertical plane, the resulting multivortex flow field can further accelerate interspecies transport (Figure V-1).

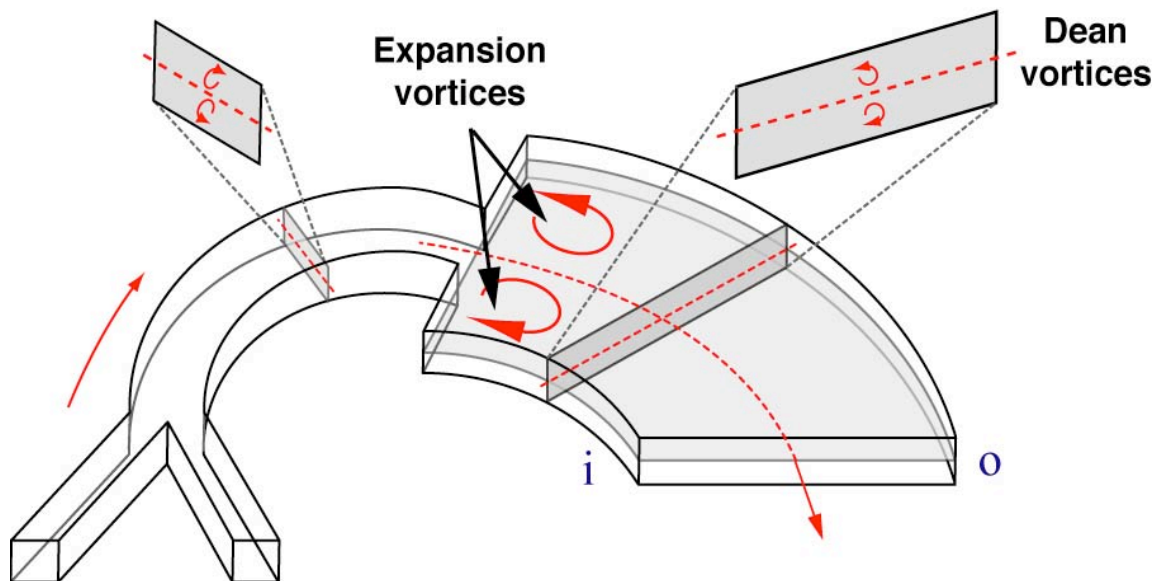


Figure V-1. Multivortex phenomena in a microchannel. Schematic of coupled transverse Dean flow (vertical plane) and expansion vortex (horizontal plane) effects in the vicinity of an abrupt increase in the width of the conduit (i and o denote inner and outer channel walls respectively).

Flow visualization in a curved channel with an expansion

The combined effect of the multi-vortex system was observed by direct visualization of colored dye streams in a curved microchannel having a radius of curvature of $630\ \mu\text{m}$ and incorporating an expansion from 100 to $500\ \mu\text{m}$ in width (Figure V-2). Corresponding cross-sectional confocal images of parallel aqueous streams with one of them fluorescently labeled indicate that beyond a critical flow rate rapid mixing can be achieved in both the horizontal and vertical planes on the channel.

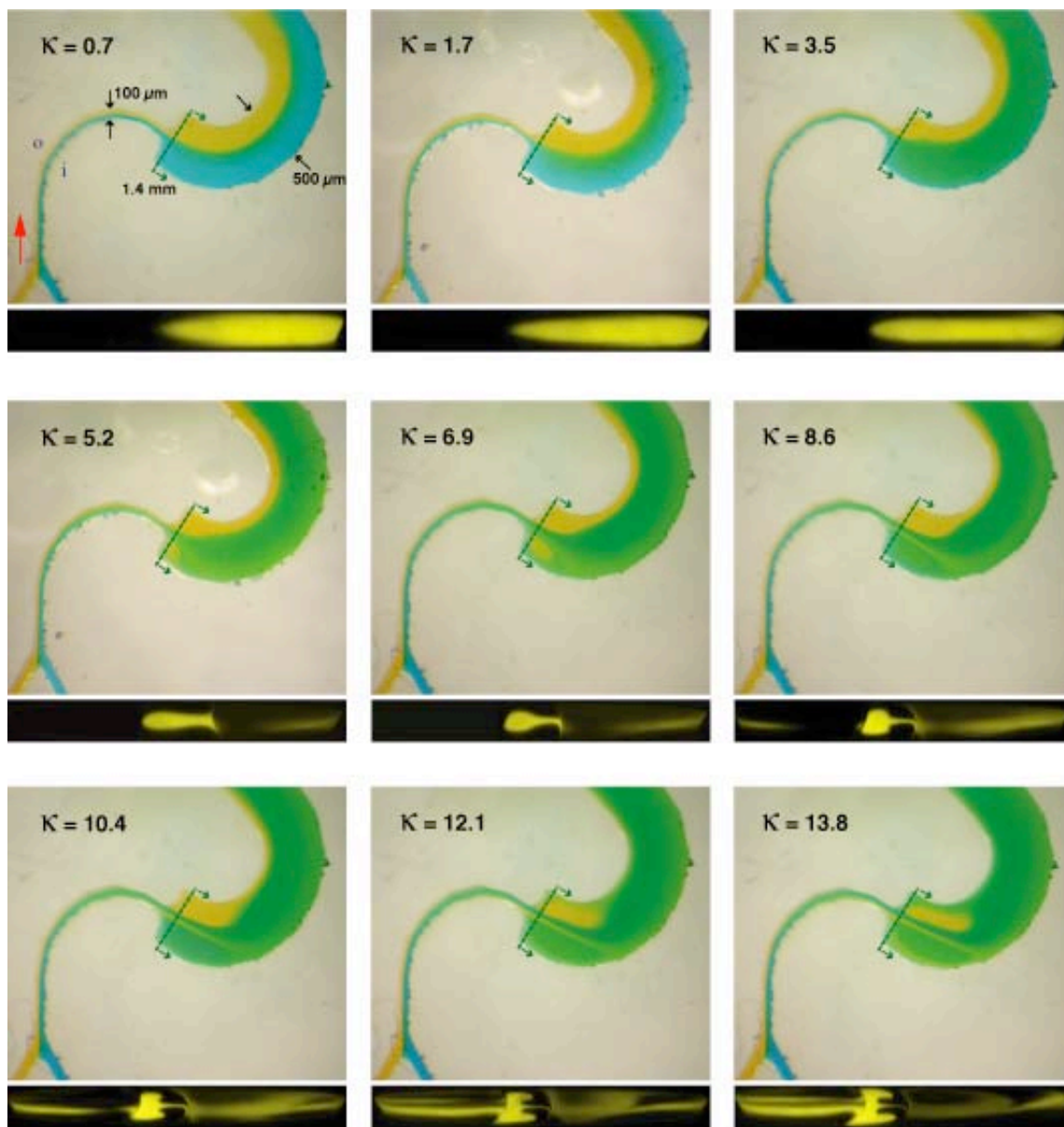


Figure V-2. Multivortex micromixing. Top-view images (above) and corresponding confocal cross-sectional images (below) taken at the entrance to an expansion in width from 100 to 500 μm occurring 1.5 mm downstream from the entrance depicting vortex formation with increasing κ (κ computed based on the 100 μm wide segment, “i” and “o” denote the inner and outer channel walls). As κ increases expansion vortices are generated and simultaneously the strength of the Dean vortices increase and rapid micromixing is achieved.

Asymmetric serpentine mixer (ASM)

Design

The effectiveness of this multi-vortex arrangement to perform micromixing is demonstrated in an asymmetric serpentine micromixer (ASM) design consisting of a curved serpentine microchannel incorporating abrupt expansions patterned at the last quarter of each opposing semi-circular arc (Figure V-3). The expansions are $500\ \mu\text{m}$ wide and the rest of the channel is $100\ \mu\text{m}$ wide. The channel has a uniform height of $29\ \mu\text{m}$ and the radius of curvature is $630\ \mu\text{m}$.

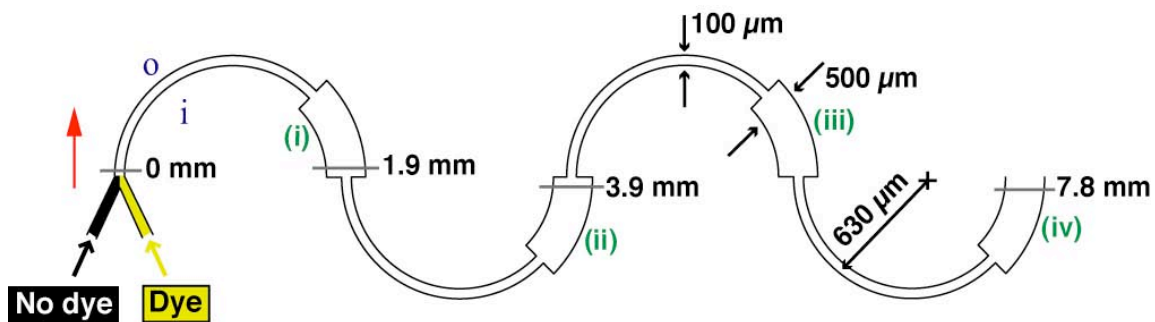


Figure V-3. ASM design. Design of micromixer coupling transverse Dean (vertical plane) and expansion vortex (horizontal plane) effects in the vicinity of an abrupt increase in width from 100 to $500\ \mu\text{m}$ over the last quarter of each semi-circular arc ($29\ \mu\text{m}$ tall, $630\ \mu\text{m}$ radius of curvature, “i” and “o” denote inner and outer walls).

Flow visualization

The combined effect of the multi-vortex system was observed direct visualization of colored dye streams in a curved microchannel incorporating an expansion from 100 to 500 μm in width. Cross-sectional confocal imaging shows that mixing is only enhanced above a critical flow rate at which the strength of both Dean and expansion vortices become significant (Figure V-4). Figure V-5 shows cross-sectional images taken along the ASM for $\kappa = 8.6$ ($Re = 32.2$)

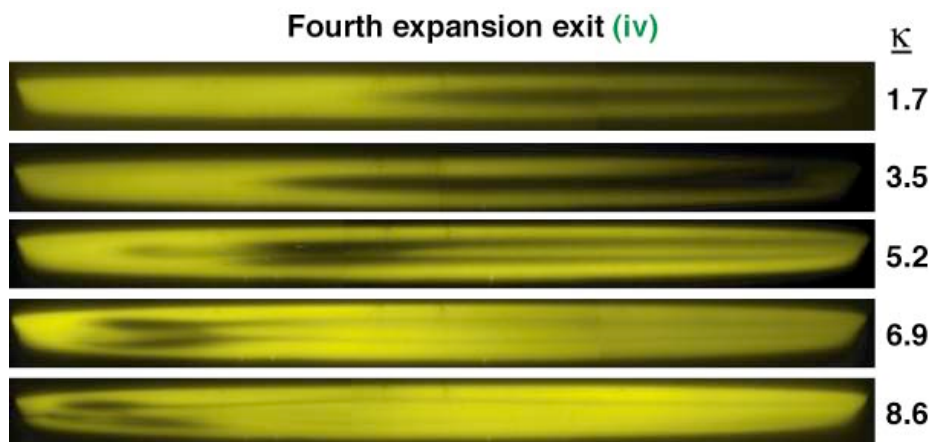


Figure V-4. Confocal cross-sectional images at the fourth expansion exit. Images are taken at 7.8 mm downstream (corresponding to position iv from Figure V-3) from $6.4 < Re < 32.2$ ($1.7 < \kappa < 8.6$, κ and Re are computed based on the 100 μm wide segment). As κ is increased the two species become almost completely intermixed, as indicated by uniform fluorescence over the channel cross-section.

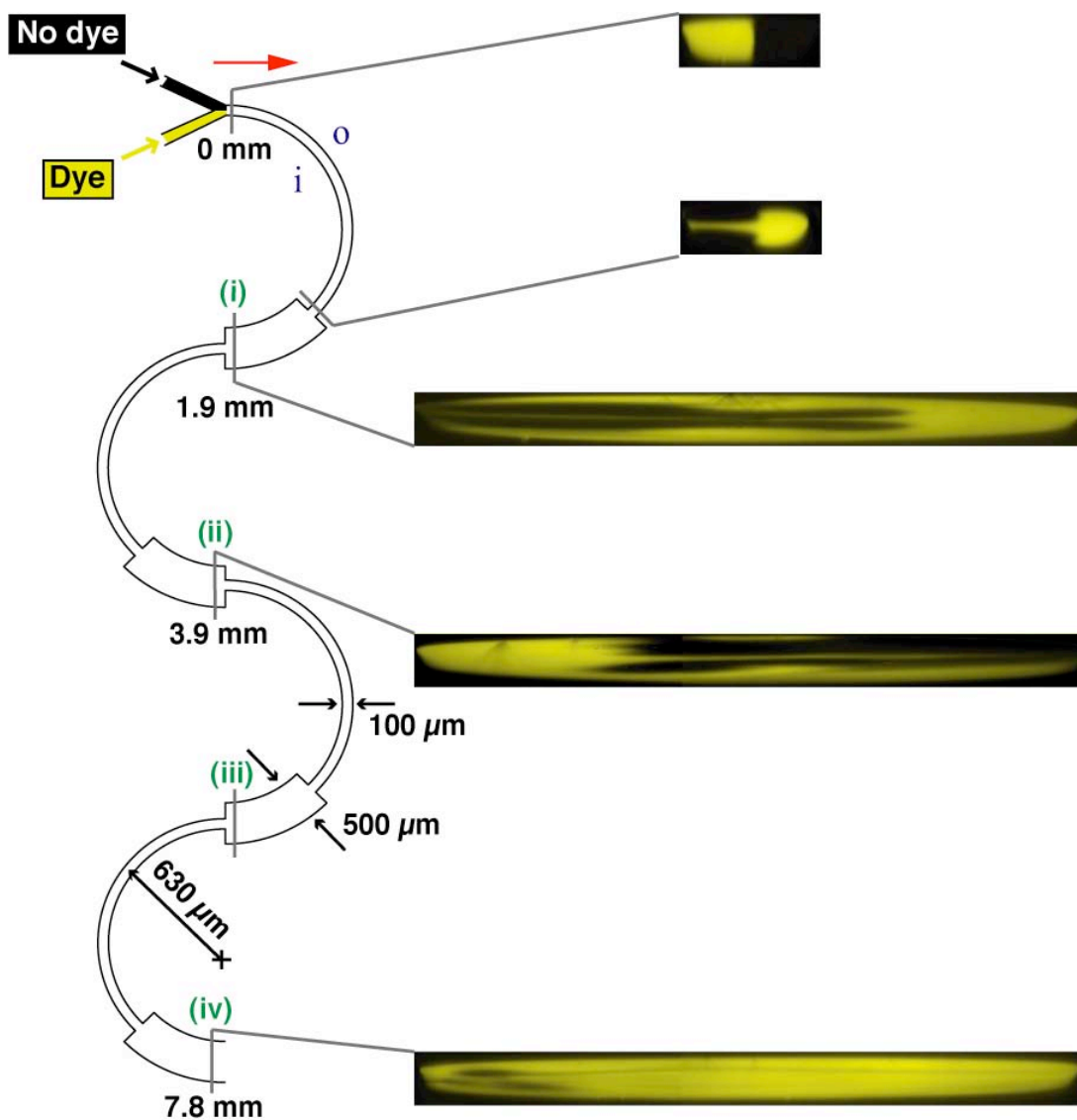


Figure V-5. Cross-sectional images at $\kappa = 8.6$ images along the ASM. A level of 80 % mixing is achieved at the end of the fourth expansion (7.8 mm from the entrance, corresponding to position iv, κ is computed based on the 100 μm wide segment).

With this simple modification to the serpentine microchannel geometry, a level of 80% mixing is achieved at the 7.8 mm downstream position at $Re \sim 32$, with even greater efficiencies possible at higher flow rates (Figure V-6). Mixing is not enhanced at low flow rates or in the absence of expansion segments, consistent with observations in serpentine and square wave flow geometries of uniform cross-section.^{63, 71, 88} Figure V-7 shows the evolution of σ with downstream distance for $1.7 < \kappa < 8.6$ ($6.4 < Re < 32.2$).

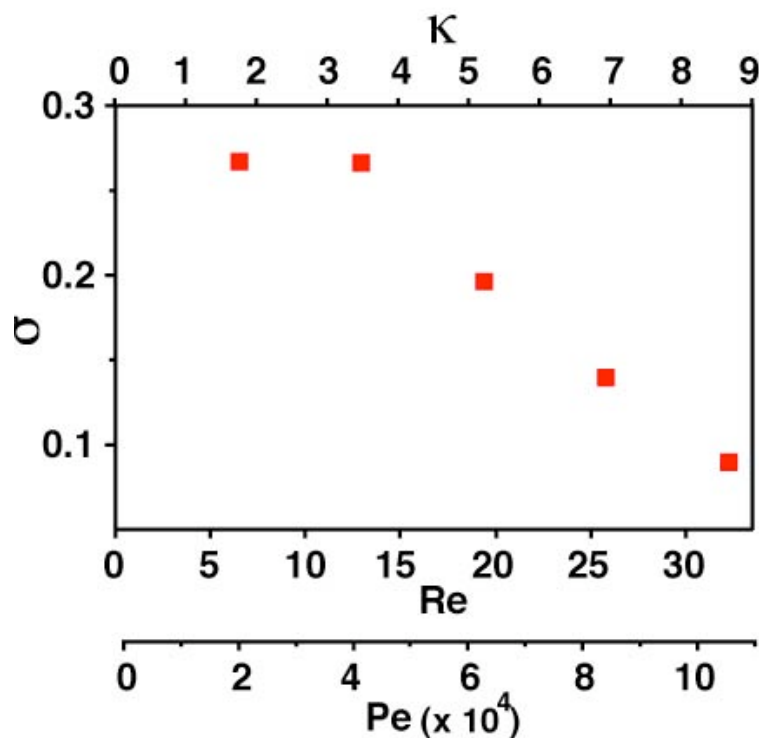


Figure V-6. Mixing levels measured at the fourth expansion exit. Plot of σ computed from the confocal image sequence in Figure V-4 (position iv in Figure V-3) as a function of the κ , Re , and Pe (Pe was computed using $D = 3 \times 10^{-6} \text{ cm}^2/\text{s}$ for Rhodamine 6G).

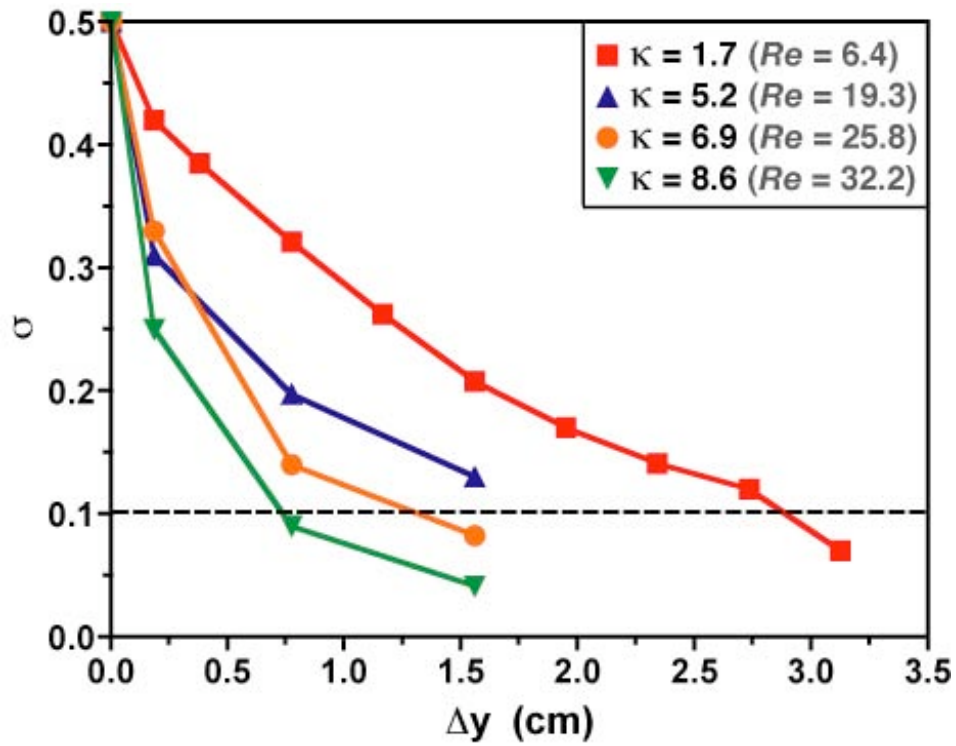


Figure V-7. Mixing performance of ASM. Flow rate dependence on the evolution of σ with downstream distance. The dashed line indicates the point where a level of 80% is achieved.

Binding application

We examined the practical utility of the ASM design by observing its influence on binding interactions between a fluorescent intercalating dye and double-stranded

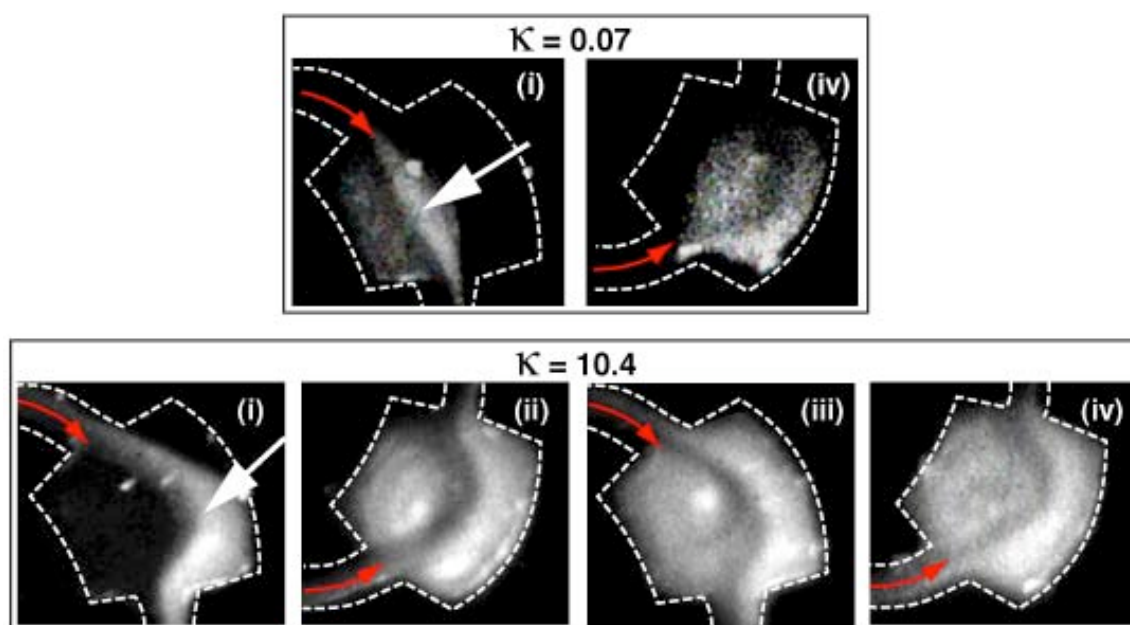


Figure V-8. Practical applicability of ASM. Binding enhancement between double-stranded DNA (calf thymus, 2.5 $\mu\text{g}/\text{mL}$) and an intercalating dye (ethidium bromide, 50 $\mu\text{g}/\text{mL}$) with increasing κ (dashed lines denote the microchannel walls). Images are taken at the positions indicated in (Figure V-3), red arrows indicate the flow direction, and white arrows indicate increased fluorescence above the background level of the unbound dye due to intercalation at the interface between streams.

DNA (Figure V-8). Fluorescence intensity is confined to the vicinity of the channel centerline at $\kappa = 0.07$, but grows to occupy the entire cross-section at $\kappa = 10.4$, indicative of an enhancement in interspecies encounters leading to an increase in the population of bound complexes.

Optimal ASM design

Optimal ASM design involves two geometric considerations. First, expansions should be positioned at downstream locations where simultaneous counter-rotations of at least 90° have occurred in the upper and lower halves of the cross-section in order to align the interface between species with the horizontal plane and maximize expansion effects on both species. This location can be determined using the same analysis discussed for the P-SAR design (Figure IV-12). Figure V-9 shows flow images of parallel aqueous streams labeled with blue and yellow food coloring for different downstream locations of the expansion.

Second, these phenomena depend on the expansion ratio (i.e., the ratio of inlet (narrow) to outlet (wide) cross-sectional areas). Our ASM design incorporates a 1:5 expansion ratio, providing a balance between favorable micromixing and ease of fabrication (e.g., avoiding problems associated with microchannel sagging at high expansion ratios).

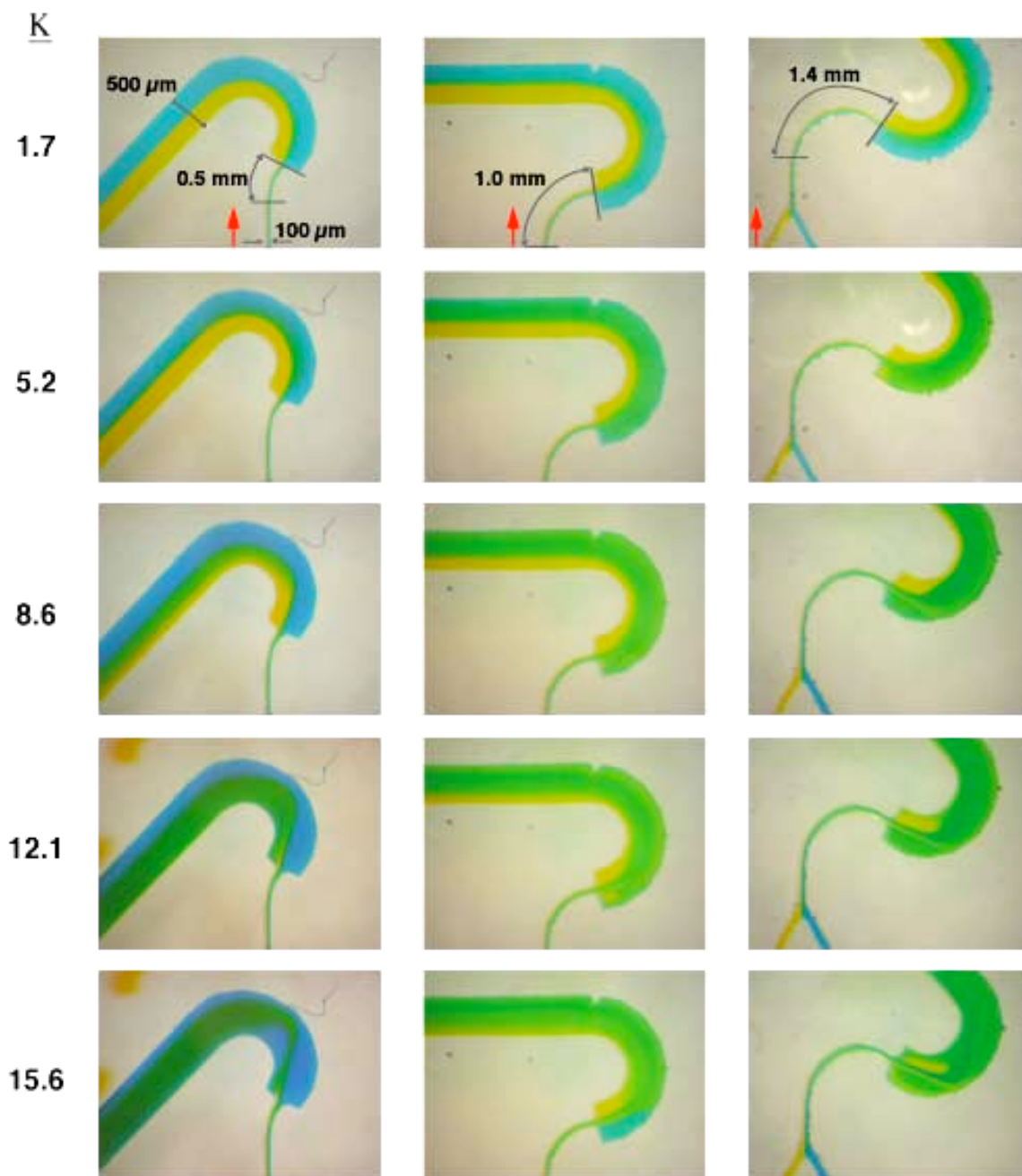


Figure V-9. Flow images at different expansion locations with increasing κ . Top-view images of aqueous streams of blue and yellow food dye taken in curved channels having an expansion in width from 100 to 500 μm . The expansions occur at different downstream locations from the entrance (indicated in the topmost image of each sequence) and the images are taken with increasing κ .

A measure of the strength of expansion vortex effects in the horizontal plane can be inferred by considering the friction loss accompanying a sudden expansion. In engineering nomenclature, these effects can be characterized in terms of the friction loss f_e for the case of incompressible inviscid flow along a streamline (i.e., losses associated with deviations from behavior describable in terms of Bernoulli's equation). For a sudden expansion

$$f_e = K_e(u^2/2g) \quad (\text{V-1})$$

where u is the average velocity in the narrow (inlet) channel segment, g is gravitational acceleration, and K_e is an *expansion-loss coefficient* given by**

$$K_e = (1 - S_a/S_b) \quad (\text{V-2})$$

where S_a and S_b are the cross-sectional areas of the narrow (inlet) and wide (outlet) segments respectively. Thus, an increase in the value of K_e corresponds to an increase in friction loss, which serves as an indication of increased expansion vortex strength. The expansion ratio chosen in the ASM design is $S_a/S_b = 1:5$ (100:500 μm) and as seen from Figure V-10, expansion ratios greater than 1:5 yield only a minimal increase in the value of K_e . Moreover, channel widths larger than 500 μm cause the channel to sag, as the material of construction is inherently soft. For these reasons we find an expansion ratio of 1:5 to be optimal for generating expansion vortices.

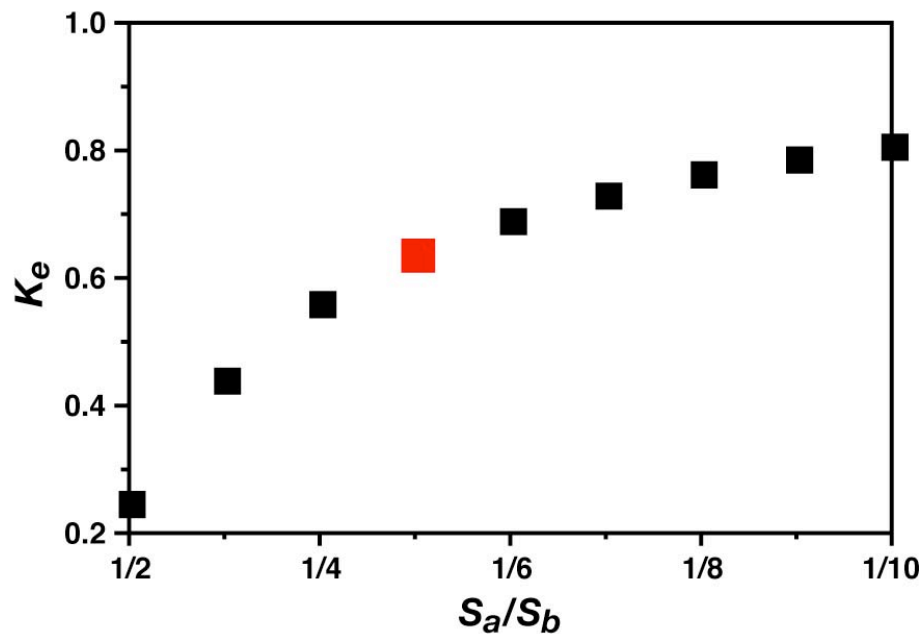


Figure V-10. Optimal expansion ratio for the ASM design. Based on this graph an expansion ratio of 1/5 (red data point) would be optimal considering the fact that fabricating wider microchannels may result in the roof of the channel to sag or collapse upon bonding.

In terms of flow conditions, the ASM is effective at $Re > 1$ (i.e., where there is sufficient inertial driving force to generate transverse flow). At higher flow rates, an inverse relationship between mixing length and Péclet number is observed (Figure V-11), in contrast to chaotically-driven configurations which display a signature logarithmic dependence of mixing length on Pe .⁶⁰

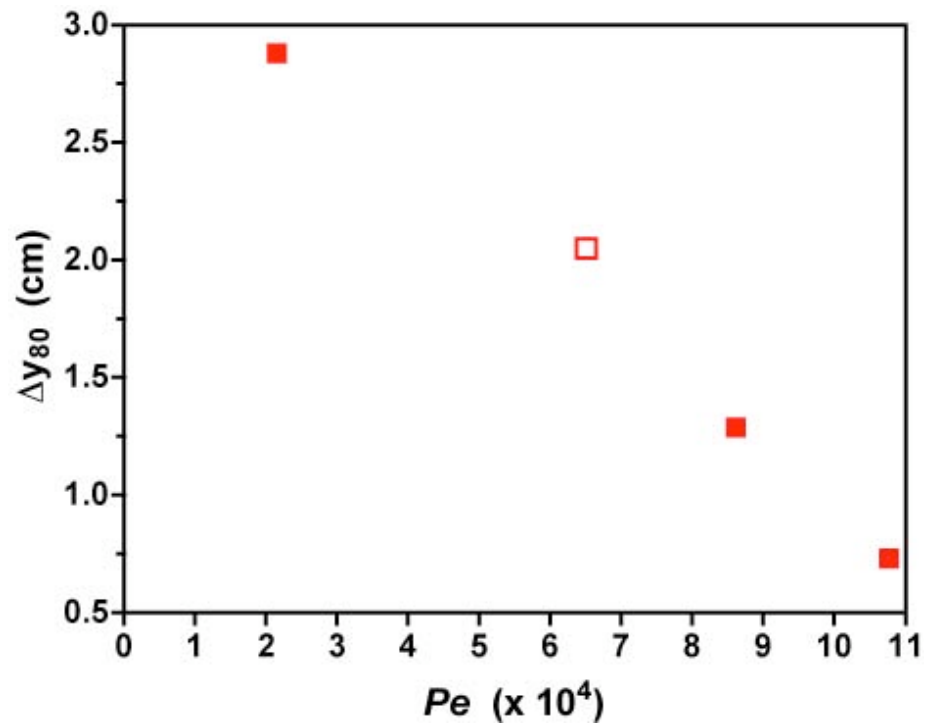


Figure V-11. Downstream distance to achieve 80% mixing at different Pe . Δy_{80} is determined from intersection of mixing intensity data with the dashed line in Figure V-7 with Péclet number. The open symbol at $Pe \sim 6.5 \times 10^4$ indicates that this mixing length was estimated by extrapolation. In contrast to chaotic systems where there is a logarithmic dependence of mixing length with Pe , an inverse relationship between mixing length and Pe is observed in the ASM design.

ASM effective flow rate range

In order to make a direct comparison between the asymmetric serpentine mixer (ASM) and the staggered herringbone mixer (SHM) design of Stroock *et al.*,⁶⁰ it is required to (i) determine the corresponding flow rates for the SHM in the case of an *aqueous* working fluid, and (ii) evaluate flow parameters (e.g., Reynolds and Péclet numbers) with respect to the channel hydraulic diameter. From the operating range of $2 \times 10^3 < Pe < 9 \times 10^5$ given in Figure 3c of Stroock *et al.*,⁶⁰ we determined the corresponding flow velocities from

$$V = PeD/d \quad (V-3)$$

where $D = 2 \times 10^{-8} \text{ cm}^2/\text{s}$ for a fluorescently labeled polymer in a 80% glycerol/20% water solution and $d = 0.01 \text{ cm}$.¹²⁵ Using these velocity values, we then computed equivalent Reynolds numbers based on the channel hydraulic diameter under the same operating conditions using

$$Re_h = d_h V / \nu \quad (V-4)$$

where $d_h = 0.0119 \text{ cm}$ is the hydraulic diameter and $\nu = 0.56 \text{ cm}^2/\text{s}$ is the kinematic viscosity of the glycerol medium. Next, flow velocities corresponding to an aqueous working fluid at the same Reynolds number were determined for the SHM from

$$V_{aq} = Re_h \mu_{aq} / d_h \rho_{aq} \quad (V-5)$$

where $\mu_{aq} = 0.01 \text{ g/cm s}$ and $\rho_{aq} = 0.9982 \text{ g/cm}^3$. These velocities were then used to compute corresponding flow rates from

$$Q_{aq} = V_{aq} A \quad (V-6)$$

where $A = 0.00017 \text{ cm}^2$ is the channel cross-sectional area. These values are summarized in Table V-1, and the flow conditions needed to achieve a given mixing length using the SHM and ASM designs are compared in Figure V-12. From this analysis, it can be seen that based on fluid properties of water at room temperature the corresponding flow rates required to achieve a level of 80% mixing in a downstream distance of $\sim 7 \text{ mm}$ are $Q > 10^{-1} \text{ mL/min}$ for the ASM design and $Q < 10^{-6} \text{ mL/min}$ for the SHM.

Table V-1. Flow rates computed for the SHM for an aqueous working fluid.

Pe^{60}	$V \text{ (cm/s)}$	Re_h	$V_{aq} \text{ (cm/s)}$	$Q_{aq} \text{ (ml/min)}$
2×10^3	4×10^{-3}	8.52×10^{-5}	7.17×10^{-5}	7.32×10^{-7}
2×10^4	4×10^{-2}	8.52×10^{-4}	7.17×10^{-4}	7.32×10^{-6}
2×10^5	4×10^{-1}	8.52×10^{-3}	7.17×10^{-3}	7.32×10^{-5}
9×10^5	1.8	3.83×10^{-2}	3.23×10^{-2}	3.29×10^{-4}

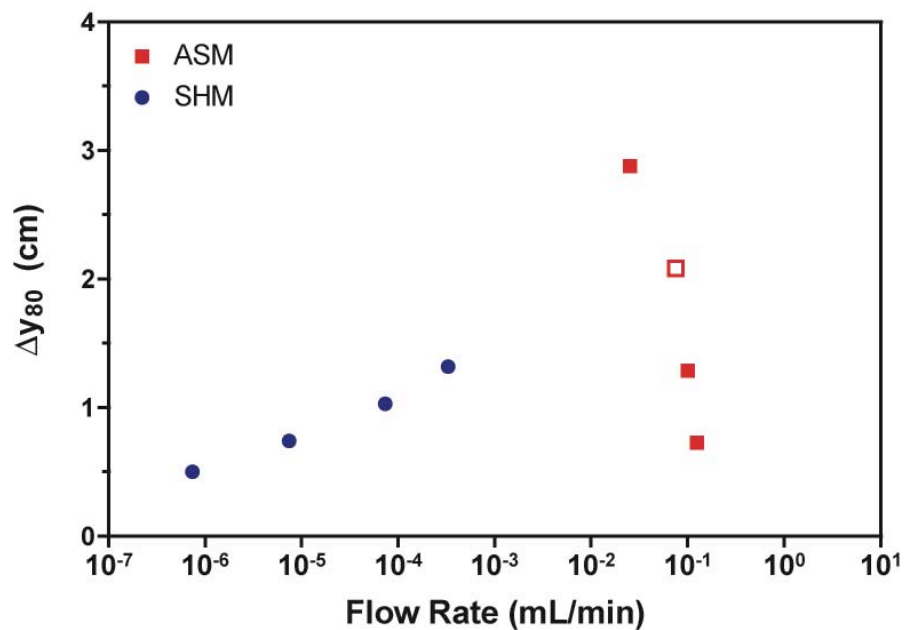


Figure V-12. Operating range of ASM and SHM for an aqueous system. The flow rate dependence of the downstream distance required to mix liquid streams to a level of 80% is shown for both designs (the open symbol indicates that this mixing length was estimated by extrapolation from Figure V-7).

Note that the use of tracers with different diffusion coefficients means that although the values of Pe are similar in both the ASM and SHM systems, the values of the Schmidt number (Sc)

$$Sc = n/D \quad (\text{V-7})$$

are quite different ($\sim 10^3$ in our experiments, versus $\sim 10^7$ in Stroock *et al.*⁶⁰).

Summary

A novel micromixing technique based on a multivortex system was discussed in this chapter. The mixer consisted of patterning a conventional serpentine channel with abrupt expansions at prescribed locations along the channel. In this Asymmetric Serpentine Mixer design, a first pair of vortices was induced by transverse Dean rotation in the vertical plane and the second pair of vortices was induced by the abrupt expansions in the horizontal plane. The combined action of these vortices was effectively used to mix liquid species in downstream distances comparable to conventional chaotic mixers. The biggest advantage of the ASM design was that it was fabricated from a single soft lithography step.

Recent work involving computational and experimental investigation of flow in sudden expansion microchannels in straight geometries demonstrates that the critical value for flow separation to occur in a microchannel with an expansion ratio of 1/3 (100:300 μm and 50 μm tall) is $Re = 22.5$.¹²⁶ The expansion ratio of 1/5 chosen in the ASM design here was found to be optimal based upon the fact that an increased ratio yielded only a minimal increase in the strength of the expansion vortices and that a wider channel would result in the top to sag or collapse upon thermal bonding. In terms of flow conditions for aqueous fluids, the corresponding flow rates required to achieve a level of 80% mixing in a downstream distance of ~ 7 mm are $Q > 10^{-1}$ mL/min for the ASM design and $Q < 10^{-6}$ mL/min for the SHM. It is noteworthy to mention that mixing can be achieved in shorter downstream distances by simply increasing the flow rates. This would result in a combined effect of faster transverse Dean rotation and increased

strength of the expansion vortices. However, it would be hard to sustain the necessary pressure drop required to achieve higher flow rates.

CHAPTER VI

HYBRID MICROMIXING APPROACHES

Techniques for combining different micromixing strategies in order to widely enhance the range of flow rates where efficient mixing can be achieved are proposed and discussed in this chapter. Initial results in two such *hybrid* techniques suggest that rapid micromixing can be achieved at short downstream distances over a greatly expanded Re range spanning over four orders of magnitude, an accomplishment that has yet to be demonstrated in a single micromixer design. The first technique involves the integration of chaotic mixing with the ASM design and the second technique involves the combination of spiral and ASM channel configurations.

Current generation micromixers generally have a limited range wherein efficient mixing is possible (e.g., see Table I-1). For example, the staggered herringbone mixer mixes fluids efficiently at $Re < 1$ with increasing efficiency at lower flow rates.⁶⁰ The C-shaped mixer on the other hand has an effective range of $Re > 1$ with increasing efficiency at higher Re .⁶³ The P-SAR micromixer discussed in this research works best at the flow rates where the Dean vortices have induced transverse rotations such that the fluid layers form a sandwich before entering the individual split streams. The ASM, similar to the C-shaped mixer, provides good mixing above $Re > 1$ with shorter mixing lengths at increased flow rates. Hence, there exists a need to combine the efficiencies of different micromixing strategies in order to design mixers that are capable of efficient mixing at *virtually* any given flow rate. From a practical standpoint, the mixer should

have the ability to perform rapid mixing at $0.01 < Re < 100$. This would encompass the operating range and conditions of most realistic microfluidic systems.

ASM combined with slanted barriers

Concept

The concept of this mixer involves the unification of two distinct techniques operating at two different flow regimes. The use of Dean flows in a curved channel with periodic expansions has been shown to be effective at $Re > 1$ through the ASM channel design in Chapter V. To enhance the effectiveness of this mixer we propose the idea of incorporating slanted barriers placed along the bottom surface of the channel (Figure VI-1). Chaotic mixing induced by barriers is an extremely effective technique for fluid mixing at $Re < 1$.^{59, 60} The combination of these two strategies in a single *hybrid* format would be an extremely useful mixer to carry out reactions in a microsystems.

For Stokes flow regime ($Re < 1$) and for $\alpha < 0.3$ (where α is the relative height of the barriers) it has been shown that the form of the flow is independent of Re .⁶⁰ Furthermore, the average rate of barrier-induced transverse rotation can be determined by a simple model and it was found that the rotation depends on geometric parameters like channel width (w), height (h), angle at which the barriers are aligned to the flow (θ) and the principal wavevector of the barriers (q).^{60, 127} The maximum transverse flow occurs for $\theta = 45^\circ$ and for $\alpha q h \sim 2$. Figure VI-2 shows mixing images in a straight channel patterned with slanted barriers on the bottom surface of the channel. The 15 μm tall barriers are arranged in alternating sets of 15 barriers each that are aligned at 45° and

140° respectively to the direction of the flow. The difference in the direction and angle of the barrier-sets was made to alter the center of the transverse flow-field with the aim of being as close to θ being on the order of 45°. Flow was initially studied in channels having alternating sets of 3 and 7 barriers and it was found qualitatively that in all the cases investigated an overall channel length of about 1.5 cm was required to achieve reasonable levels of mixing.

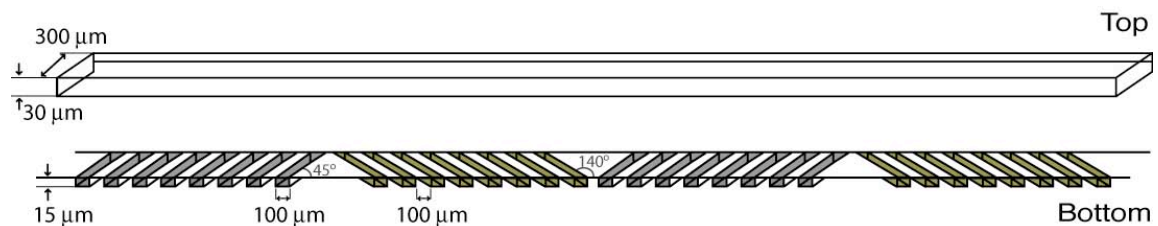


Figure VI-1. Schematic of microchannel with barriers along the channel floor. Slanted barriers in sets of seven are aligned in an alternating manner at 45° and 140° to the direction of the flow ($\alpha qh \sim 0.48$) in order to change the center of transverse rotation of the flow field produced by the barriers.

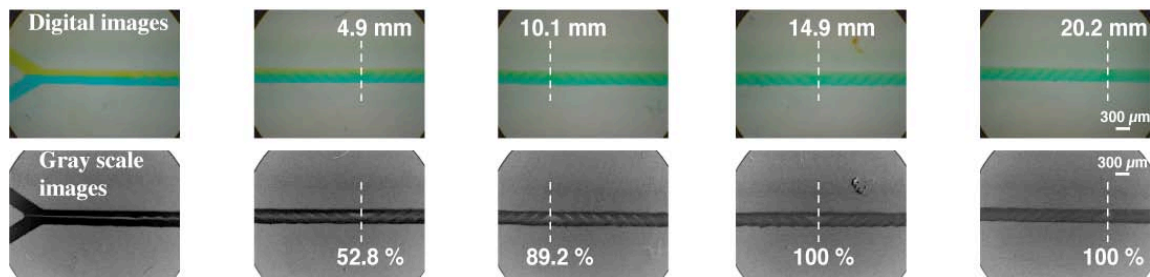


Figure VI-2. Top-view images in a straight channel with barriers on the floor. The channel is $300\ \mu\text{m}$ wide, the top is $29\ \mu\text{m}$ tall and the barriers on the floor are $15\ \mu\text{m}$ tall. The distance between the start of consecutive barriers measures $100\ \mu\text{m}$ and $\alpha qh \sim 0.48$. Digital color images (above) of parallel blue and yellow aqueous streams and corresponding gray-scale images (below) depicting the evolution of the green mixed interface are shown for $Re = 0.01$.

Design

The hybrid micromixer is a combination of the ASM design (from Chapter V) and a microchannel with slanted barriers (Figure VI-1). The top layer was a modification of the ASM design, such that the expansion region was made longer to incorporate path-length for barriers that were patterned on the bottom surface (Figure VI-3). The top surface had a uniform height of $29\ \mu\text{m}$ and the expansion ratio was

maintained at 1:5 with the narrow channel having a width of 100 μm and the wider expansion having a width of 500 μm . The radius of curvature was maintained at 630 μm along the narrower arcs while the expansion regions were composed of straight segments. Along the floor of these straight segments, slanted barriers having a width of 100 μm and height of 15 μm were placed. The distance between barriers was maintained at 100 μm ($\alpha qh \sim 0.48$). These barriers were constructed on a separate layer and carefully aligned to the top surface prior to thermal bonding. A 1/2-oz PC board was used to make the master mold to pattern the bottom surface. Fifteen barriers in each individual expansion region were uniformly aligned to the flow direction but alternated from 45° to 140° from one expansion to the other in order to compensate for the barrier induced flow symmetry, which is characteristic of alternating barrier sets that are aligned at the same angle but in opposing direction.⁶⁰ It should be noted that the expansions in the upper surface were positioned at downstream locations where simultaneous counter-rotations of at least 90° occurred in the upper and lower halves of the cross-section in order to align the interface between species with the horizontal plane and maximize expansion effects on the two species being mixed.

Flow visualization

Top-view mixing images of aqueous streams labeled with blue and yellow food coloring were obtained. The green mixed interface between the two streams was filtered out and converted to gray-scale images (Figure VI-4). Images were captured for a wide range of flow rates ranging from $Re = 0.03$ to 32.2. At lower flow rates ($Re < 1$) mixing is attributed to the transverse chaotic flows induced by the slanted barriers from the bottom of the channel and at higher flows ($Re > 1$) rapid fluid mixing is generated by the combined effect of Dean vortices in the vertical plane and expansion vortices in the horizontal plane. It is important to note that flow properties were measured using the hydraulic diameter calculated from the narrow 100 μm wide segments. Although initial results qualitatively suggest that this design is capable of performing mixing at the range of flow rates studied, further characterization using cross-sectional confocal imaging needs to be carried out.

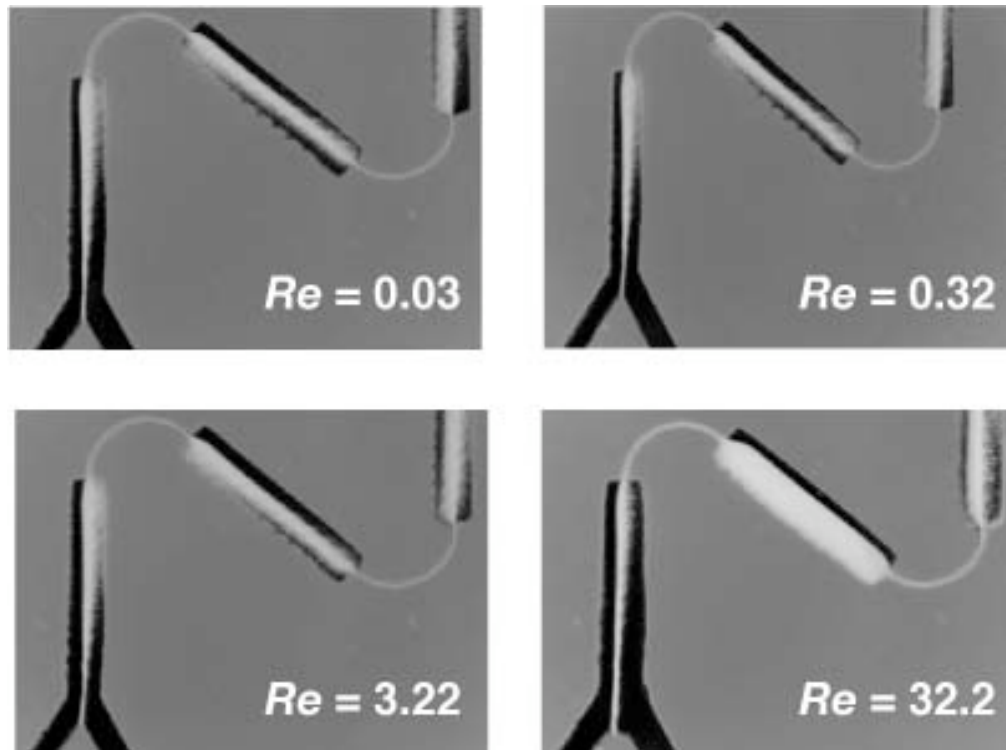


Figure VI-4. Flow images in an ASM channel with barriers patterned along the floor. The mixed interface between parallel aqueous streams of blue and yellow dyes is shown in these gray-scale images.

ASM combined with spiral mixing sections

Concept

The hybrid mixer proposed here is a combination of the ASM channel design (Chapter V) and a spiral mixing section (Chapter III). A tremendous advantage of this design over the hybrid mixer with slanted barriers described above is that the mixer can be fabricated from a single lithography step and does not require any aligning procedures prior to bonding. At high flow rates, mixing is achieved by the combined effect of the

Dean and expansion vortices. At lower flow rates however, mixing is achieved via transverse diffusion and the incorporation of the spiral section at the end of the ASM implies that the overall path length can be maintained for diffusion-based mixing to occur. Using this approach micromixing of fluid streams can be achieved at a wide range of flow rates.

Design

The ASM design from Chapter V is combined with the 8-arc spiral design from Chapter III to construct this hybrid mixer (Figure VI-5). The spiral section is placed after the ASM mixer having eight expansions that are 500 μm wide. The 1-mm long 'S'-section joining the 8-arc inlet and outlet spirals is modified to incorporate a short expansion segment (400 μm wide) in order to compensate for the uniform reversal of transverse Dean rotation (at flow rates corresponding to $Re > 1$) that occurs in geometries of opposing curvature. The abrupt increase in width helps in altering the symmetry of the flow field by generating expansion vortices on either side of the entrance to this segment. The rest of the channel has a uniform width of 80 μm and the entire channel is 29 μm tall. The overall path-length of the mixer is 4.26 cm and the mixing region occupies a total footprint area of 14.39 mm \times 3.42 mm. The inlet and outlet spirals are designed to have a radius of curvature ranging from 1.98 cm to 0.42 cm by a uniform decay of 80% every 90°.

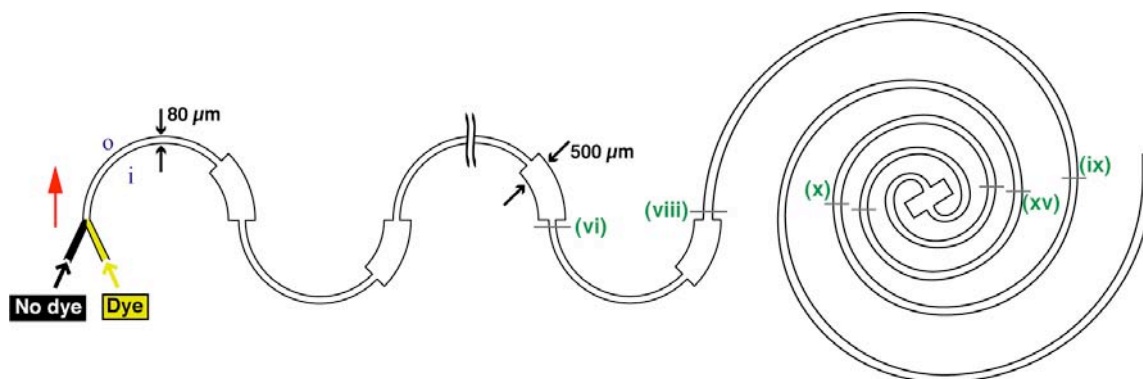


Figure VI-5. Design of an ASM-spiral hybrid micromixer. The expansion regions have a width of $500\ \mu\text{m}$ while the rest of the channel has a uniform width of $80\ \mu\text{m}$. The channel has a uniform height of $29\ \mu\text{m}$. The ASM portion incorporates eight expansions and the spiral section has a short expansion segment that connects the inlet and outlet spirals. The radius of curvature of the ASM region is maintained at $630\ \mu\text{m}$ while the spiral section has a maximum radius of curvature of $1.98\ \text{mm}$ on the inlet and outlet spirals that decays by 80% every 90° . The overall path-length of mixer is $4.26\ \text{cm}$ and occupies a footprint area of $14.39 \times \text{mm } 3.42\ \text{mm}$. In the figure “i” and “o” denote inner and outer walls).

Flow visualization

The effectiveness of the ASM design for flow rates corresponding to $Re > 1$ has already been discussed in Chapter V. In this section the performance of the hybrid design to mix fluids at $Re < 1$ is demonstrated. Cross-sectional images of two parallel aqueous streams with one of them labeled with Rhodamine 6G were obtained using confocal microscopy (Figure VI-6). It can be seen from the images that mixing is achieved purely by lateral diffusion, and a level of 80% mixing is achieved at the $2.4\ \text{cm}$

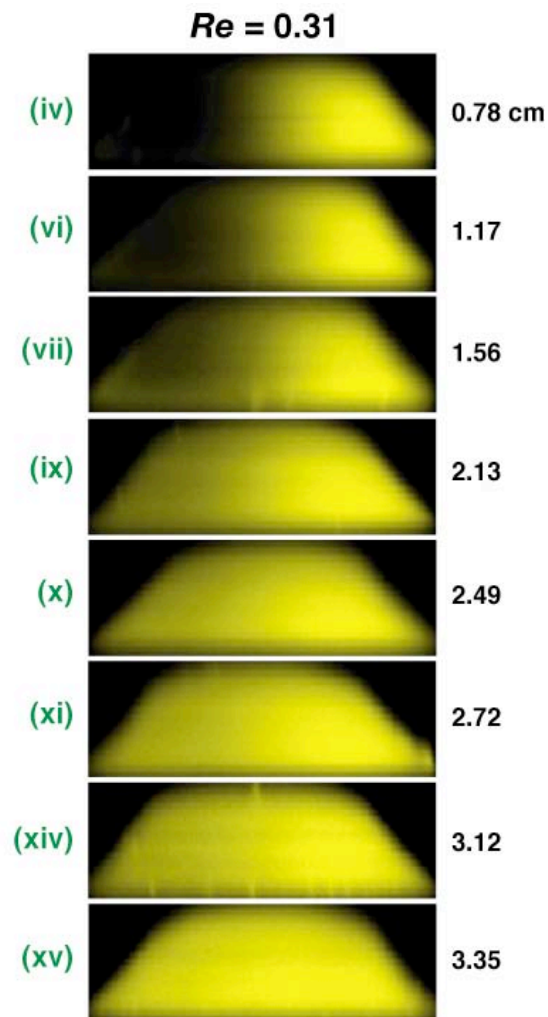


Figure VI-6. Confocal cross-sectional images in the ASM-spiral hybrid micromixer. Images of parallel aqueous streams with one of them labeled with Rhodamine 6G are taken for $Re = 0.31$ at downstream positions ranging from 0.78 – 3.35 cm as indicated next to each figure and corresponding to positions in Figure VI-6 (positions i – viii correspond to the end of each of the eight semi-circular arcs of the ASM and positions xi – xv correspond to every 180° arc-length of the spiral exclusive of the central s-section. A level of 80% mixing is achieved at 2.5 cm downstream.

downstream position at $Re \sim 0.3$, with even greater efficiencies possible at lower flow rates (Figure VI-7). Figure VI-8 shows the downstream distance required to achieve a level of 80% mixing for different values of Pe .

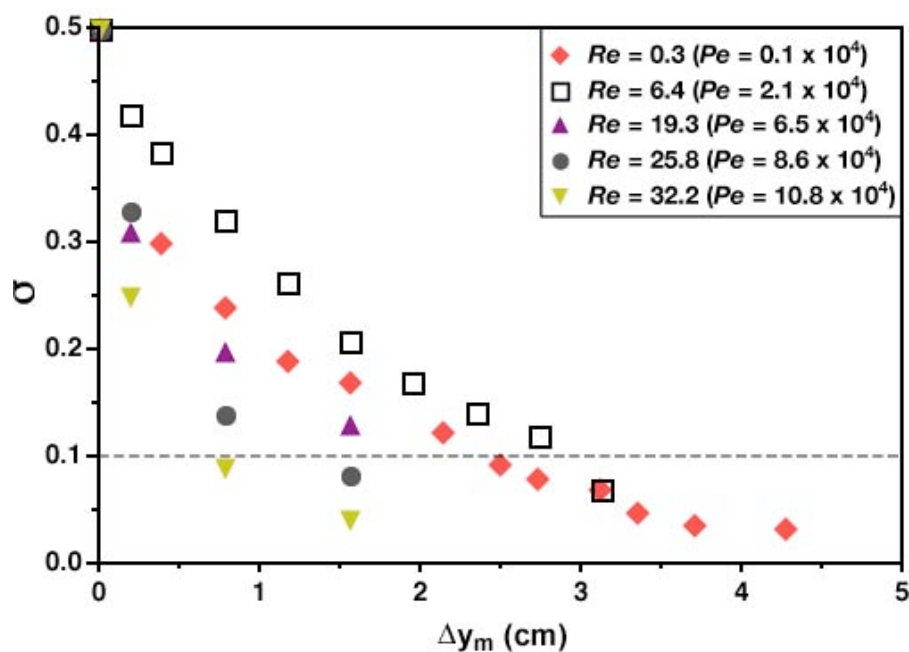


Figure VI-7. Mixing performance of ASM-spiral hybrid micromixer. Flow rate dependence on the evolution of σ with downstream distance. An 8-arc spiral section having a path length of 26.9 mm was incorporated at the end of a 15.7 mm long ASM channel having eight expansions. The data set corresponding to $Re = 6.4$ (indicated by open symbols) was obtained from an ASM channel of length 31.7 mm incorporating sixteen expansions.

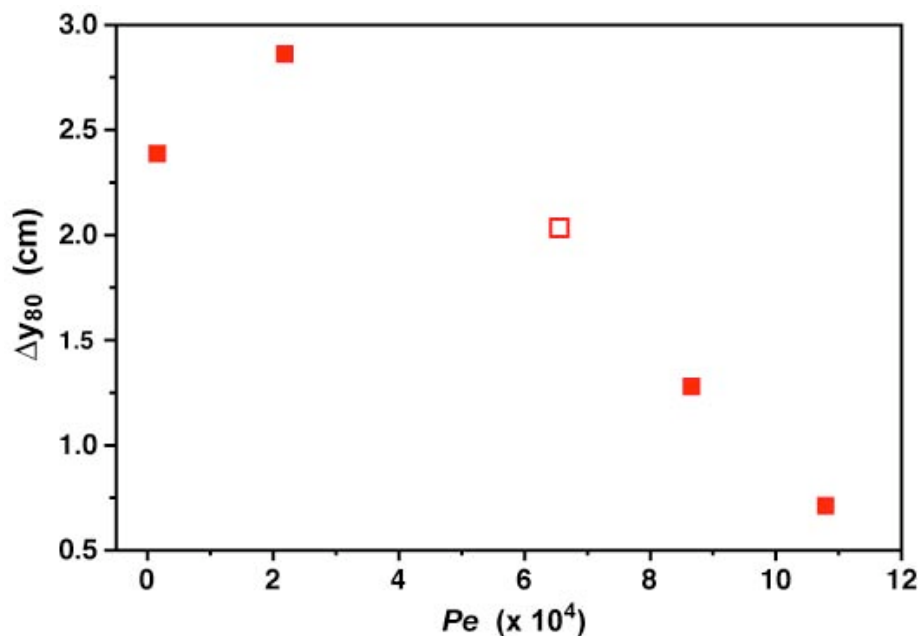


Figure VI-8. Performance of ASM-spiral hybrid mixer as a function of Pe . Downstream distance to achieve 80% mixing at different Pe in the ASM-spiral hybrid design. Δy_{80} is determined from intersection of mixing intensity data with the dashed line in Figure VI-7 with Péclet number. The open symbol at $Pe \sim 6.5 \times 10^4$ indicates that this mixing length was estimated by extrapolation.

Summary

In this chapter techniques for combining different micromixing strategies have been demonstrated. The first technique involves the combination of chaotic mixing with multivortex intermixing from the ASM design. At low flow rates corresponding to $Re < 1$, mixing is achieved by transverse flows induced by the barriers, whereas at higher flow rates corresponding to $Re > 1$, mixing is achieved by a combination of Dean vortices and expansion vortices. The second technique involves the addition of a spiral mixing

section at the end of the ASM design. Mixing at low flow rates ($Re < 1$) is achieved purely by diffusion as the spiral section permits accommodation of the path-length that is required. Both these techniques greatly expand mixing efficiency and considerable levels of mixing can be achieved at Re range spanning several orders of magnitude.

CHAPTER VII

CONCLUSIONS

This research work has demonstrated that enhanced micromixing can be achieved using topologically simple and easily fabricated planar 2-D microchannels by merely introducing curvature and changes in width in a prescribed manner. This was accomplished by harnessing a synergistic combination of (i) Dean vortices that arise in the vertical plane of curved channels as a consequence of an interplay between inertial, centrifugal, and viscous effects, and (ii) expansion vortices that arise in the horizontal plane due to an abrupt increase in a conduit's cross-sectional area. Mixing effects were characterized using both top-view imaging of aqueous streams labeled with tracer dyes and cross-sectional confocal microscopy of aqueous fluorescent dye streams. Practical utility was demonstrated by observing binding interactions between an intercalating dye and double-stranded DNA. The planar fabrication techniques involved in constructing these mixers are uncomplicated and straightforward and can be routinely carried out with any conventional microfabrication technique including those where soft lithography cannot be employed (e.g., glass, quartz, silicon).

Micromixing designs investigated

Spiral micromixers

Micromixers with spiral mixing sections arrayed along the flow path were investigated. The spiral sections were designed to have an inlet and outlet spiral wherein the radius of curvature decayed by 80% every 90°. Altering the number of arcs present can control the overall path-length of each spiral section. As fluid travels downstream into the spiral, it experiences an increase in the magnitude of centrifugal Dean effects that continually increase with decreasing radius of curvature. At low flow rates mixing is achieved purely by diffusion whereas at higher flow rates secondary flow effects contribute to the mixing performance.

Planar split-and-recombine mixer

A novel approach to perform lamination micromixing via a planar split-and-recombine format has been demonstrated. A serpentine channel was modified in such a way that the main flow channel was split at prescribed locations and then rejoined downstream. Fluid species undergo a sequence of transverse rotations in the main channel and in the individual split streams such that upon rejoining, alternating lamellae of each species are generated accompanied by a corresponding increase in interfacial area for diffusive mixing. This design is capable of efficient mixing levels without the need for employing complex 3-D channel structures.

Asymmetric serpentine mixer

An asymmetric serpentine micromixer based on a multivortex system was designed and characterized. The mixer consisted of patterning a conventional serpentine channel with abrupt expansions at prescribed locations along the channel. A first pair of vortices was induced by transverse Dean rotation in the vertical plane and the second pair of vortices was induced by the abrupt expansions in the horizontal plane. The combined action of these vortices was effectively used to mix liquid species in downstream distances comparable to conventional chaotic mixers. Increased levels of mixing can be achieved at higher flow rates.

Hybrid mixing strategies

Combining different micromixing strategies in order to enhance the mixing capabilities of each mixer have also been discussed. The first technique involved the combination of chaotic mixing via patterned barriers on the channel floor with multivortex mixing from the ASM design. At low flow rates corresponding to mixing was achieved by transverse flows induced by the barriers, whereas at higher flow rates, mixing was achieved by a combination of Dean vortices and expansion vortices. The second technique involved the addition of a spiral mixing section at the end of the ASM design. Mixing at low flow rates was achieved purely by diffusion, with a majority of mixing occurring in the spiral section. At higher flow rates fluids mixing was attributed to the multivortex system in the ASM channel.

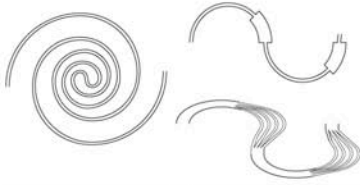
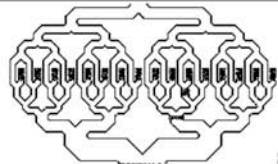
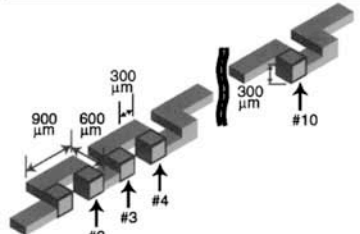
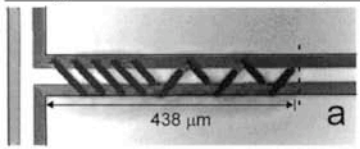
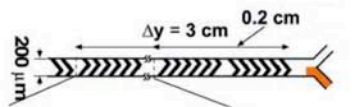
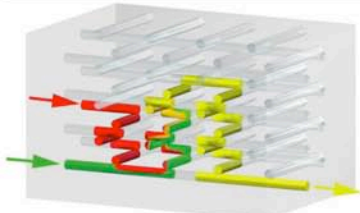
Comparison with literature

Since there is a vast body of literature involving micromixing strategies, it becomes extremely difficult to make a holistic comparison from one mixer to the other. Several factors including materials and techniques used for fabrication, percentage of mixing as a function of downstream distance, fluids and dyes used to characterize the performance of the mixer, imaging and visualization techniques need to be considered to judge the overall functionality and performance of the micromixer. A few of these factors are considered below.

Fabrication

Micromixers have been fabricated from various techniques such as soft lithography,⁶⁰ wet-etching,⁶³ direct-write,⁷¹ and stereolithography⁷² to name a few (Table VII-1). Many of the mixer designs incorporate complex 3-D structures that, from a practical standpoint are difficult and cumbersome to fabricate in a manner consistent with processes used to construct standard lab-on-a-chip components. The need to incorporate specialized processes and/or precise multilayer alignment steps makes these approaches far less attractive from both economic and process integration perspectives. The following table shows a comparison of the fabrication techniques used in this work with certain selected mixers from literature. Fabricating mixers by soft lithography of a single layer is probably the most feasible approach to perform on a routine basis.

Table VII-1. Comparison of fabrication techniques of different micromixers.

Mixer	Source	Fabrication		
		Technique (Substrate material)	Multi-level	Time
	This work	Soft lithography (Elastomer gel)	No	< 10 min
	Bessoth <i>et al.</i> ⁴⁸	Reactive ion etching (Glass and Silicon)	Yes	~ 1 h
Bessoth, F. G.; deMello, A. J.; Manz, A., Microstructure for efficient continuous flow mixing, <i>Anal. Commun.</i> 1999 , 36, 213-215 - Reproduced by permission of The Royal Society of Chemistry.				
	Liu <i>et al.</i> ⁶³	KOH wet etching (Silicon)	Yes	~ 1 h
Liu, R. H.; Stremmer, M. A.; Sharp, K. V.; Olsen, M. G.; Santiago, J. G.; Adrian, R. J.; Aref, H.; Beebe D. J., Passive mixing in a three-dimensional serpentine microchannel, <i>J. Microelectromechan. Syst.</i> 2000 , 9, 190-197. © 2000 IEEE.				
	Johnson <i>et al.</i> ⁵⁹	Hot imprinting (Polycarbonate)	Yes	~ 2 h
Reproduced with permission from Johnson, T. J.; Ross, D.; Locascio, L., Rapid microfluidic mixing, <i>Anal. Chem.</i> 2002 , 74, 45-51. © 2002 American Chemical Society.				
	Stroock <i>et al.</i> ⁶⁰	Soft lithography (PDMS)	Yes	~ 1 h
Reprinted with permission from Stroock, A. D.; Dertinger, S. K. W.; Ajdari, A.; Mezic, I.; Stone, H. A.; Whitesides, G. M., Chaotic mixer for microchannels, <i>Science</i> 2002 , 295, 647-651. © 2002 AAAS.				
	Therriault <i>et al.</i> ⁷¹	Direct-write assembly (Paraffin-based ink)	Yes	> 24 h
Reprinted with permission from Therriault, D.; White, S. R.; Lewis, J. A., Chaotic mixing in three-dimensional microvascular networks fabricated by direct-write assembly, <i>Nat. Mater.</i> 2003 , 2, 265-271. © 2003 Nature Publishing Group.				

An important factor that is often overlooked is the actual footprint area occupied by a mixer. The spiral mixer designs discussed here offer a tremendous advantage of being able to accommodate channels with long path-lengths in small footprint areas. Therriault *et al.* have shown that by building spiral towers, the overall contour length of the channel can be significantly increased while maintaining the footprint area at a constant.⁷¹ Although this technique is useful to incorporate lengthy channels, fabrication of these complex multi-level structures take several hours to days and require specialized techniques that are not easily affordable by most research laboratories. The staggered herringbone mixer on the other hand requires less complicated fabrication procedures and the mixer occupies a very minimal footprint area comparable to a conventional T-mixer.⁶⁰ Nevertheless, multiple levels of patterning and precision alignment are required prior to bonding. Moreover, since bonding is irreversible the fabrication procedures have to be repeated in case the channels happen to be misaligned. Figure VII-1 compares the mixing performance, as a function of footprint area required to achieve mixing levels of 90%, of the SHM with micromixers techniques discussed in this work.

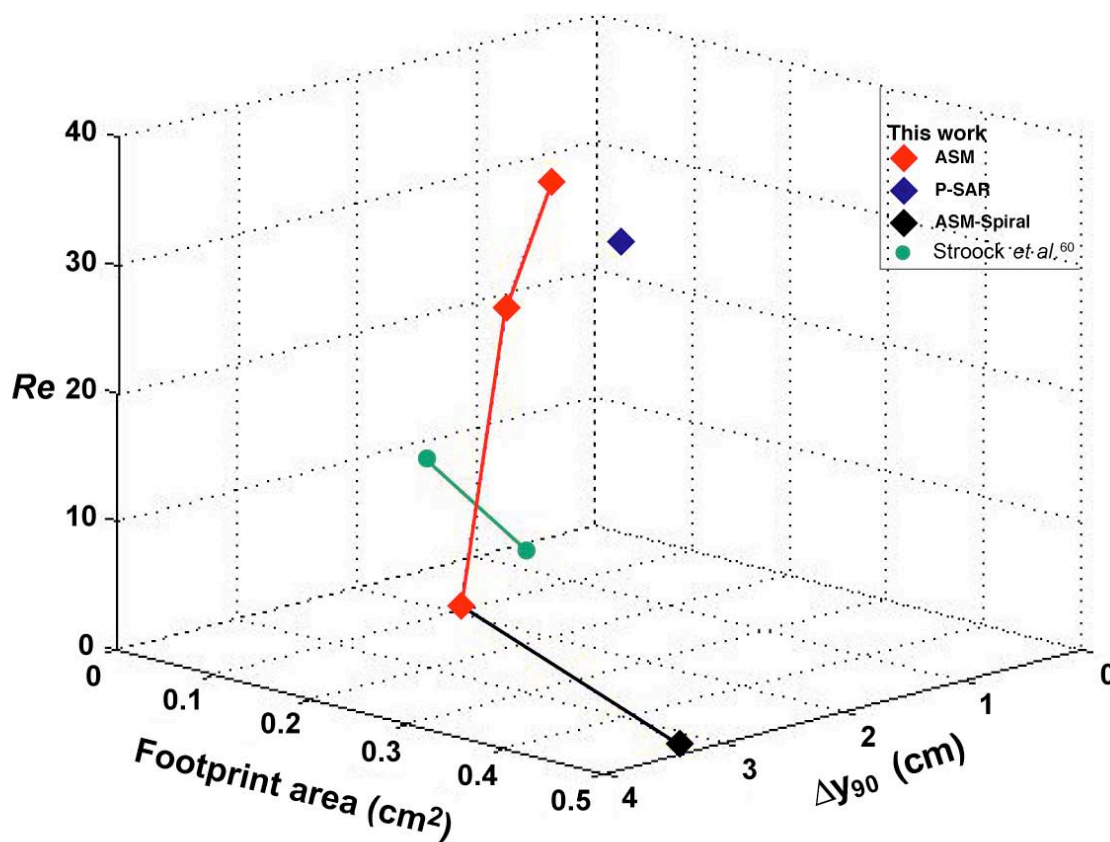


Figure VII-1. Comparison of mixing performance based on Re and footprint area. The data points indicate the length required for 90% mixing and the corresponding footprint area is measured. Mixing performance is compared with the staggered herringbone mixer. The black diamond corresponds to the ASM-spiral hybrid mixer.

Quantifying mixing

In a majority of micromixer designs, efficiency is characterized by the introduction of two parallel liquid streams and observing the minimum distance over which they become intermixed. The common protocol is to measure the length required to achieve mixing levels of 80 or 90% for different values of flow rates. Figure VII-2

shows a comparison of the lengths required to achieve 90% mixing as a function of Re for mixer geometries investigated in this work and for mixers listed in Table I-1.

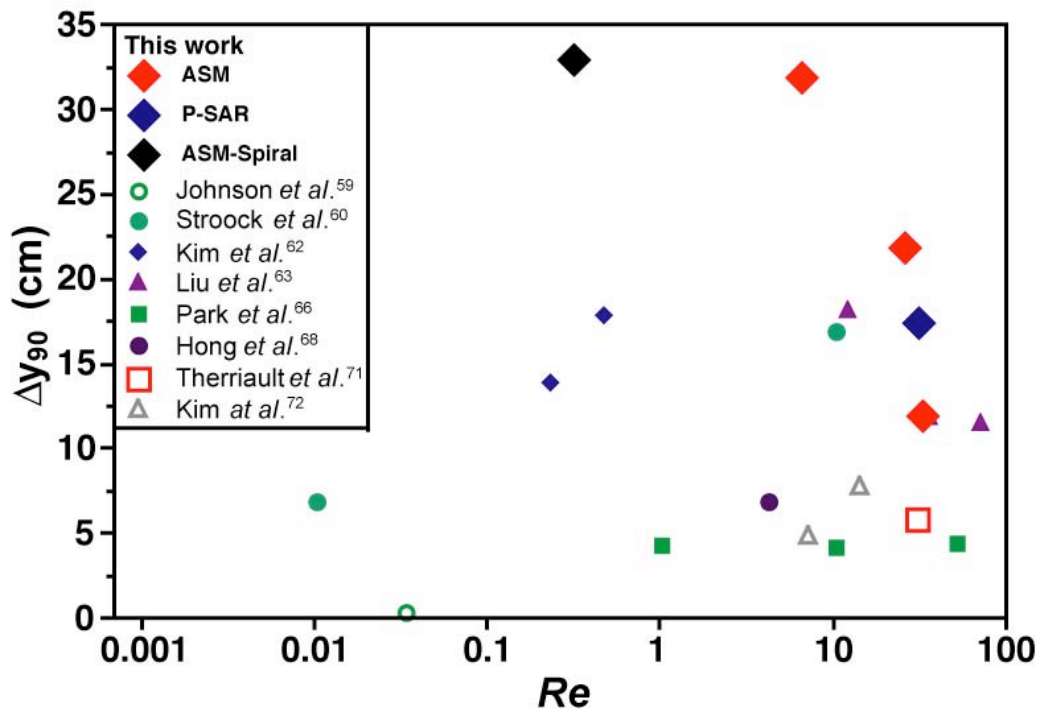


Figure VII-2. Lengths required for 90% mixing as a function of Re . Comparison is made between mixers investigated in this research with other micromixers from literature listed in Table I-1. In some cases where data was unavailable, extrapolation from existing curves was made and care was taken to be as accurate as possible.

Upon closer inspection, however, it is evident that the process of evaluating and drawing comparisons between performances of different designs based on Re alone is insufficient. Although aqueous working streams are commonly employed to study mixing, research groups have also used ethyl alcohol, sucrose solutions, glycerol/water mixtures, and phosphate buffers. Since the viscosities of these solutions vary quite considerably, it is necessary to make a comparison based on the Pe of the corresponding flow rates (Figure VII-3).

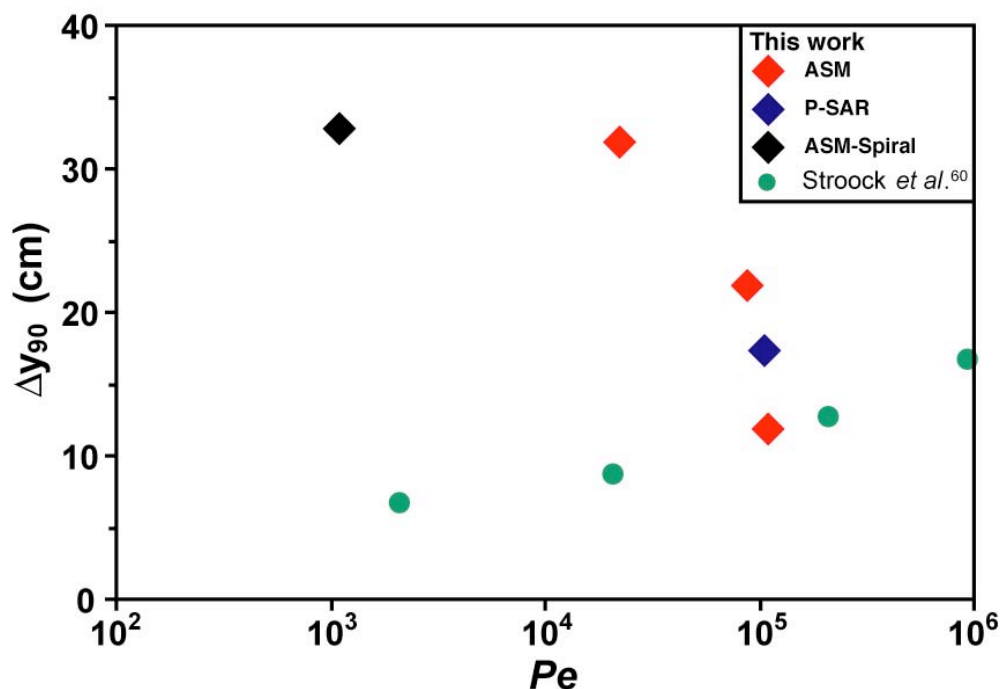


Figure VII-3. Lengths required for 90% mixing as a function of Pe . Performances of the mixer geometries investigated here and that of the staggered herringbone mixer are compared. While the ASM design demonstrates an inverse relationship with Pe , the SHM displays a signature logarithmic dependence. Data from other mixers from literature is required in order to compare efficiencies.

It is important to note that mixing experiments range from observing color changes at the interface between streams of different dyes to introducing reagents (e.g. phenolphthalein and sodium hydroxide) that react to form a visible interfacial front between streams. In addition to these “top view” measurement techniques, some research groups have employed confocal microscopy in order to image cross sectional slices of the flow field. Moreover, mixing is quantified from obtained images using various analysis algorithms. Another fundamental issue is that, in the case of non-circular conduits, flow characteristics are not always calculated using the channel hydraulic diameter. Often, the channel width has been chosen as the characteristic length-scale.

The situation becomes even more complex when this variety of experimental characterization techniques is further combined with the use of different working fluids having different dyes attached to the flow streams. Examples of these dyes include Rhodamine B, Rhodamine 6G, Fluorescein, food coloring, and FeSCN. Since these dyes have varying coefficients of diffusivity of several orders of magnitude, it is of utmost importance to characterize mixing performance as a function of the Sc (Figure VII-4). In the future mixing performances need to be compared based on Pe and Sc to account for the varying viscosities of bulk fluids and different diffusivities of dyes employed.

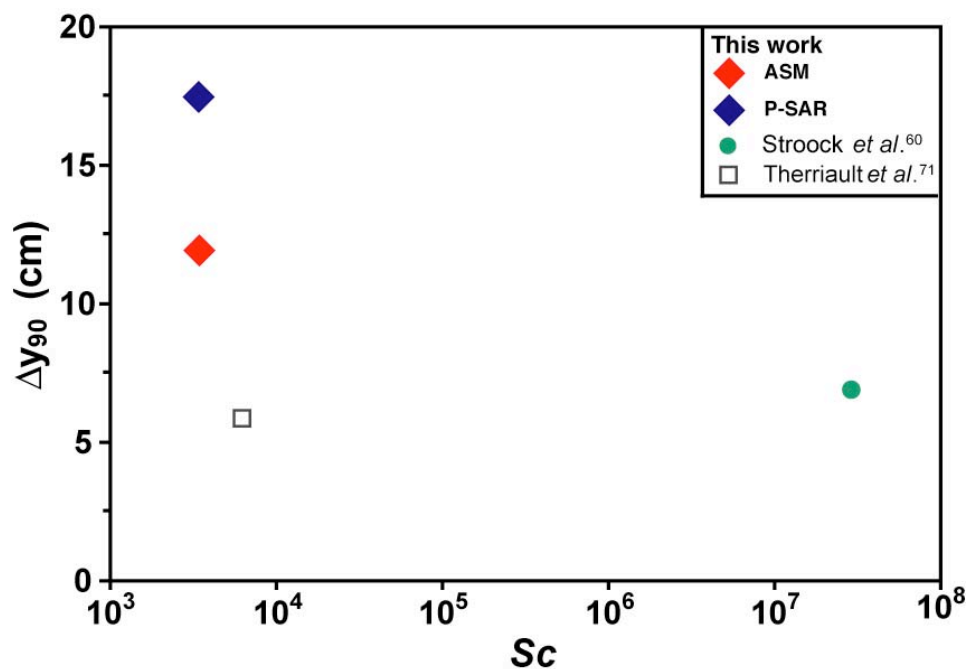


Figure VII-4. Lengths required for 90% mixing as a function of Sc . Performances of the mixer geometries investigated here are compared with that of the staggered herringbone mixer and the square spiral tower mixer. Aqueous streams were used in this work and in the case of the spiral tower mixer with dyes having diffusivities corresponding to $D_{mol} \sim 10^{-6} \text{ cm}^2/\text{s}$. For the case of the SHM, an 80% glycerol/ 20% water mixture was used with a fluorescein-labeled polymer with $D_{mol} = 2 \times 10^{-8} \text{ cm}^2/\text{s}$.

Recommendations and future work

While different techniques have been used to characterize mixing as discussed above, it is of extreme importance for mixing to be quantified based on cross-sectional imaging. Top-view imaging techniques do not necessarily give an accurate representation of the flow patterns beyond the plane of focus. As a result, the spiral

mixer geometries investigated here need to be characterized using cross-sectional confocal imaging. Furthermore, it would be useful to see whether there are any noticeable differences between the images quantified from the two techniques. Techniques from which time-resolved data could be obtained will be extremely useful for characterizing 3-D flow fields. In the confocal experiments carried out in this work, the average scan-time per cross-section is ~ 1 minute. Although faster scanning can be performed, the quality and resolution of the images decreases. As a result, it is difficult to accurately observe and characterize the existing flow patterns.

The P-SAR mixer offers a tremendous capability of performing split-and-recombine mixing in a planar format. Most SAR mixers from literature employ complex 3-D structures that are cumbersome to fabricate on a routine basis. While efficient levels of mixing have been achieved in a P-SAR employing four split streams, an increase in the number of split streams would further enhance the utility of this design. The relatively linear scaling between timescales associated with axial and transverse components of fluid motion suggest that these geometries can be easily scaled and optimized, and readily integrated in a broad range of lab-on-a-chip systems. An important aspect of the P-SAR design is that the overall mixing time continually decreases with increasing the number of split streams. Unlike conventional SAR mixers where the mixing time increases with increased amount of branching networks, the mixing time here is more or less independent of the number of individual split streams employed.

The ASM design, which is basically a modification of a conventional serpentine channel, offers mixing levels that are comparable to chaotic micromixers. Mixing in shorter downstream distances can be achieved by simply increasing the flow rate. The expansion ratio of 1:5 (100:500 μm) chosen in the ASM design is optimal both in terms of flow and fabrication. An increase in the expansion ratio will only yield a minimal increase in the value of the expansion loss-coefficient. Moreover, channel widths larger than 500 μm cause the top wall channel to sag, as the material of construction is inherently soft. For these reasons we find an expansion ratio of 1:5 to be optimal for generating expansion vortices.

The hybrid mixing approaches proposed in this research offer the capability of achieving efficient levels of mixing at Re spanning several orders of magnitude. Cross-sectional confocal imaging needs to be performed to characterize the working of the hybrid design involving the combination of ASM and chaotic mixing techniques. Although this design would involve multiple levels of fabrication, it has the ability to be efficient at a wide range of flow rates in a format that could occupy a relatively small footprint area. The ASM-spiral hybrid design on the other hand, occupies a larger footprint area but does not require a second level of patterning and the mixer has planar smooth-wall geometries through out its contour. One way of reducing the overall footprint of this hybrid design would be to pattern expansions along the spiral contour. Unfortunately, in channels that have a large radius of curvature, the centrifugal effects are not strong enough to significantly contribute to the mixing. Moreover, it is difficult to pattern expansions in the inner regions of the spiral as there is only a limited amount

of free footprint space available. Scaling down the channel geometry and by using specialized fabrication techniques, channels with smaller widths can be fabricated and expansions can be patterned in the inner regions of the spiral without overlapping adjacent channels.

From the fairly comprehensive literature review conducted here, it is evident that there is a lack of a common set of experimental and analysis protocols making it difficult to draw meaningful comparisons between the mixing performances of different designs. However, this is precisely the data needed in order to develop advanced micromixers to satisfy the demands of future miniaturized analysis systems.

To conclude this work, it is important to stress on the fact that naturally occurring transverse Dean flows offer the capability of designing and constructing extremely efficient micromixers. By simple alterations to channel widths and curvature, efficient micromixing can be achieved in smooth-walled planar microchannel geometries that can be constructed easily and routinely using any standard microfabrication technique.

LITERATURE CITED

- (1) Gravesen, P.; Branebjerg, J.; Jensen, O. *J. Micromech. Microeng.* **1993**, *3*, 168-182.
- (2) Ho, C.; Tai, Y. *Annu. Rev. Fluid Mech.* **1998**, *30*, 579-612.
- (3) Becker, H.; Gartner, C. *Electrophoresis* **2000**, *21*, 12-26.
- (4) Jakeway, S.; deMello, A.; Russell, E. *Fresenius J. Anal. Chem.* **2000**, *366*, 525-539.
- (5) Whitesides, G.; Stroock, A. *Phys. Today* **2001**, *54*, 42-48.
- (6) Beebe, D. J.; Mensing, G. A.; Walker, G. M. *Annu. Rev. Biomed. Eng.* **2002**, *4*, 261-286.
- (7) Stone, H. A.; Stroock, A. D.; Ajdari, A. *Annu. Rev. Fluid Mech.* **2004**, *36*, 381-411.
- (8) Squires, T. M.; Quake, S. R. *Rev. Mod. Phys.* **2005**, *77*, 977-1026.
- (9) Knight, J. *Nature* **2002**, *418*, 474-475.
- (10) Haswell, S. J. *Nature* **2006**, *441*, 705.
- (11) Liu, G. L.; Kim, J.; Lu, Y.; Lee, L. P. *Nat. Mater.* **2006**, *5*, 27-32.
- (12) Whitesides, G. M. *Nature* **2006**, *442*, 368-373.
- (13) Burns, M. A.; Johnson, B. N.; Brahmasandra, S. N.; Handique, K.; Webster, J. R.; Krishnan, M.; Sammarco, T. S.; Man, P. M.; Jones, D.; Heldsinger, D.; Mastrangelo, C. H.; Burke, D. T. *Science* **1998**, *282*, 484-487.
- (14) Shaikh, F. A.; Ugaz, V. M. *Proc. Natl. Acad. Sci. U. S. A.* **2006**, *103*, 4825-4830.

- (15) Krishnan, M.; Ugaz, V. M.; Burns, M. A. *Science* **2002**, *298*, 793.
- (16) Krishnan, M.; Agrawal, N.; Burns, M. A.; Ugaz, V. M. *Anal. Chem.* **2004**, *76*, 6254-6265.
- (17) Chou, H.-P.; Spence, C.; Scherer, A.; Quake, S. R. *Proc. Natl. Acad. Sci. U. S. A.* **1999**, *96*, 11-13.
- (18) Cho, B. S.; Schuster, T. G.; Zhu, X.; Chang, D.; Smith, G. D.; Takayama, S. *Anal. Chem.* **2003**, *75*, 1671-1675.
- (19) Sammarco, T. S.; Burns, M. A. *AIChE J.* **1999**, *45*, 350-366.
- (20) Dunn, D. A.; Feygin, I. *Drug Discovery Today* **2000**, *5*, S84.
- (21) Thorsen, T.; Maerkl, S. J.; Quake, S. R. *Science* **2002**, *298*, 580-584.
- (22) Lucchetta, E. M.; Lee, J. H.; Fu, L. A.; Patel, N. H.; Ismagilov, R. F. *Nature* **2005**, *434*, 1134-1138.
- (23) Belder, D.; Ludwig, M.; Wang, L.-W.; Reetz, M. T. *Angew. Chem. Int. Ed.* **2006**, *45*, 2463-2466.
- (24) Chiu, D. T.; Pezzoli, E.; Wu, H.; Stroock, A. D.; Whitesides, G. M. *Proc. Natl. Acad. Sci. U. S. A.* **2001**, *98*, 2961-2966.
- (25) Jensen, K. *Nature* **1998**, *393*, 735-737.
- (26) Stone, H. A.; Kim, S. *AIChE J.* **2001**, *47*, 1250-1254.
- (27) *Lab Chip* **2006**, *6*, 1118-1121.
- (28) Chen, D. L.; Gerdts, C. J.; Ismagilov, R. F. *J. Am. Chem. Soc.* **2005**, *127*, 9672-9673.

- (29) El-Ali, J.; Gaudet, S.; Günther, A.; Sorger, P. K.; Jensen, K. F. *Anal. Chem.* **2005**, *77*, 3629-3636.
- (30) Vanka, S. P.; Winkler, C. M.; Coffman, J.; Linderman, E.; Mahjub, S.; Young, B. *In Proceedings of the 4th ASME/JSME Joint Fluids Engineering Conference*; Honolulu, HI, 2003; pp 887-892.
- (31) Hertzog, D. E.; Michalet, X.; Jäger, M.; Kong, X.; Santiago, J. G.; Weiss, S.; Bakajin, O. *Anal. Chem.* **2004**, *76*, 7169-7178.
- (32) Hertzog, D. E.; Ivorra, B.; Mohammadi, B.; Bakajin, O.; Santiago, J. G. *Anal. Chem.* **2006**, *78*, 4299-4306.
- (33) Vijayendran, R. A.; Motsegood, K. M.; Beebe, D. J.; Leckband, D. E. *Langmuir* **2003**, *19*, 1824-1828.
- (34) Bynum, M. A.; Gordon, G. B. *Anal. Chem.* **2004**, *76*, 7039-7044.
- (35) McQuain, M. K.; Seale, K.; Peek, J.; Fisher, T. S.; Levy, S.; Stremmer, M. A.; Haselton, F. R. *Anal. Biochem.* **2004**, *35*, 215-226.
- (36) Liu, J.; Williams, B. A.; Gwartz, R. M.; Wold, B. J.; Quake, S. *Angew. Chem. Int. Ed.* **2006**, *45*, 3618-3623.
- (37) Liao, A.; Karnik, R.; Majumdar, A.; Cate, J. H. D. *Anal. Chem.* **2005**, *77*, 7618-7625.
- (38) Floyd, T. M.; Schmid, M. A.; Jensen, K. F. *Ind. Eng. Chem. Res.* **2005**, *44*, 2351-2358.
- (39) Ottino, J. M.; Wiggins, S. *Philos. Trans. R. Soc. London Ser. A* **2004**, *362*, 923-935.

- (40) Stremler, M. A.; Haselton, F. R.; Aref, H. *Philos. Trans. R. Soc. London Ser. A* **2004**, *362*, 1019-1036.
- (41) Nguyen, N.-T.; Wu, Z. *J. Micromech. Microeng.* **2005**, *15*, R1-R16.
- (42) Hardt, S.; Drese, K. S.; Hessel, V.; Schönfeld, F. *Microfluid. Nanofluid.* **2005**, *1*, 108-118.
- (43) demello, A. J. *Nature* **2006**, *442*, 394-402.
- (44) Oddy, M. H.; Santiago, J. G.; Mikkelsen, J. C. *Anal. Chem.* **2001**, *73*, 5822-5832.
- (45) Lu, L.-H.; Liu, K. S. R. *J. Microelectromechan. Syst.* **2002**, *11*, 462-469.
- (46) Liu, R. H.; Yang, J.; Pindera, M. Z.; Athavale, M.; Grodzinski, P. *Lab Chip* **2002**, *2*, 151-157.
- (47) Yang, Z.; Goto, H.; Matsumoto, M.; Maeda, R. *Electrophoresis* **2000**, *21*, 116-119.
- (48) Bessoth, F. G.; deMello, A. J.; Manz, A. *Anal. Commun.* **1999**, *36*, 213-215.
- (49) Kirner, T.; Albert, J.; Günther, M.; Mayer, G.; Reinhäkel, K.; Köhler, J. M. *Chem. Eng. J.* **2004**, *101*, 65-74.
- (50) Schwesinger, N.; Frank, T.; Wurmus, H. *J. Micromech. Microeng.* **1996**, *6*, 99-102.
- (51) Branbjerg, J.; Gravesen, P.; Krog, J. P.; Nielsen, C. R. *In Proceedings of IEEE Micro Electro Mechanical Systems Workshop*; San Diego, CA, 1996; pp 441-446.
- (52) Chen, H.; Meiners, J.-C. *Appl. Phys. Lett.* **2004**, *84*, 2193-2195.
- (53) Schönfeld, F.; Hessel, V.; Hoffman, C. *Lab Chip* **2004**, *4*, 65-69.

- (54) Lee, S. W.; Kim, D. S.; Lee, S. S.; Kwon, T. H. *J. Micromech. Microeng.* **2006**, *16*, 1067-1072.
- (55) Miyake, R.; Lammerink, T. S. J.; Elwenspoek, M. *In Proceedings of IEEE Micro Electro Mechanical Systems Workshop*; San Diego, CA, 1993; pp 248-253.
- (56) Voldman, J.; Gray, M. L.; Schmid, M. A. *J. Microelectromechan. Syst.* **2000**, *9*, 295-302.
- (57) Song, H.; Tice, J. D.; Ismagilov, R. F. *Angew. Chem. Int. Ed.* **2003**, *42*, 768-772.
- (58) Günther, A.; Jhunjhunwala, M.; Thalmann, M.; Schmidt, M. A.; Jensen, K. F. *Langmuir* **2005**, *21*, 1547-1555.
- (59) Johnson, T. J.; Ross, D.; Locascio, L. *Anal. Chem.* **2002**, *74*, 45-51.
- (60) Stroock, A. D.; Dertinger, S. K. W.; Ajdari, A.; Mezić, I.; Stone, H. A.; Whitesides, G. M. *Science* **2002**, *295*, 647-651.
- (61) Howell, P. B.; Mott, D. R.; Fertig, S.; Kaplan, C. R.; Golden, J. P.; Oran, E. S.; Ligler, F. S. *Lab Chip* **2005**, *5*, 524-530.
- (62) Kim, D. S.; Lee, S. W.; Kwon, T. H.; Lee, S. S. *J. Micromech. Microeng.* **2004**, *14*, 798-805.
- (63) Liu, R. H.; Stremmer, M. A.; Sharp, K. V.; Olsen, M. G.; Santiago, J. G.; Adrian, R. J.; Aref, H.; Beebe, D. J. *J. Microelectromechan. Syst.* **2000**, *9*, 190-197.
- (64) Kim, D. J.; Oh, H. J.; Park, T. H.; Choo, J. B.; Lee, S. H. *Analyst* **2005**, *130*, 293-298.
- (65) Kim, D. S.; Lee, S. H.; Kwon, T. H.; Ahn, C. H. *Lab Chip* **2005**, *5*, 739-747.

- (66) Park, S.-J.; Kim, J. K.; Park, J.; Chung, S.; Chung, C.; Chang, J. K. *J. Micromech. Microeng.* **2004**, *14*, 6-14.
- (67) Chung, Y.-C.; Hsu, Y.-L.; Jen, C. P.; Lu, M.-C.; Lin, Y.-C. *Lab Chip* **2004**, *4*, 70-77.
- (68) Hong, C.-C.; Choi, J.-W.; Ahn, C. H. *Lab Chip* **2004**, *4*, 109-113.
- (69) Melin, J.; Giménez, G.; Roxhed, N.; Wijngaart, W.; Stemme, G. *Lab Chip* **2004**, *4*, 214-219.
- (70) Bertsch, A.; Heimgartner, S.; Cousseau, P.; Renaud, P. *Lab Chip* **2001**, *1*, 56-60.
- (71) Therriault, D.; White, S. R.; Lewis, J. A. *Nat. Mater.* **2003**, *2*, 265-271.
- (72) Kim, D. S.; Lee, I. H.; Kwon, T. H.; Cho, D.-W. *J. Micromech. Microeng.* **2004**, *14*, 1294-1301.
- (73) Berger, S. A.; Talbot, L. *Annu. Rev. Fluid Mech.* **1983**, *15*, 461-512.
- (74) Erdogan, M. E.; Chatwin, P. C. *J. Fluid Mech.* **1967**, *29*, 465-484.
- (75) Ruthven, D. M. *Chem. Eng. Sci.* **1971**, *26*, 1113-1121.
- (76) Nunge, R. J.; Lin, T. S.; Gill, W. N. *J. Fluid Mech.* **1972**, *51*, 363-383.
- (77) Janssen, L. A. M. *Chem. Eng. Sci.* **1976**, *31*, 215-218.
- (78) Johnson, M.; Kamm, R. D. *J. Fluid Mech.* **1986**, *172*, 329-345.
- (79) Jones, S. W.; Thomas, O. M.; Aref, H. *J. Fluid Mech.* **1989**, *209*, 335-357.
- (80) Yi, M.; Bau, H. H. *Int. J. Heat Fluid Flow* **2003**, *24*, 645-656.
- (81) Dean, W. R. *Philos. Mag. Ser. 7* **1927**, *4*, 208-223.
- (82) Dean, W. R. *Philos. Mag. Ser. 7* **1928**, *5*, 673-695.
- (83) Gelfgat, A. Y.; Yarin, A. L.; Bar-Yoseph, P. Z. *Phys. Fluids* **2003**, *15*, 330-347.

- (84) Castelain, C.; Berger, D.; Legentilhomme, P.; Mokrani, A.; Peerhossaini, H. *Int. J. Heat Mass Transfer* **2000**, *43*, 3687-3700.
- (85) Jiang, F.; Drese, K. S.; Hardt, S.; Küpper, M.; Schönfeld, F. *AIChE J.* **2004**, *50*, 2297-2305.
- (86) Schönfeld, F.; Hardt, S. *AIChE J.* **2004**, *50*, 771-778.
- (87) Yamaguchi, Y.; Takagi, F.; Watari, T.; Yamashita, K.; Nakamura, H.; Shimizu, H.; Maeda, H. *Chem. Eng. J.* **2004**, *101*, 367-372.
- (88) Yamaguchi, Y.; Takagi, F.; Yamashita, K.; Nakamura, H.; Maeda, H.; Sotowa, K.; Kusakabe, K.; Yamasaki, Y.; Morooka, S. *AIChE J.* **2004**, *50*, 1530-1535.
- (89) Howell, P. B.; Mott, D. R.; Golden, J. P.; Ligler, F. S. *Lab Chip* **2004**, *4*, 663-669.
- (90) Vanka, S. P.; Luo, G.; Winkler, C. M. *AIChE J.* **2004**, *50*, 2359-2368.
- (91) Mengeaud, V.; Josserand, J.; Girault, H. H. *Anal. Chem.* **2002**, *74*, 4279-4286.
- (92) Love, J. C.; Wolfe, D. B.; Jacobs, H. O.; Whitesides, G. M. *Langmuir* **2001**, *17*, 6005-6012.
- (93) Sudarsan, A. P.; Ugaz, V. M. *Anal. Chem.* **2004**, *76*, 3229-3235.
- (94) Sudarsan, A. P.; Wang, J.; Ugaz, V. M. *Anal. Chem.* **2005**, *77*, 5167-5173.
- (95) Kleppinger, R.; Mischenko, N.; Reynaers, H. L.; Koch, M. H. J. *J. Polym. Sci., Part B* **1999**, *37*, 1833-1840.
- (96) Kleppinger, R.; Mischenko, N.; Theunissen, E.; Reynaers, H. L. *Macromolecules* **1997**, *30*, 7012-7014.

- (97) Kleppinger, R.; van Es, M.; Mischenko, N.; Koch, M. H. J.; Reynaers, H. *Macromolecules* **1998**, *31*, 5805-5809.
- (98) Laurer, J. H.; F., M. J.; Khan, S. A.; Spontak, R. J.; Bukovnik, R. *J. Polym. Sci., Part B* **1998**, *36*, 2379-2391.
- (99) Laurer, J. H.; Mulling, J. F.; Khan, S. A.; Spontak, R. J.; Lin, J. S.; Bukovnik, R. *J. Polym. Sci, Part B* **1998**, *36*, 2513-2523.
- (100) Mischenko, N.; Reynders, K.; Koch, M. H. J.; Mortensen, K.; S., P. J.; Fontaine, F.; Graulus, R.; Reynaers, H. *Macromolecules* **1995**, *28*, 2054-2062.
- (101) Mortensen, K.; Almdal, K.; Kleppinger, R.; Mischenko, N.; Reynaers, H. *Physica B* **1998**, *241-243*, 1025-1028.
- (102) Quintana, J. R.; Díaz, E.; Katime, I. *Macromolecules* **1997**, *30*, 3507-3512.
- (103) Quintana, J. R.; Díaz, E.; Katime, I. *Polymer* **1998**, *39*, 3029-3034.
- (104) Soenen, H.; A., L.; Reynders, K.; Berghmans, H.; Winter, H. H.; Overbergh, N. *Polymer* **1997**, *38*, 5661-5665.
- (105) Soenen, H.; Berghmans, H.; Winter, H. H.; Overbergh, N. *Polymer* **1997**, *38*, 5653-5660.
- (106) Watanabe, H.; Kuwahara, S.; Kotaka, T. *J. Rheol.* **1984**, *28*, 393-403.
- (107) Maanen, G. J. v.; Seeley, S. L.; Capracotta, M. D.; White, S. A.; Bukovnik, R. R.; Hartmann, J.; Martin, J. D.; Spontak, R. J. *Langmuir* **2005**, *21*, 3106-3115.
- (108) Fichet, G.; Stutzmann, N.; Muir, B. V. O.; Huck, W. T. S. *Adv. Mater.* **2002**, *14*, 47-51.

- (109) Trimbach, D.; Feldman, K.; Spencer, N. D.; Broer, D. J.; Bastiaanses, C. W. M. *Langmuir* **2003**, *19*, 10957-10961.
- (110) US Patent Number: 6066329.
- (111) US Patent Number: 5879694.
- (112) US Patent Number: 5578089.
- (113) US Patent Number: 5221534.
- (114) Wu, H.; Odom, T. W.; Chiu, D. T.; Whitesides, G. M. *J. Am. Chem. Soc.* **2003**, *125*, 554-559.
- (115) Lee, J. N.; Park, C.; Whitesides, G. M. *Anal. Chem.* **2003**, *75*, 6544-6554.
- (116) Murakami, T. *Arch. Histol. Jap.* **1973**, *35*, 323-326.
- (117) Murakami, T. *Arch. Histol. Jap.* **1975**, *38*, 151-168.
- (118) Erbacher, C.; Bessoth, F. G.; Busch, M.; Verpoorte, E.; Manz, A. *Mikrochim. Acta* **1999**, *131*, 19-24.
- (119) Grumann, M.; Geipel, A.; Riegger, L.; Zengerle, R.; Ducrée, J. *Lab Chip* **2005**, *5*, 560-565.
- (120) Ducrée, J.; Brenner, T.; Haeberle, S.; Glatzel, T.; Zengerle, R. *Microfluid. Nanofluid.* **2006**, *2*, 78-84.
- (121) Speziale, C. G.; Thangam, S. *J. Fluid Mech.* **1983**, *130*, 377-395.
- (122) Kheshgi, H. S.; Scriven, L. E. *Phys. Fluids* **1985**, *28*, 2968-2979.
- (123) Cherdon, W.; Durst, F.; Whitelaw, J. H. *J. Fluid Mech.* **1978**, *84*, 13-31.
- (124) Alleborn, N.; Nandakumar, K.; Raszillier, H.; Durst, F. *J. Fluid Mech.* **1997**, *330*, 169-188.

- (125) Li, C.; Chen, T. *Sensors Actuators B* **2005**, *106*, 871-877.
- (126) Tsai, C.-H.; Chen, H.-T.; Wang, Y.-N.; Lin, C.-H.; Fu, L.-M. *Microfluid. Nanofluid.* **2006**, DOI 10.1007/s10404-10006-10099-10402.
- (127) Ajdari, A. *Phys. Rev. E* **2002**, *65*, 016301.

VITA

Name: Arjun Penubolu Sudarsan

Address: 3122 TAMU, College Station, TX 77843-3122.

Email: arjunps@gmail.com

Education: B.E., Chemical Engineering, BMS College of Engineering, Bangalore University, 2001
M.S., Chemical Engineering, Texas A&M University, 2003

Publications: Sudarsan, A. P.; Ugaz, V. M., Multivortex micromixing, *Proc. Natl. Acad. Sci. U. S. A.* **2006**, *103*, 7228-7233 (*Science* Editor's Choice **2006**, *312*, 1280).

Sudarsan, A. P.; Ugaz, V. M., Fluid mixing in planar spiral microchannels, *Lab Chip* **2006**, *6*, 74-82.

Sudarsan, A. P.; Wang, J.; Ugaz, V. M., Thermoplastic elastomer gels: an advanced substrate for microfluidic device construction, *Anal. Chem.* **2005**, *77*, 5167-5173.

Sudarsan, A. P.; Ugaz, V. M., Novel techniques for rapid fabrication of plastic-based microfluidic devices, *Anal. Chem.* **2004**, *76*, 3229-3225.